UNIVERSITY OF CALIFORNIA,
IRVINE

Biological Controls and Biogeochemical Outcomes of Marine Elemental Stoichiometry

DISSERTATION

submitted in partial satisfaction of the requirements
for the degree of

DOCTOR OF PHILOSOPHY

in Biological Sciences

by

Allison Renee Moreno

Dissertation Committee:
Professor Adam C. Martiny, Chair
Professor Steven Allison
Professor Matthew Bracken
Professor Francois Primeau

2019

DEDICATION

To my family.

To the elders, who brought us into this world.

To my loving parents for, all the patience and being the heart of my support system.

To my best friend and beautiful sister, every piece of work I complete has a little bit of you.

To my aunts and uncles, for showing me it's okay to be me.

To my cousins, you can accomplish anything you set your mind to, I have.

"You have two choices…

One will lead to happiness,
the other ~ to the madness!...

My advice to you
is don't step aside!..."

-Alice in Wonderland

TABLE OF CONTENTS

LIST OF FIGURES

LIST OF TABLES

ACKNOWLEDGMENTS

I would like to thank my family. Every single one of you has provided me with the strength to push through the hard times. You let me be a crazy talkative scientist with no apology! You inspire me to be the best person I can be. Thank you! Love you past the heavens!

I would like to express my appreciation to my committee chair, Dr. Adam Martiny, who opened my eyes to my niche, marine biogeochemistry. I am grateful that you took a chance on me in your lab. My knowledge and skills have grown larger than I ever thought was possible under your mentorship.

I thank my committee members: Dr. Steve Allison, Dr. Matt Bracken, and Dr. Francois Primeau. Steve was always ready to hear the progress of my diverse projects and provide amazing feedback on how to improve them. Through Matt's questions on both my research and my phrasing of it, I have improved my communication skills immensely. Francois has always been excited to collaborate and teach me new aspects on my research. Through our collaborations, I have published much of my work.

I would like to thank all my co-authors: Adam (Chapters 1-3), Adam J. Fagan (Chapter 2), and George I. Hagstom, Francois W. Primeau, and Simon A. Levin (Chapter 3). I thank the Annual Reviews group for permission to include Chapter 1 of my dissertation, which was originally published in Annual Reviews of Marine Science. Financial support was provided by funding from the National Science Foundation (NSF) Graduate Research Fellowship Program and from the National Science Foundation Biological Oceanography Program (grants OCE-1046297 and OCE-1559002). I thank David Talmy at the Massachusetts Institute of Technology, George Hagstrom at Princeton University, and Alyse Larkin at UCI, for many helpful comments.

I thank the Frontiers group for permission to include Chapter 2 of my dissertation, which was originally published in Frontiers in Marine Science. Financial support was provided by the UCI Undergraduate Research Opportunities Program, NSF Graduate Research Fellowship Program, and NSF Biological Oceanography Program (grant OCE-1848576). I would also like Professor Yu for advice on ENSO cycles, and Tanya Lam, Sarah Bowen, and Jenna Lee for contributing to the MICRO time-series.

I thank the Copernicus Publications group for permission to include Chapter 3 of my dissertation, which was originally published in Biogeosciences. Financial support was provided by NSF Graduate Research Fellowship Program, grants OCE-1756906, OCE-1046001 and GEO-1211972, OCE-1046297 and OCE-1559002), DOE Office of Biological and Environmental Research award DE-SC0012550, and Simons Foundation Grant 395890.

I would like to thank you all members of Ocean Biogeochemistry Group for broadening my view of ocean biogeochemical processes. You are an amazing group of scientists! I thank my lab mates: Stacy Suarez (girl you know), Alyssa Kent, Jenna Lee, Alyse Larkin, Catherine Garcia, and Lucas Ustick for their feedback, lunches, coffee hours (eating all the cakes I made), and being rubber duckies (as well as letting my ducks fly). I thank all the undergraduates: Alessandra Flaherty, Maggie Chiang, Sarah Joy Bowen, and Teghveer Kooner (TK); who brought happiness and fun to lab. Thank you for letting me teach and mentor you, in and out of lab. I thank Katherine Mackey and her lab: Belen cario Johann Lopez, Christopher McGuire, Raisha Lovindeer, Joanna Tavares-Reager, and Jessica Walden for letting me be an honorary member and assisting/commenting on projects.

CURRICULUM VITAE
Allison Renee Moreno

EDUCATION

2014 – Present	University of California, Irvine, CA Ph.D. student Ecology and Evolutionary Biology M.S. Ecology and Evolutionary Biology- Awarded Spring 2018
2010 – 2014	California State University Monterey Bay, Seaside, CA B.S. Marine Science Minors: General Biology, Mathematics
2008 – 2010	East Los Angeles College, Monterey Park, CA A.A. Natural Sciences

FELLOWSHIP AWARDED

2019	UC President's Postdoctoral Fellowship: Finalist (not awarded)
2019	NOAA Climate & Global Change (C&GC) Postdoctoral: Finalist (not awarded)
2018 – 2019	UCI Chancellors' Club Fellowship ($12,000)
2017 – 2018	UCI OCEANS Fellowship Award ($6,000)
2014 - 2017	NSF Graduate Research Fellowship Award ($132,000)
2017	UCI Travel Award
2013	Sanctuary Currents Symposium First Place Undergraduate Student Poster Competition
2012	AGU Travel Award
2011	NSF REU Fellowship

PUBLICATIONS

1. **AR Moreno** and ALM Haffa. (2014). The Impact of Fish and the Commercial Marine Harvest on the Ocean Iron Cycle. PLoS ONE 9(9).
2. **AR Moreno** and AC Martiny. (2018). Ecological Stoichiometry of Ocean Plankton. Annual Review of Marine Science. (10) 43-69. *Highlighted in Ratios Matter August 2018; 2(3).*
3. **AR Moreno**, GI Hagstrom, FW Primaeu, SA Levin and AC Martiny. (2018). Phytoplankton Stoichiometry Mediates Nonlinear Interactions between Phosphorus and Atmospheric CO_2. Biogeosciences. (15) 2761–2779.
4. AJ Fagan†, **AR Moreno†** and AC Martiny. (*Frontiers in Marine Science*). ENSO Event Impacts California Coastal Elemental Stoichiometric Ratios and Macronutrient Concentrations.
†Co-first authors
5. **AR Moreno**, CA Garcia, AA Larkin, JA Lee, W Wang, FW Primeau, JK Moore, and AC Martiny. (*Submitted*). Latitudinal gradient in the carbon-to-oxygen respiration quotient and the implications for ocean oxygen availability.

In preparation

6. **AR Moreno** and AC Martiny. Coastal Respiration Quotient and its Limitations.
7. **AR Moreno**, JA Lee, AA Larkin, and AC Martiny. Diel Cycling in the Atlantic Ocean Respiration Quotient.

LEADERSHIP AND PROFESSIONAL EXPERIENCE

June – July 2018 Hopkins Microbiology Course
Stanford University

Sept 2017 – Present Teaching Assistant
University of California, Irvine
Course: Genetics, Organisms to Ecosystems, Physiology Lab, Physiology in Extreme Environments

PRESENTATIONS

AR Moreno, CA Garcia, JA Lee, AA Larkin, JK Moore, FW Primeau and AC Martiny. Pacific Ocean Biome Variation in the Respiration Quotient of Particulate Organic Matter. 2019. Southern California Geobiology Symposium. University of Southern California, Los Angeles, CA (Poster)

AR Moreno, AC Martiny. 2019. Quantifying the Marine Respiration Quotient. 2019 Winter Ecology and Evolutionary Biology Graduate Student Symposium (WEEBGSS). University of California, Irvine, Irvine, CA (Presentation)

AR Moreno, CA Garcia, JA Lee, AA Larkin, JK Moore, FW Primeau and AC Martiny. 2018. Biome Variation in Oxidative Demand of Particulate Organic Matter and Biogeochemical Implications. 2nd Annual Environmental Poster Symposium. University of California, Irvine, Irvine, CA (Poster)

C Hopkins, AA Larkin, **AR Moreno**, AC Martiny. 2017. Quantitation Analysis of Synechococcus Diversity in the Indian Ocean. Summer Research Symposium. University of California, Irvine, Irvine, CA (Poster)

AJ Fagan, **AR Moreno**, AC Martiny. 2017. Coastal Nutrients, Stoichiometry, and Particulate Organic Matter when affected by an ENSO Event. UCI Undergraduate Research Symposium. University of California, Irvine, Irvine, CA (Poster)

AJ Fagan, **AR Moreno**, AC Martiny. 2017. Coastal Nutrients, Stoichiometry, and Particulate Organic Matter when affected by an ENSO Event. West Coast Biological Sciences Undergraduate Research Conference. Santa Clara University, Santa Clara, CA (Poster)

AR Moreno, AC Martiny. 2017. Redfield Revisited: Proximate and Ultimate Responses behind Marine Phytoplankton Stoichiometric Variability. Southern California Geobiology Symposium. University of Southern California, Los Angeles, CA (Poster)

AJ Fagan, **AR Moreno**, AC Martiny. 2017. The Effect of an ENSO on Coastal Nutrients and Particulate Organic Matter Concentrations and Ratios. ASLO Aquatic Sciences Meeting 2017. Honolulu, Hawaii (Poster)

AR Moreno, GI Hagstrom, FW Primaeu, SA Levin, AC Martiny. 2017. Marine Phytoplankton Physiology and Stoichiometry in Major Ocean Biomes Effect on Atmospheric CO2. ASLO Aquatic Sciences Meeting 2017. Honolulu, Hawaii (Poster)

AR Moreno, AC Martiny. 2017. Redfield Revisited: Physiology Behind Variable Stoichiometry. 2017 Winter Ecology and Evolutionary Biology Graduate Student Symposium (WEEBGSS). University of California, Irvine, Irvine, CA (Presentation)

AR Moreno, GI Hagstrom, AC Martiny. 2016. Feedback Effects of Phytoplankton Physiology and Stoichiometry on Atmospheric CO2. Southern California Geobiology Symposium. California Institute of Technology, Pasadena, CA (Poster)

K Linzner, AG Kent, **AR Moreno**, AC Martiny. 2016. Stoichiometric Response of E. Coli Adapted to High Temperature. Southern California Geobiology Symposium. California Institute of Technology, Pasadena, CA (Poster)

*__AR Moreno__, JE Canner, ALM Haffa. 2014. Fisheries Impact on the Global Ocean Iron Cycle. Toward a Sustainable 21st Century; Ocean Health, Global Fishing and Food Security. Arnold and Mabel Beckman Center of the National Academies of Sciences and Engineering, Irvine, CA (Presentation)
* Invited Speaker

AR Moreno, JE Canner, ALM Haffa. 2014. Global Commercial Harvest Impact on Ocean Iron Cycling. Marine Science Capstone. CSU Monterey Bay, Seaside, CA (Presentation)

AR Moreno, JE Canner, ALM Haffa. 2013. The Impact of Global Commercial Harvest on the Oceanic Iron Cycle. Sanctuary Currents Symposium. CSU Monterey Bay, Seaside, CA (Poster)

AR Moreno, JE Canner, ALM Haffa. 2012. The Impact of Global Commercial Harvest on the Oceanic Iron Cycle. American Geophysical Union Fall Meeting. Moscone Center, San Francisco, CA (Poster)

AR Moreno, ALM Haffa. 2012. The Impact of Global Commercial Harvest on the Ocean Iron Cycle. 6th Annual Hartnell College Science, Technology, Engineering and Mathematics (STEM) Student Intern Research Symposium. Hartnell College, Salinas, CA (Poster)

AR Moreno, N Kelley, CB Batmalle, AS Amend, AC Martiny. 2012. Fungi and Salinity Gradient in California Affect Nutrient Ratios. Sanctuary Currents Symposium. CSU Monterey Bay, Seaside, CA (Poster)

AR Moreno, N Kelley, CB Batmalle, AS Amend, AC Martiny. 2011. Fungi and Salinity Gradient in California Affect Nutrient Ratios. REU Earth System Science Department Presentation. UC Irvine, Irvine, CA (Poster)

N Kelley, **AR Moreno**, AS Amend, AC Martiny. 2011. Stoichiometry and homeostasis of terrestrial fungi. REU Earth System Science Department Presentation. UC Irvine, Irvine, CA (Poster)

SERVICE

2017 - Present	Environmental Research Poster Symposium - *Cofounder and Organizer*
2014 – Present	Active Member; CLEAN Education (http://sites.uci.edu/clean/)
2018 - 2019	Earth Day- Co-leading the Oceans Booth
2018	OC Regional Science Olympiad - Test Writer for Ecology
2017	Water UCI/OCEANS Plastic Ocean Art Exhibit Opening Night Reception
2016	Head Judge; Roosevelt High Magnet School Chemistry Fair
2013 – 2014	Peer-to-Peer Student Coordinator, CSU Monterey Bay
2012 – 2014	Peer-to-Peer Mentor, CSU Monterey Bay

ABSTRACT OF THE DISSERTATION

Biological Controls and Biogeochemical Outcomes of Marine Elemental Stoichiometry

By

Allison Renee Moreno

Doctor of Philosophy in Biological Sciences

University of California, Irvine, 2019

Professor Adam C. Martiny, Chair

Redfield proportions (106C:16N:1P:138-O_2) have been used to describe ocean biogeochemical patterns since the 1950s. However, recent research demonstrates variation in this ratio over latitudinal gradients, time, and seasons. As a result, determining the controls on, and predictability of, variable stoichiometry will improve our understanding of global biogeochemical cycle dynamics. To address these missing components, I examined the environmental and physiological conditions associated with changes in stoichiometry and performed predictive modeling to demonstrate the impact of variable stoichiometry on marine biogeochemical cycles.

I examined the direct environmental and physiological effects on fluctuations in stoichiometry in two ways. First, I synthesized scientific literature and revealed that specific physiological mechanisms have a strong impact on stoichiometry in nutrient-rich environments, whereas biogeochemical interactions are important in the oligotrophic gyres. Second, I utilized the 2015 El Niño as an example of extreme environmental conditions, where high temperatures and low nutrient availability were expected to affect stoichiometric ratios. These conditions resulted in a reduction in POM concentrations and

an increase in C:N, C:P, and N:P ratios. El Niño conditions are representative of future scenarios, as such, this study provides evidence that stoichiometry is affected by extreme environmental shifts.

To estimate the impact of variable stoichiometry on global biogeochemical cycles, I modelled and predicted future carbon and oxygen concentrations. First, I created a simple ocean box model to estimate the atmospheric CO_2. I found that variation in allocation of cellular resources led to higher carbon export and declines in atmospheric CO_2 compared to Redfield proportions. Second, I quantified the variability in the respiration quotient, or the oxygen required to oxidize one unit of carbon, $r_{-O2:C}$ in marine organic matter. The $r_{-O2:C}$ ratio was found to vary regionally due to temperature controls on plankton community composition and their physiological state. Deoxygenation, which had previously been estimated to occur during high temperature conditions, increased in regions where $r_{-O2:C}$ was low.

In summary, my work has demonstrated the importance of understanding, utilizing, and quantifying variable stoichiometry in order to better characterize global biogeochemical cycles.

INTRODUCTION

In 1934, Alfred Redfield demonstrated that the surface plankton elemental composition is homogeneously similar to that of deep ocean dissolved nutrients, defining the Redfield ratio of 106C:16N:1P:138-O_2 (following Eq. 1; Redfield 1958). Redfield proposed that microorganisms set the concentrations of nutrients in the deep ocean through their ability to fix C and N (Augueres & Loreau 2015; Lenton & Klausmeier 2007). Present ocean circulation models use the static Redfield ratio to estimate global carbon export and predict CO_2 cumulative emissions over the next century (Dunne et al. 2005; Teng et al. 2014). In recent years, studies have demonstrated systematic variation in the particulate C:N:P across ocean regions and seasons, challenging Redfield's ratio.

$$(CH_2O)_{106}(HN_3)_{16}(H_3PO_4) + 138\ O_2 \leftrightarrow 106\ CO_2 + 16\ HNO_3 + H_3PO_4 + 122\ H_2O \quad (1)$$

Variation in elemental stoichiometry stems from the celluar C, N, and P pools within a cell. To link biochemical regulation with the elemental stoichiometry of a cell, we must consider the molecular components (Geider & La Roche 2002; Sterner & Elser 2002). Molecules rich in C include carbohydrates and lipids. Molecules rich in N include proteins and photosynthetic components. Molecules rich in P include membrane lipids, polyphosphates, and nucleic acids. In addition to variation among the cellular component ratios, there is also variation in the abundance of each component within a cell. Anderson (1995) estimated the average cell contains 54.4% protein, 25.5% carbohydrate, 16.1% lipid, and 4.0% nucleic acid by organic dry weight. More recent predictions found that the median composition of microalgae is 32.2% protein, 15.0% carbohydrate, 17.3% lipid,

17.3% ash, 5.6% RNA, 1.1% chlorophyll-a and 0.98% DNA as percent dry weight (Finkel et al. 2016). Variations in biological components result in changes of stoichiometry, for instance, C:N in one study has ranged from 4.3 to 9.0 (Parsons et al. 1961) and 5.7 to 9.3 in another (Finkel et al. 2016).

The variation in community elemental stoichiometry across ocean regions has been observed using two separate approaches: directly measuring the elemental stoichiometry of particulate organic matter (Martiny et al. 2013a,b) and using inverse models to indirectly infer this ratio from inorganic nutrient fields (DeVries & Deutsch 2014, Teng et al. 2014, Weber & Deutsch 2010). The elemental stoichiometry of marine particulate organic matter has been shown to be below or near Redfield proportions in high-latitudes and equatorial upwelling regions, but above Redfield proportions in the oligotrophic gyres (Martiny et al. 2016; Singh et al. 2015; Talarmin et al. 2016). This pattern is also observed across seasons, with ratios higher in the summer and fall (warm and nutrient depleted) and lower in the winter and spring (colder and nutrient replete).

Declining oxygen levels, along with rising sea temperatures and increasing ocean acidity, is one of the "Big 3" threats to marine life in our ocean today (Falkowski et al. 2011; Gilly et al. 2013; Gruber 2011; Schmidtko et al. 2017). A further decline in oxygen levels will lead to reduced biological productivity and diversity, changes in animal behavior, declines in fisheries, and impacts on biogeochemical cycles (Deutsch et al. 2015; Falkowski et al. 2011; Stramma et al. 2010). Our understanding of the spatial extent and potential fluctuations of hypoxic (low-oxygen) regions in a changing climate are limited by sparse observations and unknown interacting effects of environmental conditions. Rising ocean temperatures are known to exacerbate ocean deoxygenation by lowering oxygen solubility

and stagnating ocean circulation, but potentially important effects on the stoichiometry of marine organic matter have not been assessed. The aim of my dissertation is to determine which biological processes control variability in elemental stoichiometric ratios and its influence on global biogeochemical cycles.

References

Anderson LA. 1995. On the hydrogen and oxygen content of marine phytoplankton. *Deep Sea Res. Part I Oceanogr. Res. Pap.* 42(9):1675–80

Augueres AS, Loreau M. 2015. Regulation of Redfield ratios in the deep ocean. *Global Biogeochem. Cycles*. 29(3):254–66

Chavez FP. 2002. Biological and chemical consequences of the 1997-1998 El Niño in central California waters Biological and chemical consequences of the 1997 – 1998 El Nin ˜ o in central California waters. *Prog. Oceanogr.* 54:205–32

Checkley DM, Barth JA. 2009. Progress in Oceanography Patterns and processes in the California Current System. *Prog. Oceanogr.* 83:49–64

Deutsch C, Ferrel A, Seibel B, Portner H-O, Huey RB. 2015. Climate change tightens a metabolic constraint on marine habitats. *Science (80-.).* 348(6239):1132–36

Dunne JP, Armstrong RA, Gnnadesikan A, Sarmiento JL. 2005. Empirical and mechanistic models for the particle export ratio. *Global Biogeochem. Cycles*. 19(4):

Falkowski PG, Algeo T, Codispoti L, Deutsch CA, Emerson S, et al. 2011. Ocean Deoxygenation: Past, Present, and Future. *Eos, Trans. Am. Geophys. Union*. 92(46):

Finkel Z V, Follows MJ, Liefer JD, Brown CM, Benner I, Irwin AJ. 2016. Phylogenetic diversity in the macromolecular composition of microalgae. *PLoS One*. 11(5):e0155977

Geider RJ, La Roche J. 2002. Redfield revisited: variability of C : N : P in marine microalgae

and its biochemical basis. *Eur. J. Phycol.* 37(1):1–17

Gilly WF, Beman JM, Litvin SY, Robison BH. 2013. Oceanographic and Biological Effects of Shoaling of the Oxygen Minimum Zone. *Ann. Rev. Mar. Sci.* 5(1):393–420

Gruber N. 2011. Warming up, turning sour, losing breath: ocean biogeochemistry under global change. *Philos. Trans. R. Soc. a-Mathematical Phys. Eng. Sci.* 369(1943):1980–96

King AL, Barbeau KA. 2011. Dissolved iron and macronutrient distributions in the southern California Current System. *J. Geophys. Res. Ocean.* 116(3):

Lenton TM, Klausmeier C a. 2007. Biotic stoichiometric controls on the deep ocean N : P ratio. *Biogeosciences*. 4(3):353–67

Martiny AC, Talarmin A, Mouginot C, Lee JA, Huang JS, et al. 2016. Biogeochemical interactions control a temporal succession in the elemental composition of marine communities. *Limnol. Oceanogr.* 61(2):531–42

Mcgowan JA, Cayan DR, Dorman LM. 1998. Climate-Ocean Variability and Ecosystem Response in the Northeast Pacific. *Science (80-.).* 281:

Parsons TR, Stephens K, Strickland JDH. 1961. On the Chemical Composition of Eleven Species of Marine Phytoplankters. *J. Fish. Res. Board Canada*. 18(6):1001–16

Redfield AC. 1958. The biological control of the chemical factors in the environment. *Am. Sci.* 46(3):1–18

Schmidtko S, Stramma L, Visbeck M. 2017. Decline in global oceanic oxygen content during the past five decades. *Nature*. 542(7641):335–39

Singh A, Baer SE, Riebesell U, Martiny AC, Lomas MW. 2015. C : N : P stoichiometry at the Bermuda Atlantic Time-series Study station in the North Atlantic Ocean. *Biogeosciences*. 12(21):6389–6403

Sterner RW, Elser JJ. 2002. *Ecological Stoichiometry: The Biology of Elements from Molecules to the Biosphere*. Princeton, NJ: Princeton University Press

Stramma L, Schmidtko S, Levin LA, Johnson GC. 2010. Ocean oxygen minima expansions and their biological impacts. *Deep. Res. Part I Oceanogr. Res. Pap.* 57(4):587–95

Talarmin A, Lomas MW, Bozec Y, Savoye N, Frigstad H, et al. 2016. Seasonal and long-term changes in elemental concentrations and ratios of marine particulate organic matter. *Global Biogeochem. Cycles*. 30:1699–1711

Tegner MJ, Dayton PK. 1987. El Nino Effects on Southern California Kelp Forest Communities. *Adv. Ecol. Res.* 17:243–79

Teng Y-C, Primeau FW, Moore JK, Lomas MW, Martiny AC. 2014. Global-scale variations of the ratios of carbon to phosphorus in exported marine organic matter. *Nat. Geosci.* 7(12):895–98

CHAPTER 1

Ecological stoichiometry of ocean plankton

Abstract

Marine plankton elemental stoichiometric ratios can deviate from the Red- field ratio (106C:16N:1P); here, we examine physiological and biogeochemical mechanisms that lead to the observed variation across lineages, regions, and seasons. Many models of ecological stoichiometry blend together acclimative and adaptive responses to environmental conditions. These two pathways can have unique molecular mechanisms and stoichiometric out- comes, and we attempt to disentangle the two processes. We find that interactions between environmental conditions and cellular growth are key to understanding stoichiometric regulation, but the growth rates of most marine plankton populations are poorly constrained. We propose that specific physiological mechanisms have a strong impact on plankton and community stoichiometry in nutrient-rich environments, whereas biogeochemical interactions are important for the stoichiometry of the oligotrophic gyres. Finally, we outline key areas with missing information that is needed to advance understanding of the present and future ecological stoichiometry of ocean plankton.

Keywords: Redfield ratio, C:N:P, growth rate hypothesis, translation-compensation hypothesis, direct control, state factor

Introduction

In the early part of the twentieth century, Alfred Redfield suggested that the elemental compositions of surface plankton are uniformly similar to the ratios of dissolved nutrients in the deep ocean and defined the Redfield molar ratio of 106C:16N:1P (Redfield

1958). He proposed three hypotheses to explain this similarity: (a) It is merely a coincidence, (b) phytoplankton have the ability to change their stoichiometry to match the environmental supply, and (c) phytoplankton control the ocean chemistry though the remineralization of exported material. Based on the available data, the first hypothesis seemed unlikely. Instead, Redfield proposed that microorganisms set the concentrations of nutrients in the deep ocean through their ability to fix C and N and thus supported the third hypothesis (Augueres & Loreau 2015; Lenton & Klausmeier 2007). Recent studies have demonstrated systematic variation in the particulate C:N:P across ocean regions and seasons, challenging the paradigm of a constant plankton elemental (Redfield) ratio (Figure 1.1). The variation in community C:N:P across ocean regions has been observed using two separate approaches: directly measuring the elemental stoichiometry of particulate organic matter (Martiny et al. 2013a,b) and using inverse models to indirectly infer this ration from inorganic nutrient fields (DeVries & Deutsch 2014; Teng et al. 2014; Weber & Deutsch 2010). The C:N, C:P, and N:P ratios of particulate organic matter are below or near Redfield proportions in the oligotrophic gyres (Figure 1.1). This pattern is also observed across seasons, with the three ratios higher in the summer and fall (warm and nutrient depleted) and lower in the winter and spring (colder and nutrient replete) at many sites (Martiny et al. 2016b; Singh et al. 2015; Talarmin et al. 2016). In addition, there appear to be some regional differences in ratios across the oligotrophic gyres: C:P is highest in the North Atlantic gyre, next highest in the North Pacific gyre, and only slightly above Redfield proportions in the Southern Hemisphere oligotrophic gyres (Figure 1.1). The C:N ratio also shows differences among oligotrophic gyres, with the highest ratio in the South Atlatntic

and eastern North Atlantic and the lowest in the North Pacific and western North Atlantic. This raises the question, which mechanism(s) can explain the observed field patterns?

Our review build on past excellent summaries of this topic (e.g., Flynn et al. 2010; Geider & Roche 2002; Sterner & Elser 2002). First, we aim to include recent research and modeling work. Second, we aim to put forward plausible mechanism describing the observed variation in elemental stoichiometry among marine plankton lineages, regions, and seasons. To achieve this, we borrow a framework from ecology covering direct control and state factor mechanisms (Chapin et al. 2012). A direct control mechanism provides an immediate connection between an environmental condition and the cellular or community C:N:P through regulation, acclimation, and selection/adaptation. External state factors control the ecosystem structure and function and associated community stoichiometry through external biogeochemical feedbacks. In this review, we introduce some general concepts about acclimation versus adaptation and provide an overview of how the detailed molecular biochemical of a cell can be linked to the stoichiometry. We then examine the stoichiometric outcomes based on physiological changes in growth rate, temperature, nutrient limitation, light, C source, interactions between said factors, and finally lineages identity via adaptation. Then we discuss how state factors via ocean nutrient cycles and biogeochemical feedbacks may lead to difference in the overall nutrient supply and associated elemental stoichiometry of ocean regions. Finally, we outline key areas with missing information that is needed to advance understanding of the present and future ecological stoichiometry of ocean plankton, communities, and particulate matter. We use examples of marine plankton but incorporate observations from other systems to support and illustrate the broader applications of our synthesis.

Acclimation versus Adaptation

Many hypotheses of ecological stoichiometry interchange processes of acclimation and adaptation when describing the elemental stoichiometric outcome of environmental variation; however, these processes are not synonymous. Acclimation is the physiological process that modifies the cellular biochemistry and elemental requirements in response to an environmental change and occurs within an organism's lifetime. Adaptation is the evolutionary process and occurs intergenerationally, leading to lineage-specific changes in physiological capabilities and elemental composition. Here, changes in the stoichiometry of a community occur through selection. Many ecological stoichiometry models blend the two responses and predict the same effect of an environmental change within (acclimation) and across (adaptation) organisms (Figure 1.2a). An example is temperature, which regulates the enzyme kinetics and physiology of an organism. In addition, there are clear differences in plankton diversity across a gradient of temperature. As a result, temperature affects the elemental composition of marine communities owing to a combination of changes in physiology and diversity (Hall et al. 2008). These contrasting responses may not lead to the same outcome if the underlying biochemical mechanism differs (Figure 1.2b,c). For instance, a heat shock response is not the same as shifting the optimal temperature for growth. Understanding when acclimative and adaptive responses differ is crucial for properly extrapolating from experimental studies of single lineages to whole communities.

Biochemical Components

To link biochemical regulation with the elemental composition of cells, we must consider the molecular components underlying the cellular C, N, and P pools and their stoichiometry (Geider & La Roche 2002; Sterner & Elser 2002). Molecules rich in C include

carbohydrates and lipids. Peptidoglycan and chitin are two carbohydrates that do contain N, but the specific carbohydrate chemistry in marine plankton is unconstrained. Lipids are also rich in C, but membrane-bound lipids often contain polar head groups with phosphate and/or N (Van Mooy & Fredricks 2010). Molecules rich in N include proteins and photosynthetic components. Protein is the most abundant cellular macromolecule and constitutes on average 32% of the cellular dry weight in phytoplankton (Finkel et al. 2016) and up to 63% in heterotrophic bacteria (Simon & Azam 1989). Thus, protein N is expected to correlate closely with the overall N cell quota (although there is some disagreement about the exact relationship)(Finkel et al. 2016; Lourenço et al. 2004). For phytoplankton, photosynthetic components such as chlorophyll and other pigments can also be important N pools. Molecules rich in P include membrane lipids, polyphosphates, and nucleic acids. Phospholipids are relatively P rich (39C:0.8N:1P) but are often a lesser part (<10%) of the P quota in marine organisms (Mouginot et al. 2015; Van Mooy & Devol 2008). Inorganic polyphosphates are an enigmatic component of the P pool, serving as a store of both P and energy (Kornberg et al. 1999). The absolute amount of inorganic P in a marine organism is poorly constrained but could be an important control on the P quota (Daines et al. 2014). Nucleic acids are relatively low in C but contain high N and especially P and have a C:N:P ratio of 9.5:3.7:1(Sterner & Elser 2002). The ribosome is a key component of cellular biosynthesis and contains a substantial fraction of cellular proteins and RNA (Geider & La Roche 2002; Sterner & Elser 2002). As such, biosynthesis is viewed as a key P-rich and to some extent N-rich process in relation to C. Thus, many ecological stoichiometry hypotheses describing C:P and N:P are based on the regulation of biosynthetic capacity and associated requirement for P.

Physiological Models for Elemental Stoichiometry

The Growth Rate Hypothesis

The growth rate hypothesis (GRH) states that differences in organismal C:N:P ratios are generated by allocation changes in biosynthetic machinery and associated P-rich ribosomes (Elser et al. 2000). The hypothesis is based on three presumptions: (a) cells achieve a higher growth rate by increasing the abundance of ribosomes containing P-rich rRNA, (b) P allocated to rRNA constitutes the majority of the P cell quota, and (c) the P cell quota controls the C:P and N:P of an organism. Thus, the N and C cell quotas should display less or no variation at different growth rates. There are two variants of this hypothesis—namely, that the physiological regulation of the ribosomes of an individual organism is due to either (a) acclimation or (b) adaptive differences in allocation strategies that result in different C:N:P ratios among lineages (Elser et al. 2000). Thus, it is key to distinguish the two. Here, we first discuss the acclimation variant, which seeks to test the relationship between cellular components (RNA and ribosomes) and growth rate but not the absolute abundance of said components, as it relates to the three presumptions of the GRH. As will become apparent, it is important to keep track of the factor controlling growth (nutrients, temperature, light, etc.).

There is often experimental support for the first presumption, because increased growth rate generally correlates with an increase in the RNA content within many lineages (as shown in Table 1.1) (Elser et al. 2003). A clear relationship between ribosome counts and growth rate is well established in the model organism *Escherichia coli* (Gausing 1982; Schaechter et al. 1958b). A similar positive relationship has also been detected in many marine lineages. The marine cyanobacteria *Synechococcus* sp. WH8101 and WH8102 have a

positive relationship between RNA and growth rate under P-limited conditions (Garcia et al. 2016; Van Mooy & Devol 2008). A meta-analysis of diverse plankton found that the freshwater zooplankton species *Daphnia pulicaria* and *Daphnia galeata*, *Drosophila melanogaster*, *E. coli*, and lake bacteria demonstrate a clear linear relationship between RNA content and growth rate (Elser et al. 2003). Note that all species, with the exception of the freshwater zooplankton species, were grown under P-limited conditions; when grown in environments with sufficient P, *D. pulicaria*, *Daphnia pulex*, *E. coli*, and lake bacteria did not statistically show any relationship between RNA content and growth rate (Elser et al. 2003). Under N-limited conditions, Synechococcus sp. WH8102 does show a linear relationship between RNA and growth rate (Garcia et al. 2016).

In temperature-limited organisms, the link between growth rate and rRNA content is less clear. If temperature controls the growth rate in *E. coli*, there is little increase in RNA (Broeze et al. 1978; Schaechter et al. 1958b). When grown in chemostats with temperature as the controlling factor (14°C, 20°C, and 24°C), the freshwater bacterium *Pseudomonas fluorescens* displays a similar linear relationship between RNA content and growth rate, but only under medium- and high temperature conditions (Chrzanowski & Grover 2008). At 14°C, *P. fluorescens* showed a statistically significant negative linear relationship with RNA content and growth rate. At 20°C and 24°C, the relationship appears to be quadratic: RNA is high at low growth rates (i.e., 0.03 h^{-1}), has a minimum at a growth rate of 0.10 h^{-1}, and then increases at high growth rates (i.e., 0.13 h^{-1}). In the phytoplankton *Scenedesmus*, there is even a negative relationship between cellular RNA-P and growth controlled by temperature (Rhee & Gotham 1981). These results provide mixed support for higher RNA with growth under changing temperature conditions, but the data set is limited.

There is good support for a positive link between rRNA content and growth in marine phytoplankton when light controls growth (Flynn et al. 2010). Multiple strains of *Synechococcus* and *Prochlorococcus* show a three-phase relationship with growth rate: At low growth rates, rRNA content remains relatively constant; at intermediate growth rates, rRNA increases; and at extremely high growth rates, rRNA plateaus (Binder & Liu 1998; Kramer & Morris 1990; Worden & Binder 2003). However, another study of *Prochlorococcus* found a linear positive relationship (Lin et al. 2013). Thus, there appears to be some differentiation among closely related ecotypes. However, the experiments demonstrate a positive relationship between growth rate and rRNA content for most light-controlled conditions.

There are fewer experimental data supporting the second presumption in the GRH, which states that rRNA-P is the dominant fraction of the P cell quota. In a study of *E. coli*, RNA-P was commonly the majority of the overall P quota (Cotner et al. 2006). However, marine (phyto)plankton data addressing this question are scarce. Rhee (1973) quantified P allocation into RNA-P, DNA-P, lipids, and poly-P of the freshwater algae *Scenedesmus* across growth rates under P-limiting conditions (Figure 1.3). Rhee's work showed an increase in RNA-P as well as total P cell quota with growth rate and thus appears to support the GRH. However, other P pools increased with growth as well, and rRNA-P constituted only 20–30% of the P cell quota. A similar pattern was observed in marine *Synechococcus* sp.WH8102 (Garcia et al. 2016) and heterotrophic bacteria (Chrzanowski & Grover 2008). Again, RNA-P and total P increased with growth, but only 30% of the total P could be attributed to nucleic acids. Thus, rRNA-P may be only a partial contributor to the overall P cell quota, requiring a better empirical understanding of how other P pools (i.e.,

polyphosphates, phospholipids, and DNA) are regulated to fully predict how growth affects the P cell quota.

The third presumption in the GRH is that the P cell quota is the main control on C:P and N:P. Multiple experiments have shown that the C and N cell quotas are also sensitive to the growth rate, as many heterotrophic microbial lineages increase cell size with growth (Schaechter et al. 1958b; Vadia & Levin 2015). Additional support comes from the finding that the C and N cell quotas of phytoplankton increase up to 100% with growth (Garcia et al. 2016; Goldman et al. 1979; Laws & Bannister 1980). However, the exact change is dependent on the factor limiting growth (P source, N source, or light). Thus, it is important to consider changes in other quotas when predicting the outcome of growth on the elemental stoichiometry of marine plankton, and we have an incomplete understanding of how non-RNA biochemical pools respond to changing growth rates.

Overall, there is support for the underlying biochemical mechanism in the GRH of increasing rRNA with growth under some conditions across marine plankton lineages. There is also support that changes in the P quota exert control on C:P and N:P. However, it appears—based on only a few studies—that RNA-P is typically a minor component of the overall P quota. If RNA-P is only a minor component of (and does not control) the P quota, the association between C:P or N:P and growth rate under P limitation could simply be due to a nutrient limitation effect on all P pools, including storage. This conclusion would severely limit the applicability of the GRH for marine systems, and we will further examine interactions between multiple factors and the GRH below (see the section titled Interactions).

Temperature

Temperature plays a key role in regulating cellular biochemical processes and elemental composition across all taxa. The relationship between temperature and phytoplankton N:P and C:P stoichiometry has been predicted to be positive based on decreasing cellular allocation to ribosomes at elevated temperatures. We term this idea the translation-compensation hypothesis, which states that as growth rate is held constant, organisms growing at higher temperature will have higher C:P and N:P ratios. The biochemical reasoning behind this hypothesis is that the ribosome-specific protein synthesis rate is temperature sensitive (Hochachka & Somero G.N 1984; Toseland et al. 2013; Yvon-Durocher et al. 2015). As such, cells require higher ribosome content at colder temperatures than they do at warmer temperatures to achieve the same growth rate. Similarly to the GRH, this hypothesis relies on the assumption that the ribosome content is an important control on the overall cellular P pool.

There is considerable experimental support for the part that ribosome efficiency changes in response to temperature across a range of organisms (Broeze et al. 1978; Farewell & Neidhardt 1998; Toseland et al. 2013). The next question is, what happens to the ribosome concentration when temperature changes? To answer this question, it is essential to keep track of growth rate. In a batch culture experiment, a temperature increase led to increasing growth rate in *E. coli* but no clear changes in the RNA (or presumably the ribosome content)(Yun et al. 1996). In a chemostat experiment where growth was kept constant, the RNA content was negatively correlated with temperature in *E. coli* and *Aerobacter* (Tempest & Hunter 1965; Yun et al. 1996). However, another study of *E. coli* observed a more complex link between temperature and RNA under a constant growth rate (Cotner & Wetzel 1992). Toseland et al. (2013) observed that the protein

synthesis rates and ribosome counts of two phytoplankton species were sensitive to temperature and that phytoplankton growing in high-latitude environments increased their transcription of translationally linked genes, suggesting that their production of ribosomes was greatest at low temperatures. Thus, there is mixed support for a downregulation of RNA with temperature under constant growth.

A limitation of the translation-compensation hypothesis is that temperature also affects many other cellular processes (e.g., represented by the Q_{10} factor) (Geider 1987). Thus, the outcome is driven by a rebalancing of allocations to all processes. For example, temperature influences the expression and function of photosynthetic proteins, including Rubisco (Mackey et al. 2013; Maxwell et al. 1994), whose activity can limit C fixation (Davison 1991). The Q_{10} of photochemistry, including all photochemical processes, ranges from 1.0 to 2.08 (Raven & Geider 1988) but can be higher. For example, the Q_{10} for the carboxylase activity of Rubisco from both *Phaeodactylum tricornutum*, a temperate diatom, and *Nitzschia kerguelensis*, a cold-water diatom, is 2.66 (Raven & Geider 1988). These changes in photosynthetic C fixation machinery could mitigate the decline in RNA-P predicted by the translation-compensation hypothesis. Other examples include the temperature impact on lipid and carbohydrate content, which influences the cellular C quota (Henderson & Mackinlay 1989; Thompson et al. 1992; Zhu et al. 1997).

Several studies have examined how temperature influences the cellular nutrient quotas under constant growth. In *E. coli*, increasing temperature led to increased C and N and decreased P quotas (Cotner et al. 1997). Under nutrient-limited growth and a fixed growth rate, the P quota declined in *Scenedesmus* sp. and *Asterionella formosa*, as predicted by the translation-compensation theory (Rhee & Gotham 1981). The C and N quotas also

declined, but the slopes were dependent on nutrient availability (replete or limited by N or P), leading to a complex stoichiometric outcome.

The majority of experiments that examine the influence of temperature on cellular nutrient quotas do not control for growth rate, making it challenging to determine the independent effects of temperature and growth rate on elemental composition. Thus, temperature can simultaneously change the growth rate and the elemental composition, but separating the two can be difficult. The P quota in *Prochlorococcus* under nutrient-replete conditions and varying growth increased slightly with temperature (Martiny et al. 2016a); however, the C and N quotas also changed positively. Quotas were also positively affected in *Synechococcus* sp. CCMP1334 and *Prochlorococcus* sp. CCMP1986 (Fu et al. 2007) as well as in some larger phytoplankton. *Thalassiosira pseudonana*, *Pavlova tricornutum*, and *Pavlova lutheri* demonstrated a U-shaped pattern in the C and N quotas with increasing temperature (Thompson et al. 1992). *Chaetoceros calcitrans* showed a slight variation in the cellular C and N quotas, whereas *Isochrysis galbana* under an exponential growth rate demonstrated highly variable C and N quotas with increased temperature (Thompson et al. 1992). Berges et al. (2002) grew *T. pseudonana* in batch culture at three different temperatures and found that, as the temperature increased, there was an increase in the C quota but relatively no change in the N quota. In summary, it is clear that temperature affects all three cell quotas, but only a few studies provide direct support for the translation-compensation hypothesis.

Temperature can lead to direct effects on stoichiometry. In *E. coli*, the elemental ratios behave as predicted by the translation-compensation hypothesis. By contrast, *P. fluorescens* showed little systematic change in C:N:P with temperature. In the only

temperature-dependence study in phytoplankton under constant growth, N:P and C:P declined, were constant, or even increased with temperature, depending on the condition (Yvon-Durocher et al. 2015). The effect of temperature on elemental stoichiometry has also been quantified without controlling for growth rate. Fu et al. (2007) and Martiny et al. (Martiny et al. 2016a) observed high variability in C:P and N:P in closely related strains of *Prochlorococcus*, but this variability did not obey a uniform trend. In a single study of *Synechococcus* sp. CCMP1334, there was a decrease in C:N and C:P, whereas temperature changes led to a decrease of ~20% in C:N and an increase of ~25% in C:P in *Chaetoceros wighamii* (Spilling et al. 2015).

Temperature has a complex effect on cellular allocations and elemental stoichiometry. Laboratory experiments suggest that ribosomal biosynthesis has a high Q_{10}, providing support for the translation-compensation hypothesis. However, we currently have a limited molecular biological understanding of how temperature leads to a system-wide reallocation of metabolic networks in most marine phytoplankton. Thus, the translation-compensation hypothesis singles out an individual process with a clear temperature dependence but also relies on the weakly supported assumption that other processes are less dependent on temperature. For example, plankton C and N quotas often change with temperature, although systematic mechanisms explaining these observations are lacking. Additionally, our knowledge of the influence of temperature on elemental stoichiometry has been negatively affected by a paucity of experimental studies that control for the influence of temperature on growth rates. Thus, our current understanding of the influence of temperature on elemental stoichiometry is inadequate, and we cannot at this point identify a uniform effect.

Nutrient Limitation

A clear effect of nutrient limitation (i.e., the nutrient supply ratio) on cellular elemental stoichiometry has been documented extensively but shown to be dependent on the specific element limiting growth. Nutrient limitation has historically been described by a simple empirical hyperbolic relationship between cell quotas and growth rate (Droop 1968). The Droop model assumes that cell resources are partitioned into two basic cellular components: a structural pool and a storage pool. The structural pool is linked to the lineage, whereas the storage pool is controlled by specific nutrient uptake rates that determine the growth physiology. In model studies that have tracked multiple nutrients and their stoichiometry, the cellular stoichiometry is predicted to match the environmental supply at low growth rates (the "you are what you eat" phase), and as the rate of nutrient input and associated growth increase, the cellular stoichiometry converges on an optimal ratio (the "you eat what you need" phase) (Klausmeier et al. 2004; Persson et al. 2010). At maximum growth rate, the elemental stoichiometry reaches an organism-specific single value (Bi et al. 2012; Klausmeier et al. 2004; Rhee & Gotham 1980; Sterner & Elser 2002). Thus, both the ratio and rate of the nutrient supply influence the elemental stoichiometry. As discussed above, in a balanced system, the latter is directly tied to the cellular growth rate and the associated growth rate effects on stoichiometry. In this section, we discuss only the impact of the nutrient supply ratio and restrict our attention to studies that specifically control for the effect of nutrient supply on growth rate. This should make it possible to disentangle the influence of the nutrient supply ratio from that of the growth rate.

A non-Droop line of reasoning for how nutrients influence cellular allocations derives from molecular biology. Under P stress, most lineages induce a series of proteins in the phosphate regulon to increase inorganic P uptake or access P bound to organic molecules (Torriani-Gorini 1987; Wanner 1993). The proteins directly involved in transporting phosphate include an outer membrane porin (*pho*E), a phosphate-binding protein (*pst*S), and an ABC transporter (*pst*ABC). To access organically bound P, cells can to varying degrees induce enzymes that cleave phosphoesters (e.g., *pho*A or *pho*X), phosphordiesters (e.g., *pho*D), phosphonates (phn), and so on. Some of these proteins—especially *pho*A, *pho*E, and *pst*S—are highly induced under P stress in both heterotrophic bacteria and phytoplankton lineages (Martiny et al. 2006; Torriani-Gorini 1987). Assuming a constant growth rate, such induction of P acquisition proteins can greatly increase the total protein content of the cell, as seen in *Scenedesmus* (Rhee 1978).

Cells may also respond to stress by reducing P pools, which can be accomplished via several molecular mechanisms, including substituting P located in lipids (Mouginot et al. 2015; Van Mooy et al. 2006, 2009) or drawing down inorganic P storage. The mechanism for substituting lipids has been well documented, but phospholipids may contribute only up to 10% of total P (Mouginot et al. 2015; Van Mooy & Devol 2008; Van Mooy et al. 2006, 2009). There is more uncertainty associated with the regulation of cellular inorganic P (e.g., polyphosphate) accumulation (Kornberg et al. 1999). This pool may not dominate the overall particulate P in marine environments (Diaz et al. 2016), although some studies show inorganic P as a large fraction of the cellular P quota (Rhee 1973). Most stoichiometric models assume that polyphosphates serve primarily as nutrient storage, but polyphosphate has a dual role in microbial metabolism because it can serve as both energy

and P storage. The energy storage role is closely tied to growth physiology, but the absolute level of polyphosphate can vary extensively among organisms, as many other compounds can store energy (Mino et al. 1998). In cells where polyphosphates serve primarily as energy storage, we would expect a stronger regulation by growth physiology. However, the regulation of polyphosphates is largely uncharacterized in abundant marine phytoplankton lineages, and the concentration shows an unexplained negative correlation with P availability in marine environments (Diaz et al. 2016; Martin et al. 2014). Thus, there may be unknown interactions between growth rate and nutrient limitation that influence cellular P pools.

The molecular N mirrors to some extent the P stress response. Under N stress, cells can induce a series of proteins facilitating increased N uptake (Herrero et al. 1985; Tolonen et al. 2006). This includes upregulation of ammonia transport and utilization of alternative N sources, such as nitrite, nitrate, urea, and organically bound N (e.g., amino acids or nucleotides). However, it appears that, in contrast to P, N acquisition proteins are induced to a lower level and lead to a smaller change in protein content (Rhee 1978). The degree of N storage in many marine phytoplankton is poorly understood. Lineages may store N in pigment molecules (e.g., cyanophycin and phycocyanin) or amino acids, and N stress influences the cellular pigment content (Caperon & Meyer 1972; Collier & Grossman 1992; Geider et al. 1998; Harrison et al. 1976; Rhee 1978). In addition, some diatoms can store inorganic forms in the vacuole (Conover 1975). However, we lack data for N storage and allocation patterns across many marine lineages, including most of the dominant phytoplankton lineages in the ocean.

There is evidence that nutrient limitation affects the cellular biochemical makeup beyond simple partitioning between structural and storage components. The capacity of excess uptake of nutrients and the degree to which specific proteins are regulated vary both among and within phytoplankton lineages (Martiny et al. 2006; Tolonen et al. 2006) and depend on the limiting nutrient (Agren 2004; Bi et al. 2012). To capture some of the dynamics, models describing the elemental stoichiometry are just starting to consider such complex responses (Bonachela et al. 2013), but there are many unknowns. Studies have shown that the P cell quota is highly sensitive to P limitation. At a fixed growth rate, more than a quadrupling in the P cell quota can occur when shifting from P to N limitation in both large and small phytoplankton types (Elrifi & Turpin 1985; Geider & Osborne 1989; Leonardos & Geider 2004a; Mouginot et al. 2014; Rhee 1978) (Figure 1.4). The N quota can also be sensitive to N limitation, but the degree varies among lineages. In *Scenedesmus*, the N quota varies fivefold between N and P limitation under a constant growth rate (Rhee 1978). By contrast, *Synechococcus* exhibits only a small variation in N quota (Garcia et al. 2016; Mouginot et al. 2015). A shift in N source under constant growth rates appears to have little impact on cellular N quotas, and the P quota seems to be largely invariant under N limitation and constant growth (Goldman et al. 1979).

The fact that cellular quotas are affected by the availability of inorganic nutrients leads to questions of whether the sizes of the N or P quotas are equally sensitive to nutrient limitation and whether a differential response could drive overall stoichiometric changes. In a large meta-analysis, Moore et al. (2013) proposed that P quotas are most sensitive to nutrient limitation. This may be because P storage is less costly owing to its simple format (inorganic chain) and takes up less cellular space than N storage. If this idea is correct, we

should expect more variation in C:P and N:P than in C:N. In support, the P quota is more variable in size in small phytoplankton, such as marine *Synechococcus* and the small diatom *Chaetoceros muelleri* (Garcia et al. 2016; Leonardos & Geider 2004a) (Figure 1.4). However, it is less clear whether this also applies to large phytoplankton (which may possibly have a larger storage capacity for both N and P). Here, several studies have observed wide variation in both N and P quotas depending on the type of nutrient limitation (Cotner et al. 2006; Goldman et al. 1979; Lynn et al. 2000; Rhee 1978). Because only a few studies have carefully controlled growth rates while studying nutrient limitation, it is unclear whether such a distinction between large and small phytoplankton types is robust, but the possibility is intriguing (Caperon & Meyer 1972; Laws & Bannister 1980).

Few studies have directly examined the impact of nutrient limitation on the C cell quota and cell size, but this additional effect on C can affect the overall C:nutrient ratios (Flynn 2008). For some lineages (*Scenedesmus* and *Stephanodiscus minutulus*), cells and C quotas are larger under P limitation than they are under N limitation (Lynn et al. 2000; Rhee 1978). By contrast, *Synechococcus* and *C. muelleri* show less variation in cell size and C quota across limitation types (Garcia et al. 2016; Geider et al. 1996; Leonardos & Geider 2004a; Mouginot et al. 2015) (Figure 1.4a). Finally, Harrison et al. (1976) saw that a switch from Si to N limitation leads to a large decline in the C and N quotas.

The impact of nutrient limitation on C:N:P under constant growth largely follows the expected outcomes from the analysis of individual quotas. P limitation uniformly leads to increased C:P and N:P across lineages (Figure 1.4d–f). This is driven partly by a decline in the P quota, but the outcome is amplified by increases in the protein content and overall cell size in many phytoplankton (Figure 1.4). The outcome of N limitation is more varying.

For lineages with a sensitive N quota (e.g., *Scenedesmus*), the elemental ratios behave according to the model of Klausmeier et al. (Klausmeier et al. 2004), with a larger C:N and lower N:P under N limitation. However, *Synechococcus*, *C. muelleri*, and *Dunaliella* do not show this behavior, and the C:N:P can be largely constant in the N-limited range of nutrient supply ratios (Garcia et al. 2016; Goldman & Peavey 1979; Mouginot et al. 2015)(Figure 1.4). Thus, it appears that the elemental stoichiometry of phytoplankton is uniformly sensitive to P limitation, but the response is lineage dependent for N limitation.

So far, we have discussed only limitation by the two major nutrients, P and N. However, other nutrients, such as Fe and Si, also influence the growth rate and possibly the C:N:P stoichiometry of phytoplankton. In a study of the diatom *Thalassiosira weissflogii*, growth rate increased as expected with increasing Fe availability (Price 2005). This increase in Fe and growth rate led to increasing C:P and N:P but flat C:N. By contrast, studies of *Synechococcus*, *Prochlorococcus*, and *Pseudo-nitzschia* showed the opposite relationship with Fe availability and stoichiometry (Cunningham & John 2017; Marchetti & Harrison 2007). Si limitation may not affect the elemental quotas and stoichiometry beyond changing the growth rate. In *S. minutulus*, the C and N quotas were similar to those in fast-growing cells and cells growing under P limitation (Lynn et al. 2000). Furthermore, the C:N was similar to P limitation patterns and unlimited growth, and the C:P was similar to N limitation patterns and unlimited growth. Thus, Si and Fe may influence the elemental stoichiometry either directly or via a control on growth rate, but there are no data that allow differentiation of these two effects.

Light

Light availability can lead to phytoplankton photoacclimation and associated changes in cellular allocation strategies (Falkowski & LaRoche 1991; Leonardos & Geider 2004b). The main biological components involved are the biosynthetic apparatus (P rich), light-harvesting apparatus (N rich), and energy storage reserves (C rich). At a fixed growth rate, cells can be nutrient limited at high light and light limited at low light. Under high light and nutrient limitation, the cellular light-harvesting apparatus is downregulated in order to minimize the risk of photooxidative stress (Geider et al. 1996). Furthermore, energy reserves are high (C-rich lipids and polysaccharides) (Kromkamp 1987). Under low light, the photosynthetic apparatus increases in size for light harvesting, and C storage compounds decrease. Thus, we expect a strong positive impact of light on C:N and a lesser positive effect on C:P. However, if P is the main limiting nutrient at high light, the P quota will be additionally affected and modify the proposed effects.

There is support for the overall mechanism in phytoplankton of low storage C but high pigment under low light and high storage C but low pigment under high light in cultures (Behrenfeld et al. 2002; Leonardos & Geider 2004a) and field populations (Bouman et al. 2006). Because light-harvesting proteins can constitute 18–50% of cellular proteins and lipids and carbohydrates constitute 32–43% of cellular biomass, changes in these two pools should affect the C and N quotas. In support of this idea, Leonardos & Geider (2004a) found that the N quota was ~50% lower under high light than it was under low light in *C. muelleri* across a range of nutrient supply ratios. A similar pattern occurred in the cryptophyte *Rhinomonas reticulata*, but only under N limitation; under P limitation, the N quota was similar under both high and low light (Leonardos & Geider 2005; Thompson et al. 1991).

The effect of light on C:N:P can be viewed in two ways: One can either (a) identify the effect at a given growth rate and nutrient supply ratio or (b) examine the impact on the optimal C:N:P (i.e., C:N:P at μ_{max}, sometimes also called critical C:N:P). From the first perspective, C:N is positively related to light availability in several large phytoplankton lineages (Leonardos & Geider 2004a) and less varying in others (MacIntyre et al. 2002). C:P is high under high light for *Amphidinium carterae*, whereas N:P decreases with increased light for *T. weissflogii*, *Cyanothece* sp., and *A. carterae* (Finkel et al. 2006). From the second perspective, the optimal N:P is negatively correlated with light across a range of phytoplankton lineages (Thrane et al. 2016). Thus, the impact of light on stoichiometry has a clear mechanistic basis that is well supported by observations.

Light availability can also influence diel changes in cell quotas and elemental stoichiometry, as many cellular processes vary over a daily cycle in marine organisms (Olson et al. 1986; Waldbauer et al. 2012; Zinser et al. 2009) and communities (Ottesen 2014). Photosynthetic and C fixation proteins are expressed during the day, cell division proteins near sunset, and carbohydrate metabolism (glycogen catabolism and pentose phosphate pathway) proteins at night. This leads to diel variability in cellular components such as nucleic acids, pigments, and protein concentrations (Lopez et al. 2016; Matallana-Surget et al. 2014; Vaulot et al. 1995). Under a constant growth rate, the cellular C and N (and to a lesser extent P) quotas also exhibited diel cycling in *Synechococcus* (Lopez et al. 2016). Here, the C quota followed fixation rates and exhibited strong cycling, with a daily maximum before sunset and a low in the early morning. The N and P quotas showed lower amplitude and reached maxima earlier in the light period. There was also an interaction with growth physiology, whereby oscillations were stronger at a high growth rate. As a

result, C:N and C:P were highest at the end of the light period, whereas N:P showed limited oscillation. The diatom *Skeletonema* exhibited a similar cycling for the C and N quotas as well as C:N (Anning et al. 2000). Thus, we expect that diel variation in elemental stoichiometry will occur in marine communities.

Carbon Source

The ability to fix CO_2 (autotrophy) as opposed to assimilating organic C (heterotrophy) may also affect cellular allocation strategies. Heterotrophic organisms constitute a large fraction of overall marine biomass (Gasol et al. 1997) and thus an important contributor to the combined C:N:P of a community. It is hypothesized that heterotrophic organisms are mostly C limited and thus frugal with C (Godwin et al. 2016; Goldman & Peavey 1979; Tezuka 1990). Contributing to C limitation is the fact that at least half of the assimilated C is respired during growth (i.e., the yield or carbon use efficiency). In most marine regions, this should lead to a nutrient limitation of phytoplankton and a C limitation of heterotrophic organism. The outcome is low C:N and C:P in many heterotrophic organisms, such as bacteria, zooplankton, and possibly mixotrophs (Cotner et al. 2006; Fagerbakke et al. 1996; Zimmerman et al. 2014). In this way, C availability could behave as a nutrient and act like the N and P limitation presented above (Meunier et al. 2012; Sterner & Elser 2002).

The exact underlying biochemical mechanism for how C limitation influences molecular pathways and macromolecules is not clearly elucidated. The simplest argument is that heterotrophic organisms under C limitation down regulate C storage molecules (Anderson & Dawes 1990; Holme & Palmsterna 1956). There may also be an upregulation of resource acquisition enzymes targeting complex C sources (Allison & Vitousek 2005;

Arnosti et al. 2011), which would lead to a currently unconstrained increase in the N quota. Considerable experimental evidence indicates that heterotrophic bacteria exhibit a nutrient-like behavior for C acquisition. Studies have shown that specific bacteria lineages as well as whole communities display clear changes in cellular C:P along a gradient of C to P limitation (Godwin & Cotner 2015; Godwin et al. 2016; Makino et al. 2003). Marine bacteria at exponential growth under non-nutrient-limitation conditions also exhibit a broad range of C:P ratios, from 35:1 (Vrede et al. 2002) to 80:1 (Zimmerman et al. 2014) and C:N ratios from 3.8:1 to 4.5:1 (Fagerbakke et al. 1996). Despite the variation, these ratios are generally lower than those observed in phototrophs. Another group of heterotrophic plankton in the ocean is the zooplankton. These are larger organisms and perhaps more homeostatic in their biomass composition and less sensitive than phytoplankton and bacteria to C limitation (Malzahn et al. 2010; Meunier et al. 2012). Thus, the available data and models suggest that the ratio of chemoheterotrophic to photoautotrophic organisms could have a negative influence on C:P and C:N (Talmy et al. 2016).

Interactions

In addition to understanding the individual effects, we also need to consider the interactive effects of environmental factors. Two types of interactions require special attention: interactions with growth rate and interactions with nutrient limitation. As alluded to above, an organism's growth rate can have a strong modulating effect on the specific impact of an environmental factor (Hillebrand et al. 2013). This could be due to the presence of storage molecules and options for metabolic flexibility (Klausmeier et al. 2004), but many other molecular responses are possible. Thus, we need to consider these

interactive terms when predicting the impact of environmental changes on the elemental stoichiometry of plankton.

The GRH states that differences in organismal C:N:P ratios are generated by variations in allocation strategies that increase the abundance of ribosomes with growth (Elser et al. 2000) (Figure 1.5a). As described above, the effect of growth rate on stoichiometry likely depends on whether temperature, a specific nutrient, or light controls growth (Figure 1.5b). If temperature is the growth-limiting factor, we would predict a (nearly) neutral response, as cellular processes simply run faster. Under N limitation, we have seen that organisms with limited N storage, such as *Synechococcus* and heterotrophic bacteria, show a slight (or no) increase in N:P or C:P with growth rate (the opposite of the response predicted by the GRH) (Garcia et al. 2016; Goldman et al. 1979). However, a different pattern is seen in larger organisms capable of elevated N storage (Caperon & Meyer 1972; Laws & Bannister 1980). When light is controlling growth, we expect slightly negative relationships among light, growth, and N:P. Here, C:N and C:P might show the opposite trend owing to C storage. Finally, we expect to see a strong negative relationship for N:P and growth when P is the controlling factor (Hillebrand et al. 2013). Thus, depending on the factor controlling growth and possibly the ability to store N, we predict unique relationships between C:N:P and growth rate.

The specific impact of an environmental factor is also expected to be modulated by nutrient limitation and associated reduced allocation of this element. A chemostat experiment showed that *Scenedesmus* sp. and *A. formosa* N and P quotas increased with decreasing temperature (Rhee et al. 1981). Under nutrient limitation (both N- and P-limited conditions, separately), this relationship continued to hold true with increased

temperature in *Scenedesmus*. However, the N-limited samples showed a higher cellular N quota, whereas the P-limited samples showed no difference in cellular P quota under nutrient-sufficient samples. In *A. formosa*, the opposite trend occurs: Under N limitation, the cellular N quota did not differ with increased temperature, and under P limitation, the cellular P quota was higher than it was in samples grown under nutrient-sufficient conditions (Rhee et al. 1981).

Nutrient limitation also has a large impact on the relationship between light intensity and stoichiometry. Increased N:P ratios and decreased C:P ratios should correspond with decreased light. A laboratory experiment found that the N quota under N limitation was higher in low light than in high light and showed a similar relationship under P limitation (Leonardos & Geider 2004b). The P quota under N limitation was higher in low light than in high light, with a linear negative trend, but under P limitation, the P quota was not dependent on the light level (Leonardos & Geider 2004b). C:N increased during a transition from low-light, high-nutrient conditions to high-light, low-nutrient conditions in the same region (Geider et al. 1998). This is common in regions that experience spring blooms: Low-light, high-nutrient conditions occur before a bloom begins, and high-light, low-nutrient conditions occur after it has ended. However, the light-nutrient hypothesis is a good predictor with a strong positive relationship between the light:nutrient ratio and C:P ratio (Dickman et al. 2006). In sum, we find that both growth physiology and nutrient availability can have a large modulating effect on how a specific environmental factor influences C:N:P.

The Role of Adaptation and Phylogeny in Controlling C:N:P in Marine Plankton

In the above sections, we have described how acclimation mechanisms can lead to variation in C:N:P. However, there is also considerable variation in C:N:P across taxa (Finkel et al. 2016; Geider & La Roche 2002; Ho et al. 2003; Zimmerman et al. 2014). Two main categories of mechanisms lead to taxon-specific C:N:P. The first, called acclimation extensions, follows the previously discussed acclimation mechanisms but now as the outcome of adaptation. The second category, called biological uniqueness, is based on the idea that the biochemical diversity among plankton is immense and can influence the cellular composition in a variety of ways.

One can apply acclimation-extension ideas to all physiological hypotheses (i.e., growth rate, temperature optimum, nutrient uptake capabilities, etc.). The adaptive GRH variant proposes that fast-growing lineages have lower N:P than slow-growing ones (Elser et al. 2000). There is support for this hypothesis across large gradients in growth rate and organism size (Elser et al. 2000), but the hypothesis does not readily extend to marine phytoplankton (Edwards et al. 2012).

An adaptive extension of the translation-compensation hypothesis can also be evaluated for organisms with different optimal temperatures, but there are few data for such tests (Yvon-Durocher et al. 2015). The only study to our knowledge to test the adaptive version showed that the stoichiometric variation among high- and low-temperature-adapted ecotypes did not support an acclimation-extension version of the translation-compensation hypothesis (Martiny et al. 2016a). However, translation-related proteins appear to be expressed at higher relative proportions in cold-water plankton communities than in warm-water communities (Toseland et al. 2013). Thus, translation-related macromolecules may be more common in cold-water-adapted lineages, but the

impact on stoichiometric outcome is unclear. There is evidence for adjustments of pigment concentrations to light availability (Chisholm et al. 1975; Geider 1987; Moore et al. 1998; Rocap et al. 1999). For nutrient availability, there is clear evidence for molecular adaptation, but the effect on cell quotas and stoichiometry is completely unknown (Martiny et al. 2006). Thus, there is some support for a general adaptive mechanism for how light and nutrients affect cellular stoichiometry, but there are no data to support or refute such adaptive stoichiometric models for how temperature or interactions will have an effect.

All adaptive models have a strong covariance with phytoplankton cell size, as small cell types such as marine cyanobacteria dominate in warm, high-light, and low-nutrient environments (i.e., the oligotrophic gyres), whereas large cell types such as diatoms blooms in cold, low-light, and high-nutrient environments (and therefore are prevalent at high latitudes). This has led to a concept of slow-growing resource survivalists with high C:P and N:P and fast-growing bloomers with low C:P and N:P (Arrigo 2005; Klausmeier et al. 2004). Survivalists, such as *Prochlorococcus* and *Synechococcus*, dominate the stable, low-nutrient waters at low latitudes; have a low resource minimum; and have a high proportion of N-rich resource acquisition machinery, such as enzymes and photosystems. Elevated C:P and N:P in small cyanobacteria are supported by both laboratory and field studies. In the laboratory, *Prochlorococcus* and *Synechococcus* consistently have high C:P and N:P (Bertilsson et al. 2003; Garcia et al. 2016; Martiny et al. 2016a). Cell sorting also showed that *Prochlorococcus* and *Synechococcus* field populations have higher C:P and N:P than coexisting larger picoeukaryotic phytoplankton (Baer et al. 2017; Martiny et al. 2013a). Bloomers, such as diatoms, are normally larger and have a higher proportion of P-rich biosynthesis machinery. Diatoms in the Southern Ocean have lower N:P than coexisting

slower-growing *Phaeocystis* (Arrigo et al. 1999; Weber & Deutsch 2010). These studies support the idea that bloomers and survivalists have unique stoichiometries. However, recent in situ estimates of *Prochlorococcus* and *Synechococcus* show high growth rates in tropical waters that rival those of many larger phytoplankton types (Hunter-Cevera et al. 2016; Liu et al. 1998; Ribalet et al. 2015). Thus, a concept of slow growing, high-temperature, nutrient uptake specialists versus fast-growing bloomers does not fully capture the ecological roles of marine plankton communities and their predicted stoichiometric regulation.

The second category of taxon-specific C:N:P, biological uniqueness, is based on phylogenetically constrained elemental composition resulting from the myriad of biochemical behaviors found in marine plankton (Ho et al. 2003). Nearly all studies of both autotrophic and heterotrophic organisms have shown considerable differences of macromolecules, cell quotas, and ratios even among closely related marine taxa (Finkel et al. 2016; Geider & La Roche 2002; Zimmerman et al. 2014). The question is whether there are higher levels of phylogenetic organization that allow for an association of ratios with specific taxa, but limited data are available to fully evaluate this question.

Linking Mechanisms to Observed Patterns of Stoichiometric Variability

What mechanisms control the elemental stoichiometry in marine communities? The strong latitudinal covariance of light, temperature, nutrient availability, and biodiversity makes it difficult to answer the question at this point. Several papers have made competing claims for temperature, nutrient availability, and biodiversity as the dominating control on elemental stoichiometry (Galbraith & Martiny 2015; Martiny et al. 2013b; Yvon-Durocher et al. 2015). With the current data, it is impossible to statistically separate the effects of

these factors on the latitudinal gradients in C:N:P because all factors provide a fit to the regional patterns of stoichiometric variability (Martiny et al. 2013a; Toseland et al. 2013; Yvon-Durocher et al. 2015) (Figure 1.1). Thus, we need geographically (and environmentally) more diverse field observations to further tease apart these competing claims.

It is unlikely that irradiance has a large effect on the horizontal variation in C:N:P of marine phytoplankton because such a model cannot explain the lower ratios in equatorial upwelling zones. However, irradiance could influence vertical shifts in elemental ratios. In support of an impact of irradiance, C:N does increase with depth, although this pattern could also be driven by temperature and nutrient recycling (Martiny et al. 2013b; Schneider et al. 2003). However, we currently have a limited understanding of any vertical changes in C:P and N:P within the photic zone, and more work is needed to understand water column variability for C:N:P.

Based on current field observations, we propose a hypothesis that variation in community (all plankton, including autotrophic and heterotrophic species) C:N:P within different low-nutrient ocean gyres is driven mainly by the nutrient supply ratio, sourced from a combination of vertical and N fixation inputs. Plankton "are what they eat," which suggests that a biogeochemical state factor mechanism controlling the total input of N and P should describe the stoichiometry in this biome. However, owing to a lack of N storage in small plankton types, we should never observe lower than Redfield proportions in C:P and N:P and little variation in C:N. N fixation resupplies bioavailable N into these regions, tying into the fluctuations of N:P ratios. The patterns of N fixation rate and phosphate concentration suggest that N fixation rates are highest and P concentrations lowest in the

North Atlantic subtropical gyre, followed by the North Pacific subtropical gyre (Lomas et al. 2010; Wu et al. 2000). By contrast, N fixation rates are lower (and P higher) in the three Southern Hemisphere oligotrophic gyres (Mather et al. 2008; Moutin et al. 2007; Sohm et al. 2011). Based on our hypothesis and these apparent patterns of N fixation and P availability, we predict that C:P and N:P are highest in the North Atlantic, followed by the North Pacific subtropical gyres, and lowest in the Southern Hemisphere (but above Redfield proportions). In support of this prediction, the C:P and N:P ratios are greatest in the North Atlantic subtropical gyre, followed by the North Pacific gyre (Figure 1.1). By contrast, C:P and N:P are only slightly above Redfield proportions in the Southern Hemisphere gyres (Figure 1.1). The hypothesis would further suggest that the influence of Fe availability through N fixation on the N:P supply ratio (Mather et al. 2008) could serve as an important control on the elemental ratios in the oligotrophic gyres. Such variation in nutrient supply ratio and degree of P limitation would lead to a good fit between C:P and N:P and ambient phosphate concentration (Galbraith & Martiny 2015).

In nutrient-rich high-latitude environments, we hypothesize that plankton "eat what they need" and suggest that a direct control mechanism is most applicable in such biomes. In the absence of (or at least reduced) nutrient limitation, factors such as light, temperature, and unique lineage dependent ratios may all influence the particulate organic matter ratios. Field and inverse model studies have suggested that, in the Southern Ocean, diatoms may have lower C:P and N:P than *Phaeocystis* (Arrigo et al. 1999; Weber & Deutsch 2010). This is an intriguing observation but has not been fully explored in laboratory experiments. Such laboratory experiments would enable a disentanglement of the controls by individual environmental factors and controls by lineage specific behaviors. Limited

data are available on the elemental ratios in most high-latitude regions, but these observations suggest that the biogeography of specific plankton lineages could influence the elemental ratios.

Implications for Ocean Biogeochemistry

A variable C:N:P of plankton and particulate organic matter has broad biogeochemical implications, including for our understanding of nutrient limitation, the regulation of N fixation, C export, and ecosystem and food web model predictions that are tuned with Redfield stoichiometry. The N:P ratio of 16:1 is typically used to differentiate between N and P limitation; phytoplankton are said to be N limited when N:P < 16:1 and P limited when N:P > 16:1 (Falkowski 1997; Geider & Roche 2002; Tyrrell 1999).This concept becomes more fluid when different lineages have unique elemental compositions and N- and P-stressed cells coexist in the same water parcel (Alexander et al. 2015; Martiny et al. 2013b). There is also much debate between geochemists and biologists about the ultimate limiting nutrient for primary production: Geochemists argue that P is the ultimate limiting nutrient because of biological fixation of N, but biologists can demonstrate that many phytoplankton communities increase activity and biomass following N addition (Moore et al. 2013). Tyrrell (1999) tried to resolve this argument and presented a model suggesting that N is a proximate limiting nutrient and P is the ultimate limiting nutrient because of competition between regular phytoplankton and growth-penalized N fixers. However, his conclusion is dependent on the notion of a static elemental composition of phytoplankton communities. If the true elemental composition varies among lineages and environmental conditions, then the difference between proximate and ultimate limiting nutrients becomes more fluid.

Variation in the elemental composition of marine communities can also influence our understanding of how N gain and loss processes are regulated and geographically distributed. The biological source and sink of N reserves are N fixation and denitrification. N fixation is a costly process that requires a large amount of Fe, whereas denitrification is a process favored in low oxygen conditions. Deviations from the Redfield ratio in the relative concentrations of dissolved nitrate and phosphate have been used to map out regions of denitrification and N fixation. Based on this metric, Deutsch et al. (2001, 2007) suggested that gain and loss processes of N are spatially coupled in that upwelled waters that experience denitrification promote N fixation once the N-depleted waters are advected offshore. The spatial co-occurrence of N gain and loss processes was unexpected because in situ studies have suggested that water column denitrification occurs mostly within upwelling zones, whereas N fixation occurs mostly in the oligotrophic gyres (Sohm et al. 2011). Later studies have examined the impact of phytoplankton variable stoichiometry on the N cycling patterns and found that the interpreted spatial distribution is highly dependent on the assumed cellular elemental ratio (Deutsch & Weber 2012; Mills & Arrigo 2010). Allowing for high N:P and C:P in plankton growing in the gyres resulted in a much stronger correspondence between observed and predicted N fixation patterns (Weber & Deutsch 2012). The elemental stoichiometry of total marine communities also influences the proportions of electron donors and acceptors in oxygen minimum zones (Babbin et al. 2014) and associated N loss pathways (i.e., the dominance of denitrification versus anammox). Thus, knowing what sets the elemental composition of marine plankton and communities will likely affect our understanding of how marine N gain and loss processes are controlled.

The elemental compositions of marine plankton and communities may be important for how C export and the biological pump are regulated, both now and under future climate change conditions. The canonical view of C export is that rates are low in the gyres because of their low nutrient inputs and high in temperate and upwelling regions because of their elevated nutrient inputs. If one considers the surface ocean as a water parcel box and a constant C:P of particles, a mass balance dictates that C export must equal the nutrient influx times a C:P of 106:1 (Dugdale & Goering 1967; Tyrrell 1999). However, detailed studies using different metabolite mass balances and inverse models do not support higher C export fluxes in mid-latitude ecosystems than in low-latitude ecosystems, instead showing little variation in export rates between these biomes (Emerson 2014; Richardson & Jackson 2007; Teng et al. 2014). Higher C:P of exported material, however, can result in significant C export despite increased ocean stratification and reduced nutrient inputs. As was demonstrated recently using a simplified box-model simulation, variations in the C:P of phytoplankton and exported material can have a substantial impact on long-term changes in C export and atmospheric CO_2 level (Galbraith & Martiny 2015) (Figure 1.6). Such studies lend support to the conclusion that the elemental composition of exported material can have a tangible impact on future predicted C export and possible long-term ocean feedbacks to atmospheric CO_2 (Sterner 2015).

Conclusions and Outstanding Issues

It has become clear that the upper-ocean plankton and particulate organic matter elemental ratios are not constant but instead display spatial and temporal differences. The quantification of C:N:P, and especially of particulate organic P, is geographically biased, and many regions have been either sparsely sampled or not sampled at all (Martiny et al.

2013a). Thus, we need a much richer (geographically and environmentally) data set to better determine the field patterns of C:N:P and test specific models. Despite deficiencies in data coverage, there is good experimental evidence that nutrient limitation (especially P) exerts a strong influence on the elemental composition of marine plankton (Garcia et al. 2016; Goldman et al. 1979; Mouginot et al. 2015; Rhee 1978). We hypothesize that the nutrient supply ratio is the primary control in the oligotrophic gyres. If our hypothesis is correct, a clear understanding of the ultimate controls on the supply of N versus P is critical for understanding differences in C:N:P across the oligotrophic gyres. By contrast, lineage differences in the elemental composition and physiological responses to light or temperature may control the elemental composition in high-latitude environments.

It has become apparent that interactions between growth rate and specific environmental factors are important in setting the elemental composition. Thus, experiments that control growth rate (e.g., using chemostats) are critical for disentangling these interactions. Unfortunately, few such experiments have been performed, and the ones available have a disproportionate impact on current hypotheses. Furthermore, most work has been done on organisms that are not necessarily representative of a natural marine community and are rare or absent in the open ocean, and we need more experiments using abundant marine lineages. A parallel issue is that we currently have a limited understanding of the in situ growth rate for most marine phytoplankton lineages. For example, a temperature increase could lead to either increased growth rates (Eppley 1972; Sherman et al. 2016) or a reallocation of cellular machinery, as suggested by the translation-compensation hypothesis (Toseland et al. 2013), and the outcomes of these two

scenarios will lead to distinct patterns of C:N:P. These issues leave many gaps in knowledge.

The GRH has been an important guiding hypothesis for understanding ecological stoichiometry. However, it has become apparent that phosphate bound to RNA may not always be a dominant P pool, and we predict that changes in RNA will have a limited influence on C:P and N:P in many marine environments (Zimmerman et al. 2014). Nevertheless, the impact of a changing growth rate on C:N:P strongly depends on the factor controlling growth. Thus, changes in growth rates across ocean regions could be a strong moderator on how other factors influence the elemental stoichiometry and are still important to contend with.

Many stoichiometric hypotheses are based on singling out the control of a single biochemical function (e.g., ribosomes and translation). However, most environmental factors affect multiple biochemical pathways. Various "-omics" techniques may prove valuable in addressing this issue, as -omics approaches can evaluate system-wide impacts. Furthermore, we need to quantify how specific environmental conditions affect macromolecular pools (Finkel et al. 2016) and, in particular, how inorganic phosphate pools are regulated. Such data would further facilitate an integrated view of cellular reallocations in response to environmental changes and enable us to move from hypotheses centered on single biochemical pathways to system-wide effects. This is already occurring with exciting new trait-based models, but they suffer from many biochemical unknowns (Daines et al. 2014).

There is clear evidence that biological processes control the C:N:P of marine communities, leading to non-Redfield proportions in many regions and seasons, and such

processes will likely have a large impact on our understanding of many ocean biogeochemistry concepts. We propose that a linear relationship between phosphate concentration and C:P (and N:P) is a good first approximation for capturing the broad regional variation in these ratios (Galbraith & Martiny 2015). However, more sophisticated models are needed to cover the interactions among biogeochemical feedbacks, environmental conditions, growth physiology, and the biological uniqueness of marine plankton.

References

Agren GI. 2004. The C:N:P stoichiometry of autotrophs - Theory and observations. *Ecol. Lett.* 7(3):185–91

Alexander H, Jenkins BD, Rynearson TA, Dyhrman ST. 2015. Metatranscriptome analyses indicate resource partitioning between diatoms in the field. *Proc. Natl. Acad. Sci.* 112(17):E2182--E2190

Allison SD, Vitousek PM. 2005. Responses of extracellular enzymes to simple and complex nutrient inputs. *Soil Biol. Biochem.* 37(5):937–44

Anderson AJ, Dawes EA. 1990. Occurrence, metabolism, metabolic role, and industrial uses of bacterial polyhydroxyalkanoates. *Microbiol. Rev.* 54(4):450–72

Anning T, Macintyre HL, Pratt SM, Sammes PJ, Gibb S, Geider RJ. 2000. Photoacclimation in the marine diatom Skeletonema costatum. *Limnol. Ocean.* 45(8):1807–17

Arnosti C, Steen AD, Ziervogel K, Ghobrial S, Jeffrey WH. 2011. Latitudinal gradients in degradation of marine dissolved organic carbon. *PLoS One*. 6(12):8–13

Arrigo KR. 2005. Marine microorganisms and global nutrient cycles. *Nature*. 437(7057):349–55

Arrigo KR, Robinson DH, Worthen DL, Dunbar RB, DiTullio GR, et al. 1999. Phytoplankton community structure and the drawdown of nutrients and CO2 in the Southern Ocean. *Science.* 283(5400):365–67

Augueres AS, Loreau M. 2015. Regulation of Redfield ratios in the deep ocean. *Global Biogeochem. Cycles*. 29(3):254–66

Babbin AR, Keil RG, Devol AH, Ward BB. 2014. Oxygen Control Nitrogen Loss in the Ocean. *Science.* 344:406–8

Baer SE, Lomas MW, Terpis KX, Mouginot C, Martiny AC. 2017. Stoichiometry of Prochlorococcus, Synechococcus , and small eukaryotic populations in the western North Atlantic Ocean. *Environ. Microbiol.* 19:1–23

Behrenfeld MJ, Marañón E, Siegel DA, Hooker SB. 2002. Photoacclimation and nutrient-based model of light-saturated photosynthesis for quantifying oceanic primary production. *Mar. Ecol. Prog. Ser.* 228:103–17

Berges JA, Varela DE, Harrison PJ. 2002. Effects of temperature on growth rate, cell composition and nitrogen metabolism in the marine diatom *Thalassiosira pseudonana* (Bacillariophyceae). *Mar. Ecol. Ser.* 225:139–46

Bertilsson S, Berglund O, Karl DM, Chisholm SW. 2003. Elemental composition of marine *Prochlorococcus* and *Synechococcus*: Implications for the ecological stoichiometry of the sea. *Limnol. Oceanogr.* 48(5):1721–31

Bi R, Arndt C, Sommer U. 2012. Stoichiometric responses of phytoplankton species to the interactive effect of nutrient supply ratios and growth rates. *J. Phycol.* 48(3):539–49

Binder BJ, Liu YC. 1998. Growth rate regulation of rRNA content of a marine *Synechococcus* (Cyanobacterium) strain. *Appl. Environ. Microbiol.* 64(9):3346–51

Bonachela JA, Allison SD, Martiny AC, Levin SA. 2013. A model for variable phytoplankton stoichiometry based on cell protein regulation. *Biogeosciences*. 10(6):4341–56

Bouman HA, Ulloa O, Scanlan DJ, Zwirglmaier K, Li WK, et al. 2006. Oceanographic basis of the global surface distribution of *Prochlorococcus* ecotypes. *Science.* 312(5775):918–21

Broeze RJ, Solomon CJ, Pope DH. 1978. Effects of low temperature on in vivo and in vitro protein synthesis in *Escherichia coli* and *Pseudomonas fluorescens*. *J. Bacteriol.* 134(3):861–74

Caperon J, Meyer J. 1972. Nitrogen-limited growth of marine phytoplankton—I. Changes in population characteristics with steady-state growth rate. *Deep. Res.* 19:601–18

Chapin SF, Matson PA, Vitousek PM. 2012. *Principles of Terrestrial Ecosystem Ecology*

Chisholm SW, Stross RG, Nobbs PA. 1975. Light/dark-phased cell division in *Euglena gracilis* (Z) (*Euglenophyceae*) in PO_4-limited continuous culture. *J. Phycol.* 11(4):367–73

Chrzanowski TH, Grover JP. 2008. Element content of *Pseudomonas fluorescens* varies with growth rate and temperature: A replicated chemostat study addressing ecological stoichiometry. *Limnol. Oceanogr.* 53(4):1242–51

Collier JL, Grossman AR. 1992. Chlorosis induced by nutrient deprivation in *Synechococcus sp.* strain PCC 7942: Not all bleaching is the same. *J. Bacteriol.* 174(14):4718–26

Conover SAM. 1975. Partitioning of nitrogen and carbon in cultures of the marine diatom *Thalassiosira fluviatilis* supplied with nitrate, ammonium, or urea. *Mar. Biol.* 32(3):231–46

Cotner JB, Ammerman JW, Peele ER, Bentzen E. 1997. Phosphorus-limited bacterioplankton

growth in the Sargasso Sea. *Aquat. Microb. Ecol.* 13:141–49

Cotner JB, Makino W, Biddanda BA. 2006. Temperature affects stoichiometry and biochemical composition of *Escherichia coli*. *Microb. Ecol.* 52(1):26–33

Cotner JB, Wetzel RG. 1992. Uptake of dissolved inorganic and organic phosphorus compounds by phytoplankton and bacterioplankton. *Limnol. Oceanogr.* 37(2):232–43

Cunningham BR, John SG. 2017. The effect of iron limitation on cyanobacteria major nutrient and trace element stoichiometry. *Limnol. Oceanogr.*

Daines SJ, Clark JR, Lenton TM. 2014. Multiple environmental controls on phytoplankton growth strategies determine adaptive responses of the N : P ratio. *Ecol. Lett.* 17:414–25

Davison IR. 1991. Environmental effects on algal photosynthesis: Temperature. *J Phycol*. 27:2–8

Deutsch C, Key RM, Sarmiento JL, Ganachaud A. 2001. Denitrification and N2 fixation in the Pacific Ocean. *Global Biogeochem. Cycles*. 15(2):483–506

Deutsch C, Sarmiento JL, Sigman DM, Gruber N, Dunne JP. 2007. Spatial coupling of nitrogen inputs and losses in the ocean. *Nature*. 445(7124):163–67

Deutsch C, Weber T. 2012. Nutrient ratios as a tracer and driver of ocean biogeochemistry. *Ann. Rev. Mar. Sci.* 4:113–41

DeVries T, Deutsch C. 2014. Large-scale variations in the stoichiometry of marine organic matter respiration. *Nat. Geosci.* 7(12):890–94

Diaz JM, Bjorkman KM, Haley ST, Ingall ED, Karl DM, et al. 2016. Polyphosphate dynamics at Station ALOHA, North Pacific subtropical gyre. *Limnol. Oceanogr.* 61(1):227–39

Dickman EM, Vanni MJ, Horgan MJ. 2006. Interactive effects of light and nutrients on

phytoplankton stoichiometry. *Oecologia*. 149(4):676–89

Droop MR. 1968. Vitamin B12 and Marine Ecology. IV. The Kinetics of Uptake, Growth and Inhibition in Monochrysis Lutheri. *J. Mar. Biol. Assoc. UK*. 48:689–733

Dugdale RC, Goering JJ. 1967. Uptake of new and regenerated forms of nitrogen in primary productivity. *Limnol. Oceanogr.* 12:196–206

Edwards KF, Thomas MK, Klausmeier CA, Litchman E. 2012. Allometric scaling and taxonomic variation in nutrient utilization traits and maximum growth rate of phytoplankton. . 57(2):554–66

Elrifi IR, Turpin DH. 1985. Steady-state luxury consumption and the concept of optimum nutrient ratios - a study with phosphate and nitrate limited *Selenastrum minutum* (Chlorophyta). *J. Phycol.* 21(4):592–602

Elser JJ, Acharya K, Kyle M, Cotner J, Makino W, et al. 2003. Growth rate-stoichiometry couplings in diverse biota. *Ecol. Lett.* 6(10):936–43

Elser JJ, Sterner RW, Gorokhova E, Fagan WF, Markow TA, et al. 2000. Biological stoichiometry from genes to ecosystems. *Ecol. Lett.* 3(6):540–50

Emerson S. 2014. Annual net community production and the biological carbon flux in the ocean. *Global Biogeochem. Cycles*. 28(1):14–28

Eppley RW. 1972. Temperature and phytoplankton growth in the sea. *Fish. Bull.* 70(4):1063–85

Fagerbakke KM, Heldal M, Norland S. 1996. Content of carbon, nitrogen, oxygen, sulfur and phosphorus in native aquatic and cultured bacteria. *Aquat. Microb. Ecol.* 10(1):15–27

Falkowski PG. 1997. Evolution of the nitrogen cycle and its influence on the biological sequestration of CO2 in the ocean. *Nature*. 387:272–75

Falkowski PG, LaRoche J. 1991. Acclimation to spectral irradiance in algae. *J. Phycol.* 27:8–14

Farewell a, Neidhardt FC. 1998. Effect of temperature on in vivo protein synthetic capacity in *Escherichia coli*. *J. Bacteriol.* 180(17):4704–10

Finkel Z V, Follows MJ, Liefer JD, Brown CM, Benner I, Irwin AJ. 2016. Phylogenetic diversity in the macromolecular composition of microalgae. *PLoS One*. 11(5):e0155977

Finkel Z V, Quigg A, Raven JA, Reinfelder JR, Schofield OE, Falkowski PG. 2006. Irradiance and the elemental stoichiometry of marine phytoplankton. *Limnol. Oceanogr.* 51(6):2690–2701

Flynn KJ. 2008. The importance of the form of the quota curve and control of non-limiting nutrient transport in phytoplankton models. *J. Plankton Res.* 30(4):423–38

Flynn KJ, Raven JA, Rees TA V, Finkel Z, Quigg A, Beardall J. 2010. Is the Growth Rate Hypothesis Applicable to Microalgae? *J. Phycol.* 46(1):1–12

Fu FX, Warner ME, Zhang YH, Feng YY, Hutchins DA. 2007. Effects of increased temperature and CO_2 on photosynthesis, growth, and elemental ratios in marine *Synechococcus* and *Prochlorococcus* (Cyanobacteria). *J. Phycol.* 43(3):485–96

Galbraith ED, Martiny AC. 2015. A simple nutrient-dependence mechanism for predicting the stoichiometry of marine ecosystems. *Proc. Natl. Acad. Sci.* 112(27):201423917

Garcia NS, Bonachela JA, Martiny AC. 2016. Interactions between growth-dependent changes in cell size, nutrient supply and cellular elemental stoichiometry of marine *Synechococcus*. *ISME J*. 10(11):2715–24

Gasol JM, del Giorgio PA, Duarte CM. 1997. Biomass distribution in marine planktonic communities. *Limnol. Oceanogr.* 42(6):1353–63

Gausing K. 1982. Regulation of ribosome synthesis in *E. coli*. *Trends Biochem. Sci.* 7(2):65–67

Geider R, Roche J La. 2002. Redfield revisited: variability of C:N:P in marine microalgae and its biochemical basis *Eur. J. Phycol.* 37(September 2012):37–41

Geider RJ. 1987. Light and temperature dependence of the carbon to chlorophyll a ratio in microalgae and cyanobacteria: implications for physiology and growth of phytoplankton. *New Phytol.* 106:1–34

Geider RJ, La Roche J. 2002. Redfield revisited: variability of C : N : P in marine microalgae and its biochemical basis. *Eur. J. Phycol.* 37(1):1–17

Geider RJ, Macintyre HL, Kana TM. 1996. A dynamic model of photoadaptation in phytoplankton. *Limnol. Oceanogr.* 41(1):1–15

Geider RJ, MacIntyre HL, Kana TM. 1998. A dynamic regulatory model of phytoplanktonic acclimation to light, nutrients, and temperature. *Limnol. Oceanogr.* 43(4):679–94

Geider RJ, Osborne BA. 1989. Respiration and microalgal growth: A review of the quantitative relationship between dark respiration and growth. *New Phytol.* 112:327

Godwin CM, Cotner JB. 2015. Aquatic heterotrophic bacteria have highly flexible phosphorus content and biomass stoichiometry. *ISME J.* 9(MARCH):1–4

Godwin CM, Whitaker EA, Cotner JB. 2016. Growth rate and resource imbalance interactively control biomass stoichiometry and elemental quotas of aquatic bacteria. *Ecology*. 98(3):820–29

Goldman JC, McCarthy JJ, Peavy DG, Peavey DG. 1979. Growth rate influence on the chemical composition of phytoplankton in oceanic waters. *Nature*. 279(5710):210–15

Goldman JC, Peavey DG. 1979. Steady-state growth and chemical composition of the marine

Chlorophyte *Dunaliella tertiolecta* in nitrogen-limited continuous cultures. *Appl. Environ. Microbiol.* 38(5):894–901

Hall EK, Neuhauser C, Cotner JB. 2008. Toward a mechanistic understanding of how natural bacterial communities respond to changes in temperature in aquatic ecosystems. *ISME J.* 2(5):471–81

Harrison PJ, Conway HL, Dugdale RC. 1976. Marine diatoms grown in chemostats under silicate or ammonium limitation. I. Cellular chemical composition and steady state growth kinetics of *Skeletonema costatum*. *Mar. Biol.* 35:177–86

Henderson RJ, Mackinlay EE. 1989. Effect of temperature on lipid composition of the marine cryptomonad Chroomonas salina. *Phytochemistry*. 28(11):2943–48

Herrero A, Flores E, Guerrero MG. 1985. Regulation of nitrate reductase cellular levels in the cyanobacteria *Anabaena variabilis* and *Synechocystis* sp. *FEMS Microbiol. Lett.* 26:21–25

Hillebrand H, Steinert G, Boersma M, Malzahn A, Léo Meunier C, et al. 2013. Goldman revisited: Faster growing phytoplankton has lower N:P and lower stoichiometric flexibility. *Limnol. Oceanogr.* 58(6):2076–88

Ho T-Y, Quigg A, Finkel Z V., Milligan AJ, Wyman K, et al. 2003. The elemental composition of some marine phytoplankton. *J. Phycol.* 39(6):1145–59

Hochachka, Somero G.N. 1984. *Biochemical Adaptation*, Vol. 30

Holme T, Palmsterna H. 1956. On the Glycogen in *Escherichia coli B*; its Synthesis and Breakdown and its Specific Labeling with 14C. *Acta Chem. Scand.* 10:1557–62

Hunter-Cevera KR, Neubert MG, Olson RJ, Solow AR, Shalapyonok A, Sosik HM. 2016. Physiological and ecological drivers of early spring blooms of a coastal phytoplankter.

Science. 354(6310):326–29

Klausmeier CA, Litchman E, Levin SA. 2004. Phytoplankton growth and stoichiometry under multiple nutrient limitation. *Limnol. Oceanogr.* 49(4):1463–70

Kornberg A, Rao NN, Ault-Riche D. 1999. Inorganic polyphosphate: A molecule of many functions. *Annu. Rev. Biochem.* 68:89–125

Kramer JG, Morris I. 1990. Growth regulation in irradiance limited marine *Synechococcus sp.* WH 7803. *Arch. Microbiol.* 154:286–93

Kromkamp J. 1987. Formation and functional significance of storage products in cyanobacteria. *New Zeal. J. Mar. Freshw. Res.* 21:457–65

Laws EA, Bannister TT. 1980. Nutrient- and light-limited growth of *Thalassiosira fluviatilis* in continuous culture, with implications for phytoplankton growth in the ocean. *Limnol. Oceanogr.* 25(3):457–73

Lenton TM, Klausmeier CA. 2007. Biotic stoichiometric controls on the deep ocean N : P ratio. *Biogeosciences*. 4(3):353–67

Leonardos N, Geider RJ. 2004a. Responses of elemental and biochemical composition of *Chaetoceros muelleri* to growth under varying light and nitrate: phosphate supply ratios and their influence on critical N : P. *Limnol. Oceanogr.* 49(6):2105–14

Leonardos N, Geider RJ. 2004b. Effects of nitrate: phosphate supply ratio and irradiance on the C : N : P stoichiometry of *Chaetoceros muelleri*. *Eur. J. Phycol.* 39(2):173–80

Leonardos N, Geider RJ. 2005. Elemental and biochemical composition of *Rhinomonas reticulata* (Cryptophyta) in relation to light and nitrate-to-phosphate supply ratios. *J. Phycol.* 41(3):567–76

Lin Y, Gazsi K, Lance VP, Larkin AA, Chandler JW, et al. 2013. In situ activity of a dominant

Prochlorococcus ecotype (eHL-II) from rRNA content and cell size. *Environ. Microbiol.* 15(10):2736–47

Liu H, Campbell L, Landry MR, Nolla HA, Brown SL, Constantinou J. 1998. *Prochlorococcus* and *Synechococcus* growth rates and contributions to production in the Arabian Sea during the 1995 Southwest and Northeast Monsoons. *Deep Sea Res. Part II Top. Stud. Oceanogr.* 45(10–11):2327–52

Lomas MW, Burke AL, Lomas DA, Bell DW, Shen C, et al. 2010. Sargasso Sea phosphorus biogeochemistry: an important role for dissolved organic phosphorus (DOP). *Biogeosciences*. 7(2):695–710

Lopez JL, Garcia NS, Talmy D, Martiny AC. 2016. Diel variability in the elemental composition of the marine cyanobacterium *Synechococcus*. *J. Plankton Res.* 38(4):1052–61

Lourenço SO, Barbarino E, Lavín PL, Lanfer Marquez UM, Aidar E. 2004. Distribution of intracellular nitrogen in marine microalgae: Calculation of new nitrogen-to-protein conversion factors. *Eur. J. Phycol.* 39(1):17–32

Lynn SG, Kilham SS, Kreeger DA, Interlandi SJ. 2000. Effect of Nutrient Availability on the Biochemical and Elemental Stoichiometry in the Freshwater Diatom *Stephanodiscus Minutulus* (Bacillariophyceae). *J. Phycol*. 36(December 1998):510–22

MacIntyre HL, Kana TM, Anning T, Geider RJ. 2002. Photoacclimation of photosynthesis irradiance response curves and photosynthetic pigments in microalgae and cyanobacteria. *J. Phycol.* 38(1):17–38

Mackey KRM, Paytan A, Caldeira K, Grossman AR, Moran D, et al. 2013. Effect of temperature on photosynthesis and growth in marine *Synechococcus* spp. *Plant*

Physiol. 163(2):815–29

Makino W, Cotner JB, Sterner RW, Elser JJ. 2003. Are bacteria more like plants or animals? Growth rate and resource dependence of bacterial C : N : P stoichiometry. *Funct. Ecol.* 17:121–30

Malzahn AM, Hantzsche F, Schoo KL, Boersma M, Aberle N. 2010. Differential effects of nutrient-limited primary production on primary, secondary or tertiary consumers. *Oecologia*. 162(1):35–48

Marchetti A, Harrison PJ. 2007. Coupled changes in the cell morphology and elemental (C, N, and Si) composition of the pennate diatom *Pseudo-nitzschia* due to iron deficiency. *Limnol. Oceanogr.* 52:2270–84

Martin P, Dyhrman ST, Lomas MW, Poulton NJ, Van Mooy B a S. 2014. Accumulation and enhanced cycling of polyphosphate by Sargasso Sea plankton in response to low phosphorus. *Proc. Natl. Acad. Sci. U. S. A.* 111(22):8089–94

Martiny AC, Coleman ML, Chisholm SW. 2006. Phosphate acquisition genes in *Prochlorococcus* ecotypes: Evidence for genome-wide adaptation. *Proc. Natl. Acad. Sci. U. S. A.* 103(33):12552–57

Martiny AC, Ma L, Mouginot C, Chandler JW, Zinser ER. 2016a. Interactions between Thermal Acclimation, Growth Rate, and Phylogeny Influence Prochlorococcus Elemental Stoichiometry. *PLoS One*. 11(12):1–12

Martiny AC, Pham CTA, Primeau FW, Vrugt JA, Moore JK, et al. 2013a. Strong latitudinal patterns in the elemental ratios of marine plankton and organic matter. *Nat. Geosci.* 6(5):1–5

Martiny AC, Talarmin A, Mouginot C, Lee JA, Huang JS, et al. 2016b. Biogeochemical

interactions control a temporal succession in the elemental composition of marine communities. *Limnol. Oceanogr.* 61(2):531–42

Martiny AC, Vrugt JA, Primeau FW, Lomas MW. 2013b. Regional variation in the particulate organic carbon to nitrogen ratio in the surface ocean. *Global Biogeochem. Cycles*. 27(3):723–31

Matallana-Surget S, Derock J, Leroy B, Badri H, Deschoenmaeker F, Wattiez R. 2014. Proteome-wide analysis and diel proteomic profiling of the cyanobacterium *Arthrospira platensis* PCC 8005. *PLoS One*. 9(6):

Mather RL, Reynolds SE, Wolff GA, Williams RG, Torres-Valdes S, et al. 2008. Phosphorus cycling in the North and South Atlantic Ocean subtropical gyres. *Nat. Geosci.* 1(7):439–43

Maxwell DP, Falk S, CG T, Huner NPA, Maxwell DP, et al. 1994. Growth at Low Temperature Mimics High-Light Acclimation in Chlorella vulgaris. *Plant Physiol.* 105(2):535–43

Meunier CL, Haafke J, Oppermann B, Boersma M, Malzahn AM. 2012. Dynamic stoichiometric response to food quality fluctuations in the heterotrophic dinoflagellate *Oxyrrhis marina*. *Mar. Biol.* 159(10):2241–48

Mills MM, Arrigo KR. 2010. Magnitude of oceanic nitrogen fixation influenced by the nutrient uptake ratio of phytoplankton. *Nat. Geosci.* 3(6):412–16

Mino T, Van Loosdrecht MCM, Heijnen JJ. 1998. Microbiology and biochemistry of the enhanced biological phosphate removal process

Moore CM, Mills MM, Arrigo KR, Berman-Frank I, Bopp L, et al. 2013. Processes and patterns of oceanic nutrient limitation. *Nat. Geosci*. 6(9):701–10

Moore LR, Rocap G, Chisholm SW. 1998. Physiology and molecular phylogeny of coexisting

Prochlorococcus ecotypes. *Nature*. 393:464–67

Mouginot C, Kawamura R, Matulich KL, Berlemont R, Allison SD, et al. 2014. Elemental stoichiometry of Fungi and Bacteria strains from grassland leaf litter. *Soil Biol. Biochem.* 76(0):278–85

Mouginot C, Zimmerman AE, Bonachela JA, Fredricks H, Allison SD, et al. 2015. Resource allocation by the marine cyanobacterium *Synechococcus* WH8102 in response to different nutrient supply ratios. *Limnol. Oceanogr.* 60(5):1634–41

Moutin T, Karl DM, Duhamel S, Rimmelin P, Raimbault P, et al. 2007. Phosphate availability and the ultimate control of new nitrogen input by nitrogen fixation in the tropical Pacific Ocean. *Biogeosciences Discuss.* 4(4):2407–40

Olson RJ, Vaulot D, Chisholm SW. 1986. Effects of environmental stresses on the cell cycle of two marine phytoplankton species. *Plant Physiol.* 80:918–25

Ottesen E a. 2014. Multispecies diel transcriptional oscillatins in open ocean heterotrophic bacterial assemblages. *Science (80-.).* 53(9):1689–99

Persson J, Fink P, Goto A, Hood JM, Jonas J, Kato S. 2010. To be or not to be what you eat: Regulation of stoichiometric homeostasis among autotrophs and heterotrophs. *Oikos*. 119(5):741–51

Price NM. 2005. The elemental stoichiometry and composition of an iron-limited diatom. *Limnol. Oceanogr.* 50(4):1159–71

Raven JA, Geider RJ. 1988. Temperature and algal growth. *New Phytol.* 110(4):441–61

Redfield AC. 1958. The biological control of the chemical factors in the environment. *Am. Sci.* 46(3):1–18

Rhee G-Y. 1973. A continuous culture study of phosphate uptake, growth rate and

polyphosphate in *Scenedesmus sp. J. Phycol.* 9:495–506

Rhee G-Y, Gotham IJ. 1981. The effect of environmental factors on phytoplankton growth: Temperature and the interactions of temperature with nutrient limitation

Rhee G-Y, Gotham I, Chisholm SW. 1981. Use of cyclostat cultures to study phytoplankton ecology. In *Continuous Cultures of Cells*, Vol. 2, ed. PH Calcott, pp. 159–86. Boca Raton, FL: CRC Press

Rhee G -Y, Gotham IJ. 1980. Optimum N:P ratios and coexistence of planktonic algae. *J. Phycol.* 16(4):486–89

Rhee GY. 1978. Effects of N-P atomic ratios and nitrate limitation on algal growth, cell composition, and nitrate uptake. *Limnol. Oceanogr.* 23(1):10–25

Ribalet F, Swalwell J, Clayton S, Jiménez V, Sudek S, et al. 2015. Light-driven synchrony of *Prochlorococcus* growth and mortality in the subtropical Pacific gyre. *Proc. Natl. Acad. Sci.* 112(26):8008–12

Richardson TL, Jackson GA. 2007. Small Phytoplankton and Carbon Export from the Surface Ocean. *Science (80-.).* 315(5813):838–40

Rocap G, Moore LR, Chisholm SW. 1999. Molecular phylogeny of Prochlorococcus ecotypes. In *Marine Cyanobacteria*, Vol. Special Is, eds. L Charpy, AWD Larkum, pp. 107–16. Monaco: Bulletin de l'Institut Oc{é}anographique

Schaechter M, Maaloe O, Kjeldgaard NO. 1958a. Dependency on medium and temperature of cell size and chemical composition during balanced grown of *Salmonella typhimurium*. *J. Gen. Microbiol.* 19:592–606

Schaechter M, MaalOe O, Kjeldgaard NO. 1958b. Dependency on Medium and Temperature of Cell Size and Chemical Composition during Balanced Growth of Salmonella

typhimurium. *J. Gen. Microbiol.* 19(3):592–606

Schneider B, Schlitzer R, Fischer G, Nothig EM. 2003. Depth-dependent elemental compositions of particulate organic matter (POM) in the ocean. *Global Biogeochem. Cycles*. 17(2):

Sherman E, Moore J, Primeau F, Tanouye D. 2016. Temperature influence on phytoplankton community growth rates. *Global Biogeochem. Cycles*. 30(4):550–59

Simon M, Azam F. 1989. Protein content and protein synthesis rates of planktonic marine bacteria. *Mar. Ecol. Prog. Ser.* 51:201–2013

Singh A, Baer SE, Riebesell U, Martiny AC, Lomas MW. 2015. C : N : P stoichiometry at the Bermuda Atlantic Time-series Study station in the North Atlantic Ocean. *Biogeosciences*. 12(21):6389–6403

Sohm JA, Webb EA, Capone DG. 2011. Emerging patterns of marine nitrogen fixation. *Nat. Rev. Microbiol.* 9(7):499–508

Spilling K, Ylostalo P, Simis S, Seppala J. 2015. Interaction effects of light, temperature and nutrient limitations (N, P and Si) on growth, stoichiometry and photosynthetic parameters of the cold-water diatom *Chaetoceros wighamii*. *PLoS One*. 10(5):1–18

Sterner RW. 2015. Ocean stoichiometry, global carbon, and climate. *Proc. Natl. Acad. Sci. U. S. A.* 112(27):8162–63

Sterner RW, Elser JJ. 2002. *Ecological Stoichiometry: The Biology of Elements from Molecules to the Biosphere*. Princeton, NJ: Princeton University Press

Talarmin A, Lomas MW, Bozec Y, Savoye N, Frigstad H, et al. 2016. Seasonal and long-term changes in elemental concentrations and ratios of marine particulate organic matter. *Global Biogeochem. Cycles*. 30:1699–1711

Talmy D, Martiny AC, Hill C, Hickman AE, Follows MJ. 2016. Microzooplankton regulation of surface ocean POC : PON ratios. *Glob. Biogeochem. Cycles*. 30:311–32

Tempest D., Hunter JR. 1965. The Influence of Temperature and pH Value on the Macro-molecular Composition of Magnesium-limited and Glycerol-limited *Aerobacter aerogenes* Growing in a Chemostat. *J. Gen. Microbiol.* 41:267–73

Teng Y-C, Primeau FW, Moore JK, Lomas MW, Martiny AC. 2014. Global-scale variations of the ratios of carbon to phosphorus in exported marine organic matter. *Nat. Geosci.* 7(12):895–98

Tezuka Y. 1990. Bacterial Regeneration of Ammonium and Phosphate as Affected by the Carbon - Nitrogen - Phosphorus Ratio of Organic Substrates. *Microb. Ecol.* 19(3):227–38

Thompson PA, Guo MX, Harrison PJ. 1992. Effects of variation in temperature. I. on the biochemical composition of eight species of marine phytoplankton. *J. Phycol.* 28(4):481–88

Thompson PA, Harrison PJ, Parslow JS. 1991. Influence of irradiance of cell volume and carbon quota for ten species of marine phytoplankton. *J. Phycol.* 27(3):351–60

Thrane JE, Hessen DO, Andersen T, Hillebrand H. 2016. The impact of irradiance on optimal and cellular nitrogen to phosphorus ratios in phytoplankton. *Ecol. Lett.* 19(8):880–88

Tolonen AC, Aach J, Lindell D, Johnson ZI, Rector T, et al. 2006. Global gene expression of *Prochlorococcus* ecotypes in response to changes in nitrogen availability. *Mol Syst Biol*. 2:53

Torriani-Gorini A. 1987. The birth and growth of the Pho regulon. In *Phosphate Metabolism and Cellular Regulation in Microorganisms*, eds. A Torriani-Gorini, FG Rothman, S

Silver, A Wright, E Yagil, pp. 3–11. Washington, DC: American Society for Microbiology

Toseland A, Daines SJ, Clark JR, Kirkham A, Strauss J, et al. 2013. The impact of temperature on marine phytoplankton resource allocation and metabolism. *Nat. Clim. Chang.* 3(11):979–84

Tyrrell T. 1999. The relative influences of nitrogen and phosphorus on oceanic primary production. *Nature*. 400:525–31

Vadia S, Levin PA. 2015. Growth rate and cell size: A re-examination of the growth law

Van Mooy BAS, Devol AK. 2008. Assessing nutrient limitation of *Prochlorococcus* in the North Pacific Subtropical gyre by using an RNA capture method. *Limnol. Oceanogr.* 53(1):78–88

Van Mooy BAS, Fredricks HF. 2010. Bacterial and eukaryotic intact polar lipids in the eastern subtropical South Pacific: Water-column distribution, planktonic sources, and fatty acid composition. *Geochim. Cosmochim. Acta*. 74(22):6499–6516

Van Mooy BAS, Fredricks HF, Pedler BE, Dyhrman ST, Karl DM, et al. 2009. Phytoplankton in the ocean use non-phosphorus lipids in response to phosphorus scarcity. *Nature*. 458(7234):69–72

Van Mooy BAS, Rocap G, Fredricks HF, Evans CT, Devol AH. 2006. Sulfolipids dramatically decrease phosphorus demand by picocyanobacteria in oligotrophic marine environments. *Proc. Natl. Acad. Sci. U. S. A.* 103:8607–12

Vaulot D, Marie D, Olson RJ, Chisholm SW. 1995. Growth of *Prochlorococcus*, a photosynthetic prokaryote, in the equatorial Pacific Ocean. *Science (80-.).* 268:1480–82

Vrede K, Heldal M, Norland S, Bratbak G. 2002. Elemental composition (C, N, P) and cell

volume of exponentially growing and nutrient-limited bacterioplankton. *Appl. Environ. Microbiol.* 68(6):2965–71

Waldbauer JR, Rodrigue S, Coleman ML, Chisholm SW. 2012. Transcriptome and Proteome Dynamics of a Light-Dark Synchronized Bacterial Cell Cycle. *PLoS One*. 7(8):

Wanner BL. 1993. Gene regulation by phosphate in enteric bacteria. *J. Cell. Biochem.* 51(1):47–54

Weber T, Deutsch C. 2012. Oceanic nitrogen reservoir regulated by plankton diversity and ocean circulation. *Nature*. 489:419–22

Weber TS, Deutsch C. 2010. Ocean nutrient ratios governed by plankton biogeography. *Nature*. 467(7315):550–54

Worden AZ, Binder BJ. 2003. Growth regulation of rRNA content in *Prochlorococcus* and *Synechococcus* (marine cyanobacteria) measured by whole-cell hybridization of rRNA-targeted peptide nucleic acids. *J. Phycol.* 39(3):527–34

Wu J, Sunda W, Boyle EA, Karl DM. 2000. Phosphate Depletion in the Western North Atlantic Ocean. *Science (80-.).* 289(5480):759–62

Yun HS, Hong J, Lim HC. 1996. Regulation of Ribosome Synthesis in *Escherichia coli* Effects of Temperature and Dilution Rate Changes. *Biotechnol. Bioeng.* 52:615–24

Yvon-Durocher G, Dossena M, Trimmer M, Woodward G, Allen AP. 2015. Temperature and the biogeography of algal stoichiometry. *Glob. Ecol. Biogeogr.* 24(5):562–70

Zhu CJ, Lee YK, Chao TM. 1997. Effects of temperature and growth phase on lipid and biochemical composition of *Isochrysis galbana* TK1. *J. Appl. Phycol.* 9(5):451–57

Zimmerman AE, Allison SD, Martiny AC. 2014. Phylogenetic constraints on elemental stoichiometry and resource allocation in heterotrophic marine bacteria. *Environ.*

Microbiol. 16(5):1398–1410

Zinser ER, Lindell D, Johnson ZI, Futschik ME, Steglich C, et al. 2009. Choreography of the transcriptome, photophysiology, and cell cycle of a minimal photoautotroph, *Prochlorococcus*. *PLoS One*. 4(4):e5135

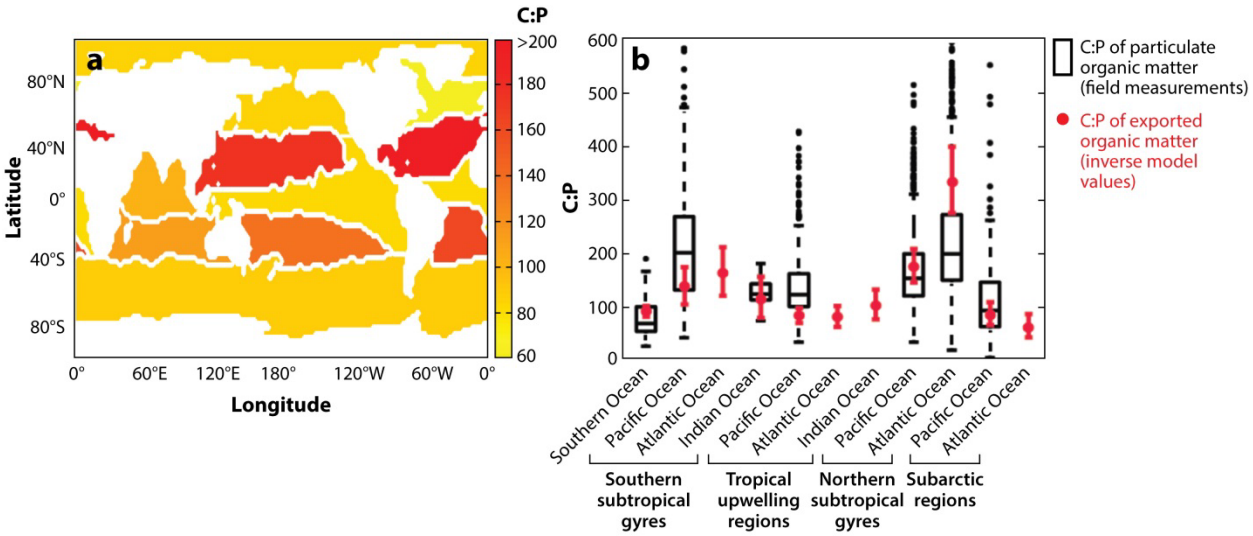

Figure 1.1 Regional variation in the elemental composition of exported organic matter and surface particulate organic matter. (a) C:P of exported matter across 11 regions classified based on the surface phosphate concentration (Teng et al. 2014). (b) A comparison of the C:P of exported organic matter (based on inverse model values) and the surface C:P of particulate organic matter (based on field measurements) of these 11 regions (Martiny et al. 2013a,b).

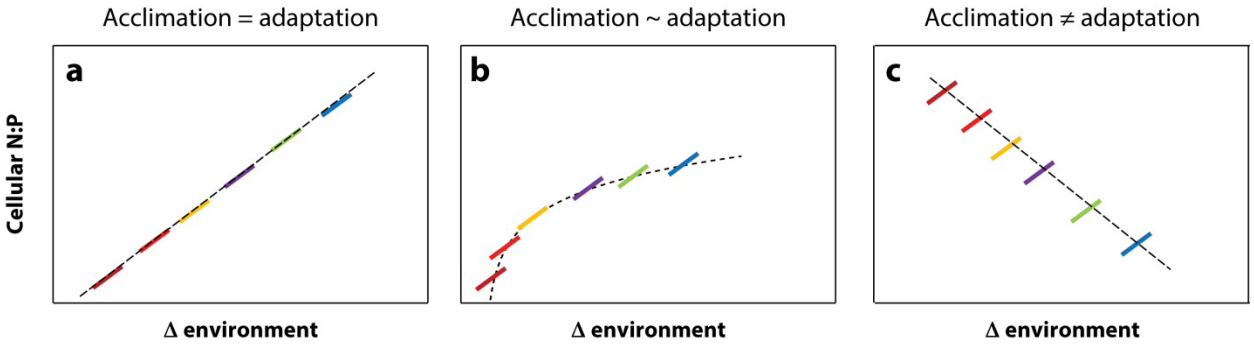

Figure 1.2 Influence of acclimation and adaptation processes on the relationship between an environmental change and the elemental composition. (a) In the first scenario, the environmental impacts on the N:P ratio in a cell that occur via acclimation and adaptation are aligned, and understanding the individual response provides a model for how communities are affected. (b) In the second scenario, the two processes are related but lead to a nonlinear interaction. (c) In the third scenario, the outcome of a physiological adjustment of the cellular chemistry is the opposite of how a cell adapts to a different environment; in this scenario, physiological models may be misguided when predicting the elemental stoichiometry across ocean gradients. Each colored line represents a different species being examined within an experiment or study.

Table 1.1 Relationship of RNA to growth rate in diverse species

Species	Controlling Mechanism	Relationship	Citation
Escherichia Coli	Replete	Positive Linear	(Gausing 1982; Schaechter et al. 1958a)
Daphnia Pulicaria	Replete	No Relationship	(Elser et al. 2003)
Daphnia Pulex	Replete	No Relationship	(Elser et al. 2003)
Escherichia Coli	Replete	No Relationship	(Elser et al. 2003)
Lake bacteria	Replete	No Relationship	(Elser et al. 2003)
Freshwater zooplankton	Replete	No Relationship	(Elser et al. 2003)
Daphnia pulicaria	P- limited	Positive Linear	(Elser et al. 2003)
Dapnia galeata	P- limited	Positive Linear	(Elser et al. 2003)
Drosophila melanogaster	P- limited	Positive Linear	(Elser et al. 2003)
Escherichia Coli	P- limited	Positive Linear	(Elser et al. 2003)
Lake bacteria	P- limited	Positive Linear	(Elser et al. 2003)
Synechococcus sp. *WH8101*	P- limited	Positive Linear	(Van Mooy & Devol 2008)
Synechococcus sp. *WH8102*	P- limited	Positive Linear	(Garcia et al. 2016)
Synechococcus sp. *WH8102*	N- limited	Positive Linear	(Garcia et al. 2016)
E. Coli	Temp (0°C to 25°C)	Positive Linear	(Broeze et al. 1978; Schaechter et al. 1958a)
Pseudomonas fluorescens	Temp (20°C and 24°C)	Positive Linear	(Chrzanowski & Grover 2008)
Pseudomonas fluroescens	Temp (14°C)	Negative Linear	(Chrzanowski & Grover 2008)
Scenedesmus	Temp (5°C and 25°C)	Negative Linear	(Rhee & Gotham 1981)
Prochlorococcus	Light	Positive Linear	(Lin et al. 2013)

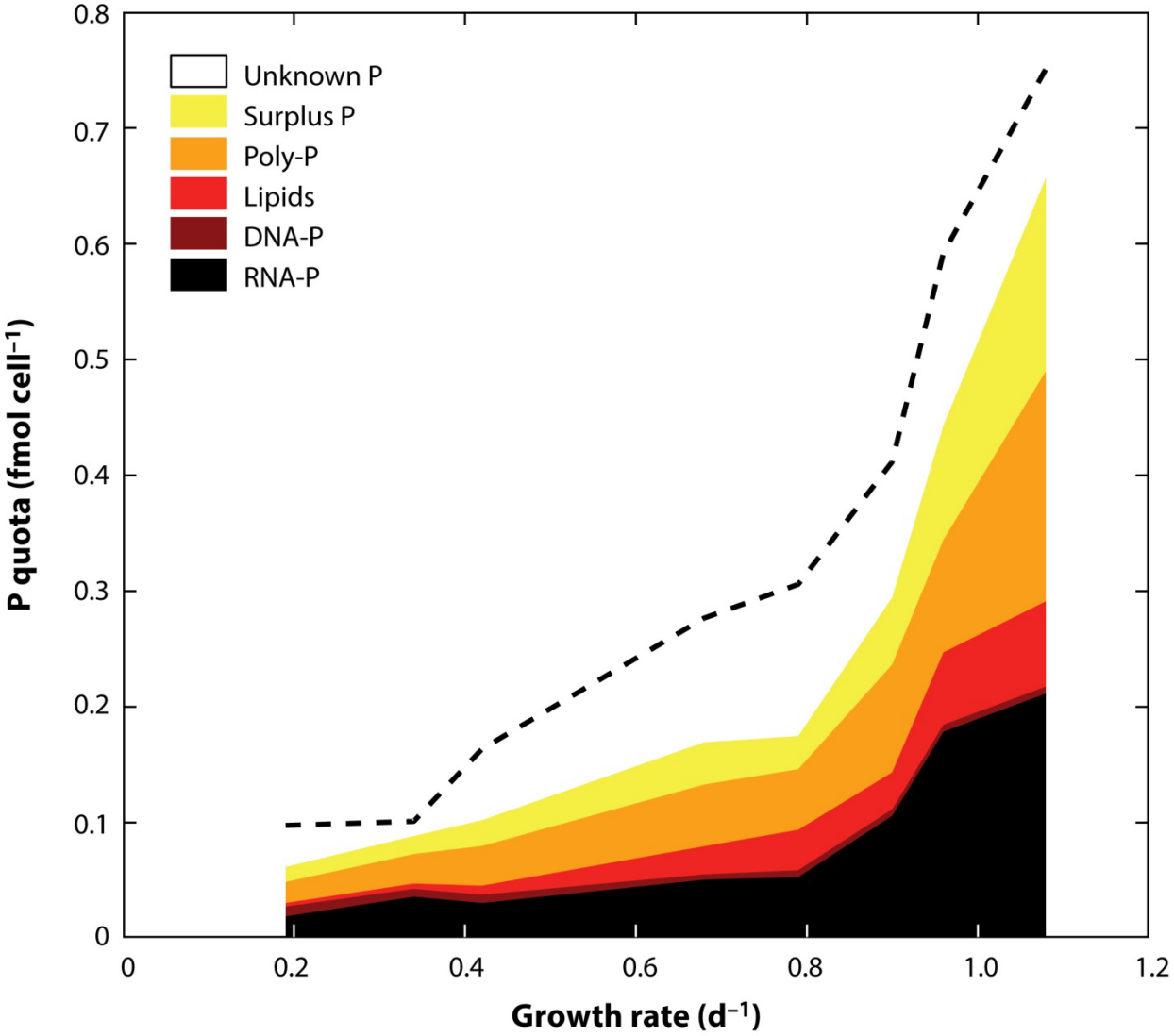

Figure 1.3 Breakdown of total P quota with increased growth rate. The dashed line represents the total P quota, and the colored regions represent the distribution of P among different cellular components. Data are from Rhee (1973).

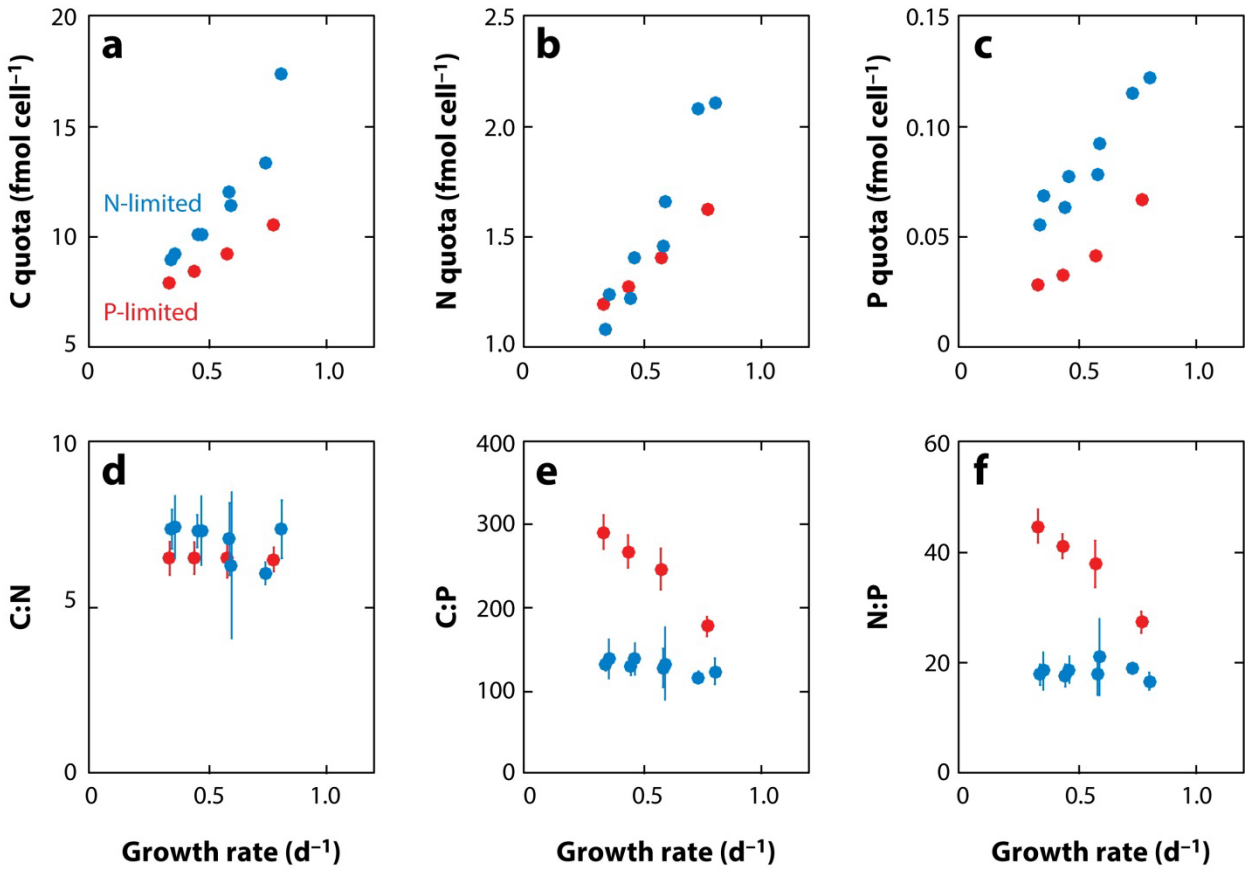

Figure 1.4 Interactive effects of nutrient limitation and growth on cellular quotas and ratios (Garcia et al. 2016). Red circles represent P-limited conditions, and blue circles represent N-limited conditions.

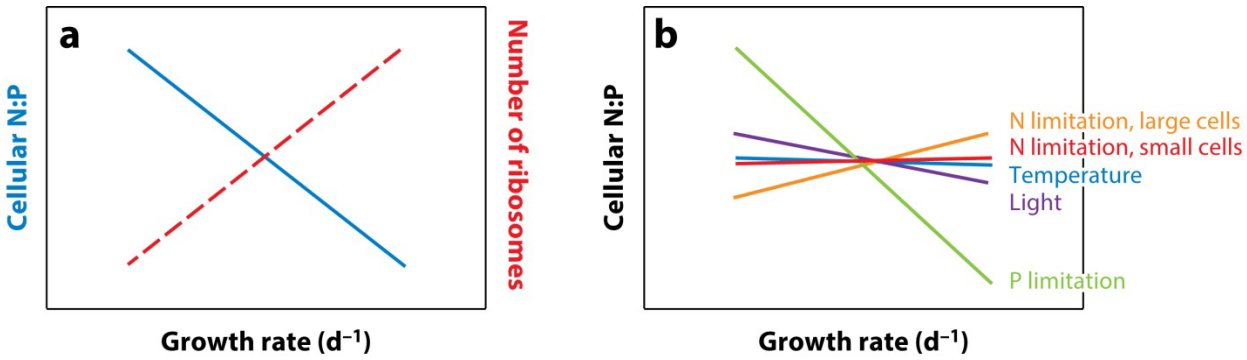

Figure 1.5 The link between cellular biochemical composition and N:P. (a) The growth rate hypothesis (GRH) prediction based on a higher number of ribosomes (dashed line), high P quota, and lower N:P (solid line). (b) A modified GRH that considers the factor limiting growth.

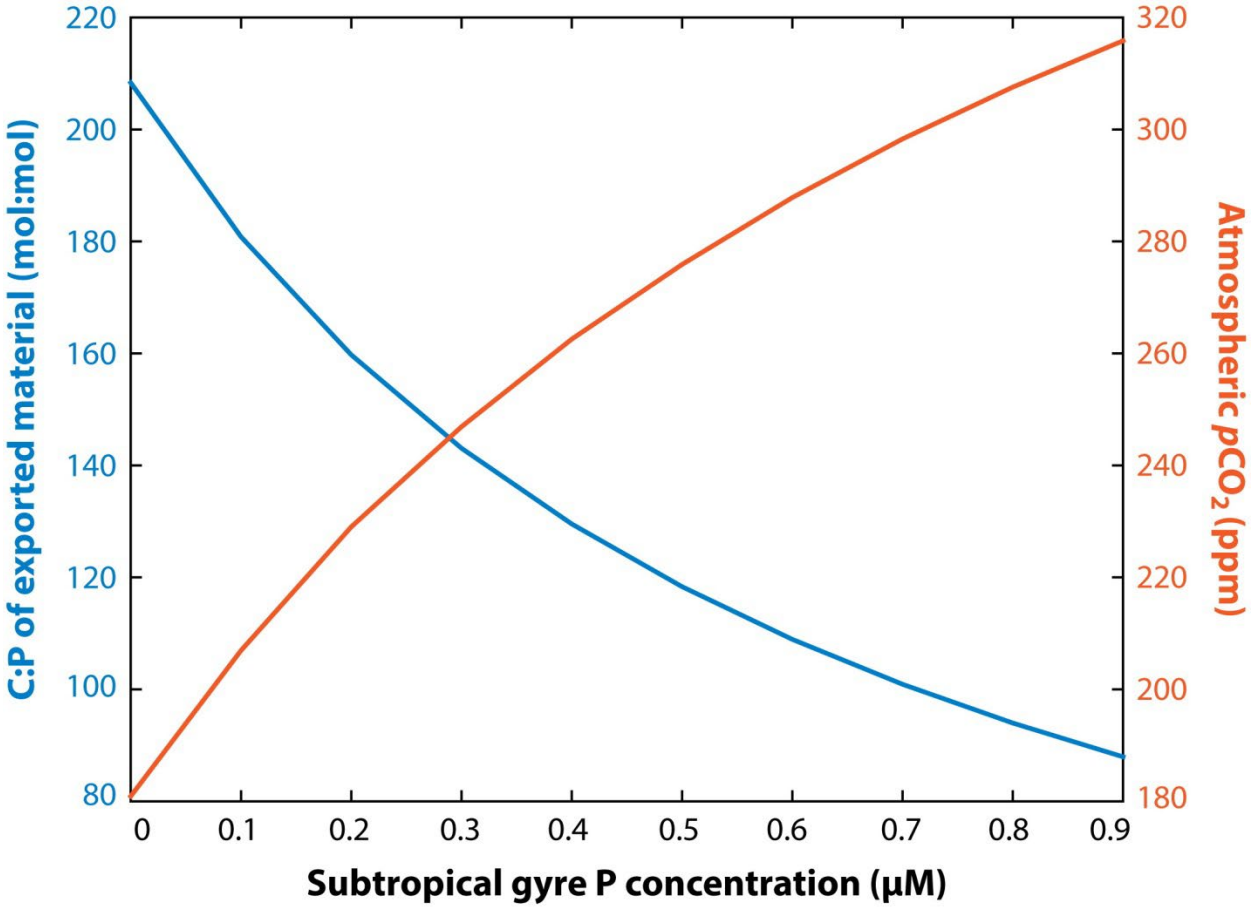

Figure 1.6 Linking subtropical gyre nutrient availability, the elemental composition of surface particles and export flux, and atmospheric pCO_2. To a first order, the C:P elemental composition of surface-ocean particles can be linked to nutrient availability (Martiny et al. 2013a). Based on this relationship, a simplified box-model simulation demonstrates how varying the C:P of exported material from low-latitude regions can lead to substantial long-term changes in atmospheric pCO_2 (Galbraith & Martiny 2015).

CHAPTER 2

Role of ENSO conditions on particulate organic matter concentrations and elemental ratios in the Southern California Bight

Abstract

El Niño Southern Oscillation (ENSO) influences multi-year variation in sea-surface temperature and the intensity of upwelling in many Pacific regions. However, it is currently unknown how El Niño conditions will affect the concentration and elemental ratios of particulate organic matter (POM). To investigate this, we have quantified POM weekly for 6 years (2012 to 2017) at the MICRO time-series station in the Southern California Bight. We found a strong influence of the 2015 El Niño on sea-surface temperature and phosphate concentration but to a lesser extent on nitrate availability. The 2015 El Niño also resulted in a short-term depression in POC and POP concentrations, whereas PON concentrations displayed an independent long-term decline regardless of the El Niño event. Reduced POM concentrations resulting from the 2015 El Niño occurred in parallel to high C:P and N:P ratios. Following the changes in PON, C:N continued to climb reaching ~9.4 at the end of our sampling period. We suggest that an Eastern Pacific- vs. a Central Pacific-type El Niño as well as a switch in the Pacific Decadal Oscillation phase significantly altered the local response in POM concentrations and ratios.

Keywords: MICRO, ecological stoichiometry, marine, ENSO, Redfield

Introduction

El Niño Southern Oscillation (ENSO) is a recurring climate cycle leading to multi-year variation in ocean environmental conditions (Dijkstra & Burges 2002; McPhaden 2015). In the California Current System, ENSO regulates sea-surface temperature (SST), upwelling source and intensity, thermocline depth, and large-scale circulation patterns

(Chavez 2002; Checkley & Barth 2009; Mcgowan et al. 1998). In the southern part of the California Current Ecosystem (i.e., the Southern California Bight, SCB), El Niño conditions are typically manifested as periods of high temperature and low nutrient availability (Chavez 2002; King & Barbeau 2011; Tegner & Dayton 1987). ENSO variability may have a negative effect on plankton growth and biomass accumulation, however this link has been elusive (Kim et al. 2009). Thus, it is currently unclear how coastal plankton will respond to recent ENSO-driven changes in ocean conditions.

There appears to be multiple modes of El Niño events including the Eastern-Pacific (EP) and Central-Pacific type (CP; Paek et al. 2017; Yu et al. 2012). The two types of El Niño conditions differentially regulate temperature anomalies including a shift in the regional location of maximum sea-surface temperature variability. A high positive temperature anomaly in the North Eastern Pacific Ocean is more indicative of an EP El Niño-type, whereas increased temperatures in the equatorial Pacific Ocean are typically associated with the CP El Niño-type (Paek et al. 2017). Furthermore, different El Niño modes result in spatially divergent patterns of declining vs. increasing phytoplankton biomass and growth (Racault et al. 2017). Generally a change in planktonic biomass and growth has an effect on the overall community structure. In the southern part of the California Current Ecosystem, the EP El Niño can result in significant shifts in community composition of phytoplankton. In contrast, CP El Niño has a proposed limited effect on phytoplankton in SCB. Thus, the mode of El Niño is predicted to differentially impact plankton communities in SCB.

A core property of ocean biogeochemistry is the elemental composition and stoichiometric ratios of particulate organic matter (POM). C:N:P of marine communities have traditionally been considered static at Redfield proportions (106C:16N:1P; Redfield

1958). However, phytoplankton acclimation and adaptation to different ocean environmental conditions can have a large impact on C:N:P (Moreno & Martiny 2018). Temperature and nutrient limitation are currently thought to be the most important regulators of C:N:P in the surface ocean although the relative contribution of each factor is subject to much debate. Increasing temperature is predicted to correspond to higher C:P and N:P in phytoplankton due to a reduced allocation to P-rich ribosomes (Toseland et al. 2013). Temperature is also known to affect microbial respiration rates (Pomeroy et al. 1991), which could affect the concentrations of POC, PON and POP. Nutrient limitation is predicted to lead to a reduced use of the respective nutrient and higher carbon-to-nutrient ratio although the effect may be higher for P vs. N limitation (Garcia et al. 2016). Temperature and nutrients may also affect stoichiometry via changes in phytoplankton community composition and growth physiology. Smaller cells thriving in warm, nutrient deplete waters are proposed to have higher C:N:P ratios compared to large cell types like diatoms (Klausmeier et al. 2004). Similarly, slower growing cells need fewer P-rich ribosomes and have higher C:N:P (Sterner & Elser 2002). Thus, shifts in temperature and nutrient concentrations during El Niño conditions are expected to impact phytoplankton community composition, physiology, and associated C:N:P. Based on current theories for the regulation of phytoplankton elemental stoichiometry, we therefore predict elevated C:N:P during El Niño events.

Recent studies have demonstrated considerable regional and temporal variation in C:N:P (Martiny et al. 2013b,a; Moreno & Martiny 2018). Higher C:N:P have been associated with warm, nutrient deplete ocean regions dominated by marine cyanobacteria and other small plankton. In contrast, colder, nutrient replete regions with high abundance of larger

phytoplankton like diatoms have depressed C:N:P. A parallel link between environmental changes and C:N:P was also observed in a past study in the Southern California Bight (Martiny et al. 2016). Here, variation in POM concentrations and ratios corresponded to seasonal oscillations in environmental conditions and phytoplankton abundances. Specifically, winter/spring periods with low temperature, high nutrient concentrations and a dominance of large phytoplankton resulted in low C:N:P and vice-versa for warmer periods during the summer and fall. Similar links between environmental conditions, phytoplankton community structure and C:N:P were also found on weekly and multi-year time-scales (Martiny et al. 2016). Based on these observations, we predict that El Niño conditions will positively impact C:N:P, but the strength of the C:N:P response will be modulated by the mode of El Niño.

We quantify the changes in SST, macronutrient concentrations, POM concentrations, and POM elemental stoichiometric ratios at the MICRO time-series in the Southern California Bight weekly from the beginning of 2012 to the end of 2017 covering the large El Niño event in 2015. Based on these observations, we aim to quantify how El Niño conditions influence ocean POM concentrations and stoichiometric ratios. We predict annually temperatures would be at its highest and macronutrient concentrations are at the lowest due to an offshore damping in upwelling during the 2015 El Niño. Through the regulation of phytoplankton ecology, we should see low POM concentrations and high carbon-to-nutrient elemental ratios. The outcome of this study will allow us to further understand how climatic drivers of ocean environmental conditions affect the link between the C, N, and P biogeochemical cycles.

Materials and Methods

Collection

Surface water was collected weekly at the MICRO time-series (33.608°N and 117.928°W; Martiny et al. 2016). Two autoclaved bottles are rinsed with ocean water and filled for processing in the lab. Water temperature data is collected from an automated shore station off of Newport Pier as part of the Southern California Coastal Ocean Observing Systems (SCCOOS).

Triplicate 300 ml samples for POC/PON or POP from each bottle are filtered within an hour of collection through pre-combusted (500°C, 5 h) 25 mm GF/F filters (Whatman, MA). Each filter is rinsed with Milli-Q water before being fitted in order to remove potential P residues. The filtrate from the initial filtration is collected and used for macronutrient quantification. The filtrate is filtered through a 0.2 μm syringe filter into a 50 ml tube. Triplicates are collected for both macronutrient and stored in the -20°C freezer.

Macronutrients

Nitrate and phosphate samples were collected in prewashed 50 mL Falcon tubes and filtered through a 0.2 μm syringe filter and stored at -20°C until further analysis. Soluble reactive phosphorus (SRP) concentrations were determined using the magnesium induced co-precipitation (MAGIC) protocol and calculated against a potassium monobasic phosphate standard (Karl & Tien 1992; Lomas et al. 2010). Nitrate samples were treated with a solution of ethylenediaminetetraacetate and passed through a column of copperized cadmium fillings (Knap et al. 1997). Measurements were conducted using the same standards and protocols throughout the time series.

Particulate Organic Carbon and Nitrogen

After thawing, POC/PON filters were allowed to dry overnight at 65°C before being packed into a 30 mm tin capsule (CE Elantech, Lakewood, New Jersey). Samples were then analyzed for C and N content on the same FlashEA 1112 nitrogen and carbon analyzer (Thermo Scientific, Waltham, Massachusetts), following the Sharp (1974) protocol. POC and PON concentrations were calibrated using known quantities of atropine.

Particulate Organic Phosphorus

Particulate organic phosphorus filters are placed in combusted glass vials. Potassium Monobasic Phosphate (1.0 mM-P) is used as a standard. 2 ml of Magnesium sulfate (0.017 M; Macron Fine Chemicals) are added to each vial, covered in tin foil, and put into an oven at 80°C overnight. The vials are wrapped in tinfoil and placed into a 500°C muffle oven for 2 h. Once cooled to room temperature, 5 ml HCl (0.2 M; EMD) is added to each vial and then capped with a Teflon coated cap and placed into the 80°C oven for 30 min and placed into a 15 ml glass centrifuge tube. Each vial is then washed with 5 ml Milli-Q water and then added to the tubes. 1 ml of mixed reagent is added to each of the tubes, centrifuged at 4000 rpm for 1 min and stored in the dark for 30 min. Each standard and sample is quantified at 885 nm. Quantifications were conducted using the same protocol, modified from Lomas et al., 2010, throughout the time series.

Data Analysis

All analyses were done on Supplementary Table S1 data in Matlab (Mathworks, MA). Using the smooth function, a four point moving average was overlaid onto the raw data time-series plots. Sum of square analysis was conducted on linear regressions to quantify the monthly and annual contributions. To detrend seasonality in our time series parameters, we apply a seasonal adjustment using a stable seasonal filter applying a 53-

point moving average, representing our weekly sampling. To determine potential covariations, a Pearson's correlation coefficient was calculated for each pair of variables, followed by a test of statistical significance (p-value ≤0.05).

El Niño Impacts

We used the ERSSTv5 estimate of the Oceanographic El Niño Index (ONI; Huang et al. 2017). Regional temperature anomalies are derived by a linear interpolation of the weekly satellite SST optimum interpolation fields to daily fields then averaging the daily values over a month (Reynolds et al. 2002) from 1983 to 2018. To estimate the mean temperature anomaly for Southern California Bight region, we used satellite observations between 29°–38°N and 115°–124°W.

Results

The ONI data indicate that a strong El Niño event followed La Niña in 2015 (Figure 2.1). Generally, the ONI index data were significantly correlated with positive temperature anomalies at our MICRO site ($R_{pearson}$ = 0.38, p < 1e-16) and more broadly in the SCB ($R_{pearson}$ = 0.44, p < 1e-22). In support, El Niño periods including the 2015 event led to positive temperature anomalies of >2°C. One notable disconnect between ONI and the temperature anomalies at MICRO and in SCB was the period following the El Niño 2015 event. Here, ONI suggested a slightly negative anomaly and La Niña conditions. However, SCB and our site still experienced strong positive temperature anomalies. This positive anomaly occurred during both the summer and winter periods and might be related to an unusually high temperature in the North Eastern Pacific Ocean (Di Lorenzo & Mantua 2016). Thus, the 2015 El Niño event led to a positive temperature anomaly in SCB and MICRO, but the period following was unexpectedly warm.

To understand the impact of El Niño conditions on the composition of marine POM, we quantified weekly macronutrient concentrations, POM concentrations, and elemental stoichiometric ratios from the beginning of 2012 to the end of 2017. Temperature oscillated annually with a peak in August and trough in January (Figure 2.2A). In 2015, the average annual temperature was higher than any other year at 22.4°C, peaking to 23.7°C (Figure 2.2A). As described earlier, nutrient availability showed a strong seasonal anti-correlation with temperature (Martiny et al. 2016) as well as some annual differences (Figure 2.2B). Nitrate concentrations also oscillated in parallel with phosphate and reached extremely low or undetectable levels during the summer (Figure 2.2C). In 2015, the nitrate level did not appear particularly low and stayed in detectable ranges through most of the year. POM concentrations all peaked during the spring bloom period and oscillated annually (Figure 2.2D–F). POC and POP concentrations did not show any consistent long-term trends, whereas PON levels declined 26% throughout the time-series. Although a slight increasing trend in C:N appeared from the start of the time series, a clear increasing trend was obvious after 2014 (Figure 2.2G). Annually, C:P peaked during the summer/fall at ~140 although we saw a big spike during the winter of 2014–2015 but this was not an annually re-occurring phenomenon (Figure 2.2H). N:P followed the annual oscillation in C:P with high values of 20 in the summer and also spiked during the same time periods (Figure 2.2I). Overall, we detected both seasonal and annual variation in both environmental conditions and POM concentrations and ratios.

The MICRO study site experienced long-term shifts in oceanographic conditions (Figure 2.3). Seasonally detrended temperature concentrations have an increasing trend during the sampling period (Figure 2.3A). Macronutrient and POM concentrations have a

slight decreasing trend, whereas the C:N and C:P ratios have increasing trends. The strongest positive correlations seen in the seasonally detrended data is POC and PON with POP demonstrating that the POM concentrations are linked (Figure 2.3B). Temperature is positively correlated with macronutrient and POM concentration and negatively correlated with stoichiometric ratios (Figure 2.3B). Thus, temperature is most likely the leading contributor to overall trends seen throughout the time series.

We sought to quantify the amount of variability for environmental conditions, POM concentration, and ratio that is attributable to monthly versus annual variance. In general, we found that monthly variability explained a higher proportion of variance in environmental metrics and POM concentrations than yearly variability (Figure 2.4). For temperature, monthly variability explained a large fraction of the total variance, representing over 60% of the variance. Monthly variability in nitrate and phosphate were the second and third highest proportion of variance explained among the environmental conditions. In contrast, yearly variability explained less than 10% of variance in temperature, nitrate, and phosphate. Similar to temperature and nutrients, monthly variability is greater among POM concentrations. As POM concentrations generally cycle in unison, there was less monthly variance in POM ratios. In contrast, we saw a larger proportion of variance in POM ratios between years. Monthly variation has more control on the environmental conditions and POM concentrations, whereas annual processes dominated for stoichiometric ratios. Thus, we should expect that POM stoichiometric ratios will be sensitive to El Niño events.

Impact of the 2015 El Niño Event

The 2015 El Niño event had some impact on the POM concentrations and ratios at MICRO (Figure 2.5). Temperature was highest in 2015, 15.9°C (Figure 2.5A). The phosphate concentration was 0.15 µM lower than in 2015 compared to 2012, although 2016 had lowest levels with a change of 0.16 µM (Figure 2.5B). However, nitrate concentrations were not particularly low that year and both 2014 and 2017 had lower levels (Figure 2.5C). POM concentrations showed divergent annual trends. POC showed a decrease of 4.7 and 3.1µM in 2014 and 2015 compared to 2012. PON also decreased during these years by 0.8 and 0.9µM, respectively. Both POC and POP displayed low levels in 2014 and 2015, which could be indicative of an El Niño effect. In contrast, PON showed a declining trend throughout the sampling period leading to a 26% drop in concentration (Figure 2.5E). The change in PON coincided with a continually rising C:N and a high average ratio of 9.4 in 2017 (Figure 2.5G). In contrast, C:P and N:P were at their highest in late 2014 and all of 2015 (Figure 2.2H,I). Thus, it appeared that the C:P and N:P were sensitive to the 2015 El Niño event, whereas C:N showed a divergent long-term increase.

Discussion

Our time-series data suggest that the 2015 El Niño event impacted SST, phosphate conditions, POM concentrations, and stoichiometric ratios in our study region. The El Niño event resulted in unusually high temperature conditions and lower phosphate concentrations. Such environmental conditions are starting to resemble open-ocean conditions although the POM concentrations are still much higher than common oligotrophic regions. The high C:P and N:P ratios during the El Niño event support our hypothesis although the underlying drivers are unclear. Due to the strong seasonal and

annual links between temperature, phosphate and phytoplankton community at our site, we are unable to identify the exact mechanism resulting in high C:P and N:P.

The C:N ratio appeared to be regulated by different processes than C:P and N:P. At our study site, we saw a long-term decline in PON concentration that led to high C:N. We hypothesize that the observed trend in C:N is regulated by an overall N limitation, shown by the declining nitrate supply (Geider & Roche 2002; Moreno & Martiny 2018). The nitrate concentration followed a different multi-year trajectory in comparison to phosphate and temperature leading to lower nitrate concentrations in later years. It is unclear if changing nitrogen, i.e., nitrate and ammonium; levels were driven by differences in nutrient run-off or by offshore shifts in source water and upwelling strength. In 1998, the Santa Ana Regional Water Quality Control Board started regulating nitrogen run-off near our study site. This regulation has led to a decline in terrestrial nitrogen inputs (French et al. 2006). Furthermore, shifts in the source water for the SCB has led to declining phosphate:nitrate levels in subsurface waters (at the σ_θ = 26.5 kg m^3 isopycnal surface; Bograd et al. 2014). Thus, there could be multiple ultimate causes for the observed declining nitrate level, but we predict that lower nitrate availability and plankton N stress has proximately led to higher C:N ratios.

We expect that the observed correspondence between changing environmental conditions and C:N:P are at least in part driven by shifts in phytoplankton community composition and physiological state. Our past work has demonstrated that increasing temperature and declining nutrient availability as observed during the El Niño event lead to increasing abundance of picophytoplankton lineages at the expense of larger eukaryotic phytoplankton (Martiny et al. 2016). Several studies have suggested that smaller

phytoplankton lineages have higher C:P and N:P ratios (Klausmeier et al. 2004). Furthermore, phytoplankton will acclimate to increasing temperature and lower nutrient availability leading to higher cellular carbon-to-nutrient ratios. Both mechanisms could possibly explain the elevated C:P and N:P seen in late 2014 and 2015 but our data does not allow for a direct identification of the underlying mechanism controlling the shift in POM stoichiometry.

El Niño events can vary in their expression leading to unique impacts on the environmental conditions and biogeochemical functioning of the SCB (Capotondi et al. 2015; Jacox et al. 2016). The 2015 event is likely an 'Eastern Pacific' type leading to a temperature anomaly in the North Eastern Pacific Ocean (Paek et al. 2017). However, there was also a strong temperature anomaly in the equatorial section of the Pacific and a high overall warming of most of the eastern part of the basin. As such, the biogeochemical impact of the 2015 El Niño event may diverge from a traditional 'Central Pacific' event. In addition to the El Niño event, we also saw a strong positive temperature and negative nitrate anomaly in 2016 and 2017. Such a long term warming of the region may be caused by a shift in the Pacific Decadal Oscillation (PDO; Newman et al. 2016). A positive PDO leads to overall high temperatures in the central/eastern part of the Pacific Ocean (Mantua et al. 1997) and a >2°C temperature anomaly in the SCB. The underlying physical driver of the PDO is currently not clear but a shift in the phase could suggest elevated temperatures in the SCB for years to come. This would further lead to low POM concentrations but high C:nutrient ratios.

El Niño events can act as a natural 'experiment' to understand climate change effects on POM concentrations and stoichiometric ratios. Future climate scenarios predict

increased SST and more stratified waters, and El Niño events share these characteristics. Due to the offshore topography at MICRO, the local conditions share similarities with pelagic waters rather than typical coastal regions. Thus, our findings suggest that elevated temperature cause changes in phytoplankton ecology with clear implications for POM concentrations and ratios. However, it is unclear whether or not future El Niño events will superimpose on or blend into the already high ocean temperatures in the region. If the former, we predict large changes in the biogeochemical and ecosystem functioning of the SCB in the future.

References

Bograd SJ, Pozo M, Di E, Castro CG, Schroeder ID, et al. 2014. Changes in source waters to the Southern California Bight. *Deep. Res. Part II*. 1–11

Capotondi A, Wittenberg AT, Newman M, Di Lorenzo E, Yu JY, et al. 2015. Understanding enso diversity. *Bull. Am. Meteorol. Soc.* 96(6):921–38

Chavez FP. 2002. Biological and chemical consequences of the 1997-1998 El Niño in central California waters Biological and chemical consequences of the 1997 – 1998 El Nin ˜ o in central California waters. *Prog. Oceanogr.* 54:205–32

Checkley DM, Barth JA. 2009. Progress in Oceanography Patterns and processes in the California Current System. *Prog. Oceanogr.* 83:49–64

Di Lorenzo E, Mantua N. 2016. Multi-year persistence of the 2014/15 North Pacific marine heatwave. *Nat. Clim. Chang.* 6(11):1042–47

Dijkstra HA, Burges G. 2002. Fluid Dynamics of El Nino Variability. *Annu. Rev. Fluid Mech.* (34):531–58

French C, Wu L, Meixner T, Kabashima J, Jury WA. 2006. Modeling nitrogen transport in the

Newport Bay / San Diego Creek watershed of Southern California. *Agric. Water Manag.* 81:199–215

Garcia NS, Bonachela JA, Martiny AC. 2016. Interactions between growth-dependent changes in cell size, nutrient supply and cellular elemental stoichiometry of marine *Synechococcus*. *ISME J*. 10(11):2715–24

Geider R, Roche J La. 2002. Redfield revisited: variability of C:N:P in marine microalgae and its biochemical basis Redfield revisited: variability of C:N:P in marine microalgae and its biochemical basis. *Eur. J. Phycol.* 37(September 2012):37–41

Huang B, Thorne PW, Banzon VF, Boyer T, Chepurin G, et al. 2017. Extended Reconstructed Sea Surface Temperature , Version 5 (ERSSTv5): Upgrades , Validations , and Intercomparisons. *Am. Meterological Soc.* 5:8179–8205

Jacox MG, Hazen EL, Zaba KD, Rudnick DL, Edwards CA, et al. 2016. Impacts of the 2015–2016 El Niño on the California Current System: Early assessment and comparison to past events. *Geophys. Res. Lett.* 43(13):7072–80

Karl DM, Tien G. 1992. MAGIC: A sensitive and precise method for measuring dissolved phosphorus in aquatic environments. *Limnol. Oceanogr.* 37(1):105–16

Kim H, Webster PJ, Curry JA. 2009. Impact of Shifting Patterns of Pacific Ocean Warming on North Atlantic Tropical Cyclones. *Science (80-.).* 325:77–80

King AL, Barbeau KA. 2011. Dissolved iron and macronutrient distributions in the southern California Current System. *J. Geophys. Res. Ocean.* 116(3):

Klausmeier CA, Litchman E, Levin SA. 2004. Phytoplankton growth and stoichiometry under multiple nutrient limitation. *Limnol. Oceanogr.* 49(4):1463–70

Knap AH, Michaels AF, Steinberg D, Bahr F, Bates NR, et al. 1997. BATS Methods Manual

Version 4. U.S. JGOFS Planning Office, Woods Hole

Lomas MW, Burke AL, Lomas DA, Bell DW, Shen C, et al. 2010. Sargasso Sea phosphorus biogeochemistry: an important role for dissolved organic phosphorus (DOP). *Biogeosciences*. 7(2):695–710

Mantua NJ, Hare SR, Zhang Y, Wallace JM, Francis RC. 1997. A Pacific Interdecadal Climate Oscillation with Impacts on Salmon Production. *Bull. Am. Meteorol. Soc.* 1069–79

Martiny AC, Pham CTA, Primeau FW, Vrugt JA, Moore JK, et al. 2013a. Strong latitudinal patterns in the elemental ratios of marine plankton and organic matter. *Nat. Geosci.* 6(5):1–5

Martiny AC, Talarmin A, Mouginot C, Lee JA, Huang JS, et al. 2016. Biogeochemical interactions control a temporal succession in the elemental composition of marine communities. *Limnol. Oceanogr.* 61(2):531–42

Martiny AC, Vrugt JA, Primeau FW, Lomas MW. 2013b. Regional variation in the particulate organic carbon to nitrogen ratio in the surface ocean. *Global Biogeochem. Cycles*. 27(3):723–31

Mcgowan JA, Cayan DR, Dorman LM. 1998. Climate-Ocean Variability and Ecosystem Response in the Northeast Pacific. *Science (80-.).* 281:

McPhaden MJ. 2015. Playing hide and seek with El Niño. *Nat. Clim. Chang.* 5(9):791–95

Moreno AR, Martiny AC. 2018. Ecological stoichiometry of ocean plankton. *Ann. Rev. Mar. Sci.* 10(1):43–69

Newman M, Alexander MA, Ault TR, Cobb KM, Deser C, et al. 2016. The Pacific Decadal Oscillation, Revisited. *Am. Meterological Soc.* 29:4399–4427

Paek H, Yu JY, Qian C. 2017. Why were the 2015/2016 and 1997/1998 extreme El Niños

different? *Geophys. Res. Lett.* 44(4):1848–56

Pomeroy LR, Wiebe WJ, Deibel D, Thompson RJ, Rowe GT, Pakulski JD. 1991. Bacterial responses to temperature and substrate concentration during the Newfoundland spring bloom. *Mar. Ecol. Prog. Ser.* 75(2–3):143–59

Racault M-F, Sathyendranath S, Brewin RJW, Raitsos DE, Jackson T, Platt T. 2017. Impact of El Niño Variability on Oceanic Phytoplankton. *Front. Mar. Sci.* 4(May):1–15

Redfield AC. 1958. The biological control of the chemical factors in the environment. *Am. Sci.* 46(3):1–18

Reynolds RW, Rayner NA, Smith TM, Stoker DC, Wang W. 2002. An Improved In Situ and Satellite SST Analysis for Climate. *J. Clim.* 15:1609–25

Sharp JH. 1974. Improved analysis for "particulate" organic carbon and nitrogen from seawater. *Limnol. Oceanogr.* 19(6):984–89

Sterner RW, Elser JJ. 2002. *Ecological Stoichiometry: The Biology of Elements from Molecules to the Biosphere*. Princeton, NJ: Princeton University Press

Tegner MJ, Dayton PK. 1987. El Nino Effects on Southern California Kelp Forest Communities. *Adv. Ecol. Res.* 17:243–79

Toseland A, Daines SJ, Clark JR, Kirkham A, Strauss J, et al. 2013. The impact of temperature on marine phytoplankton resource allocation and metabolism. *Nat. Clim. Chang.* 3(11):979–84

Yu JY, Zou Y, Kim ST, Lee T. 2012. The changing impact of El Nio on US winter temperatures. *Geophys. Res. Lett.* 39(15):

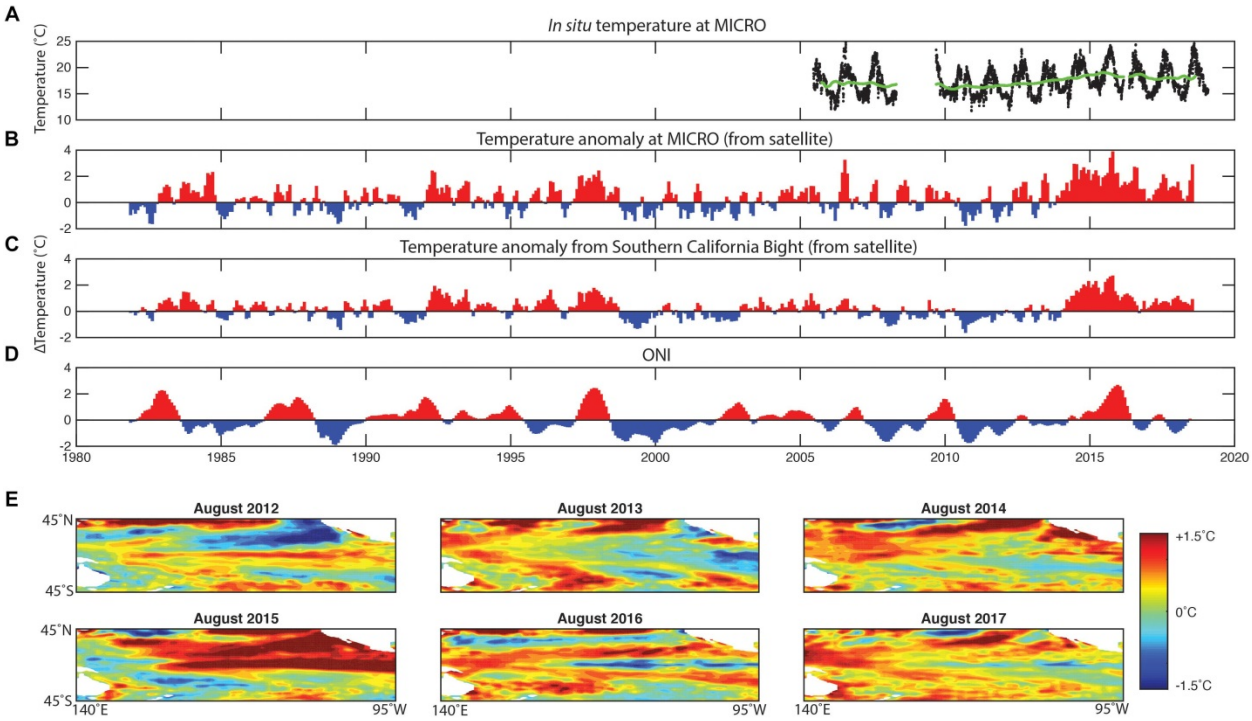

Figure 2.7 Multi-year variation in temperature at MICRO and surrounding region. (A) The in situ daily temperature from 2005 to 2018 from the SCCOOS station on Newport Pier and the 2-year moving average (green line). (B) The temperature anomaly at the MICRO time-series (estimated from satellite). (C) The temperature anomaly in the Southern California Bight. (D) Oceanographic El Niño Index (ONI). (E) Central Pacific Ocean temperature anomaly for August throughout the time-series.

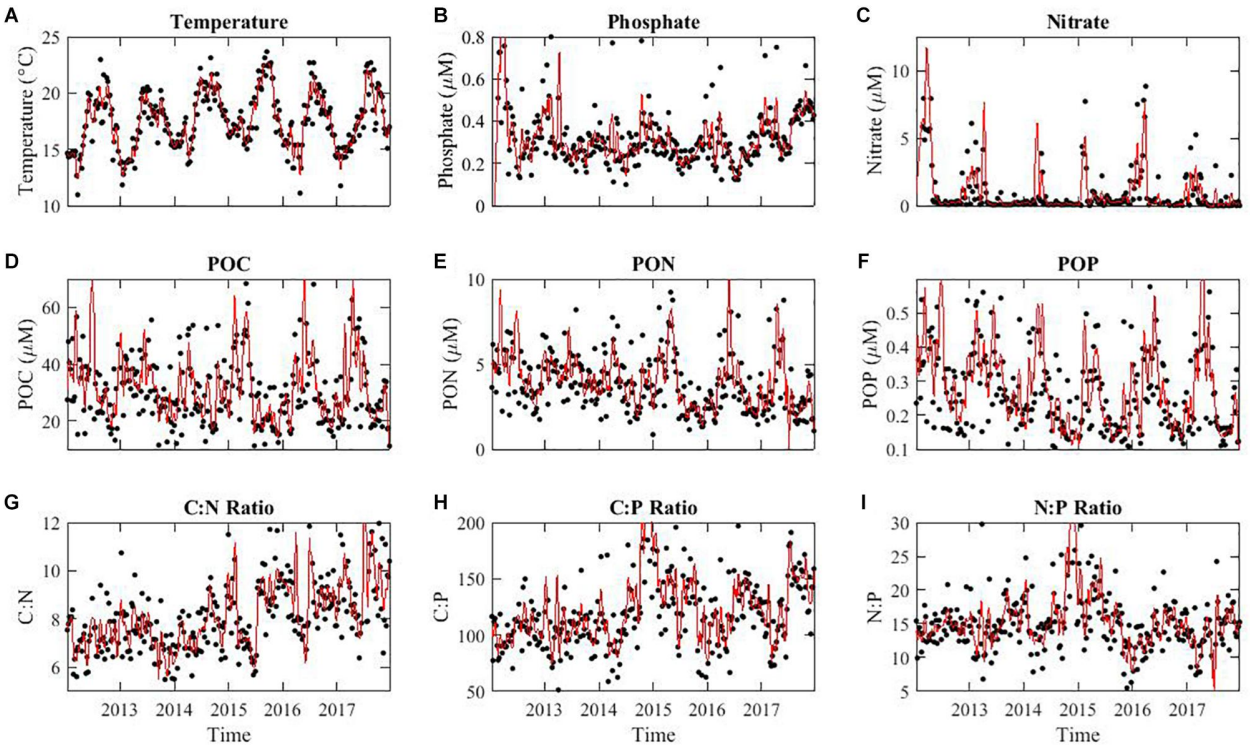

Figure 2.8 Environmental conditions (A), macronutrient concentrations (B, C), POM concentrations (D–F), and elemental stoichiometric ratios (G–I) over time at MICRO study site in Newport Pier, Newport, CA. The solid black points represent the averaged data per week from the period of 1/1/2012 to 12/31/2017. The red line represents a 4-point moving average. Stoichiometric ratios are molar.

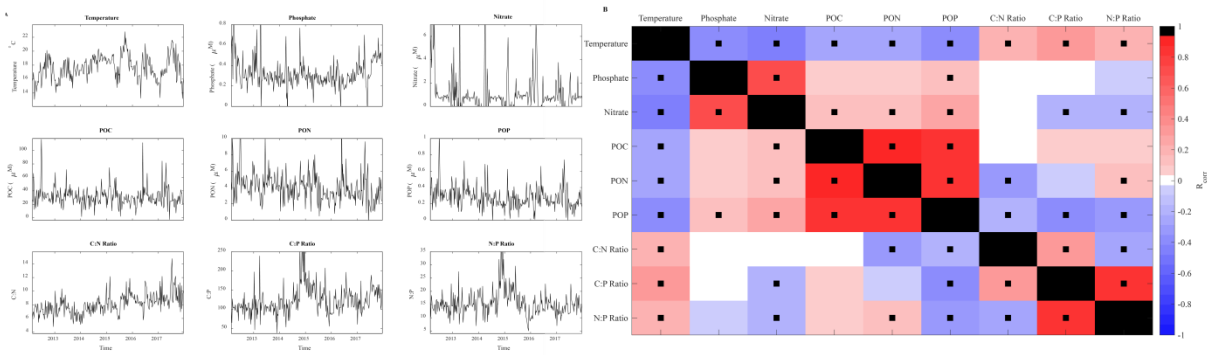

Figure 2.9 Seasonally detrended values and correlations in environmental conditions, macronutrients concentrations, POM concentrations, and stoichiometric ratios. (A) Detrended seasonal data over time for each factor. Statistical trends quantified using a Mann-Kendal analysis ($p < 0.05$). (B) Pearson correlation coefficient for each pair of factors. Redder squares signify a strong positive correlation between the two variables, while blue squares signify a strong negative correlation between the two variables. Large black squares represent a correlation of 1. The small black squares indicate that the correlation is statistically significant.

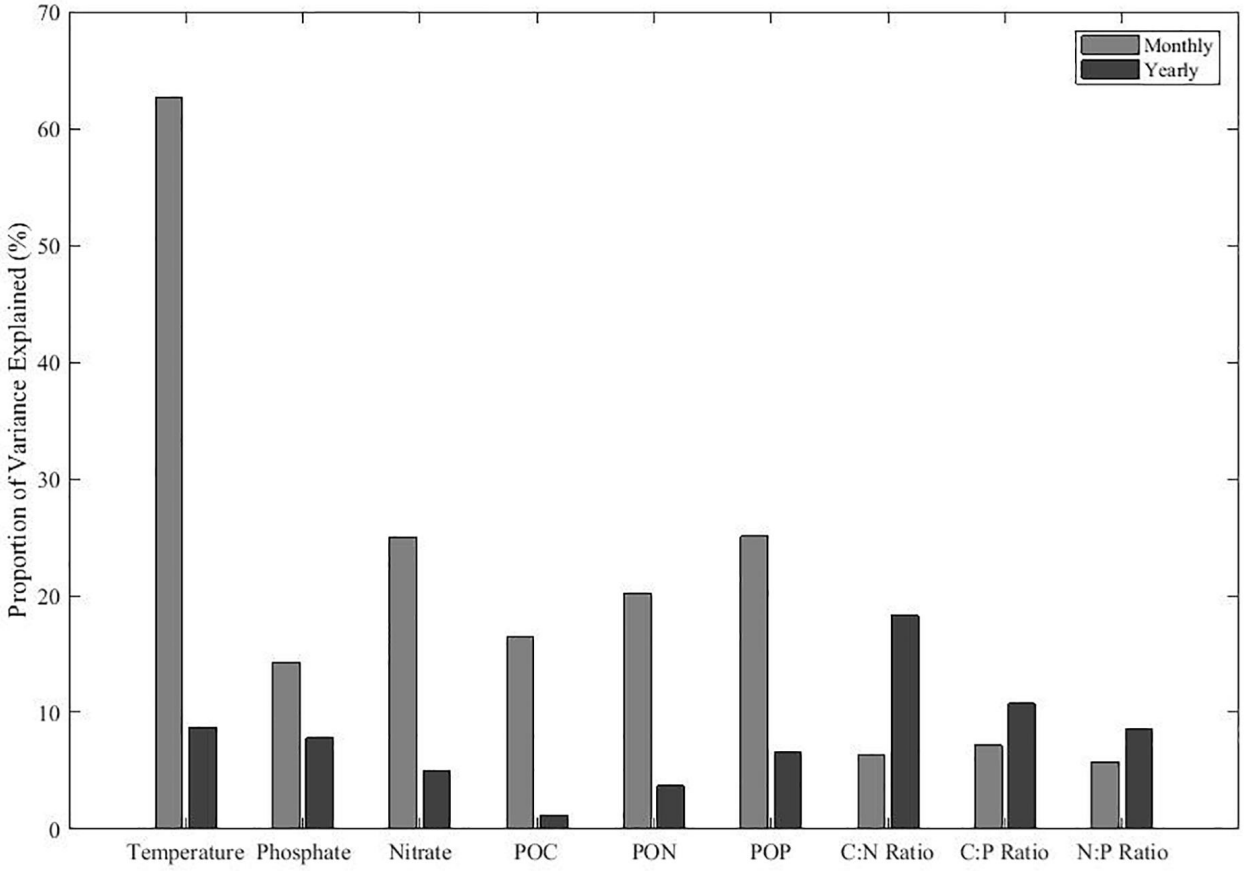

Figure 2.10 The contribution of monthly and annual variation for environmental conditions and POM concentrations and ratios. The remaining variance represents variance associated with short-term events and measurement errors. Proportions are calculated using the sum of squares from the linear regression data shown in Figure 2.5.

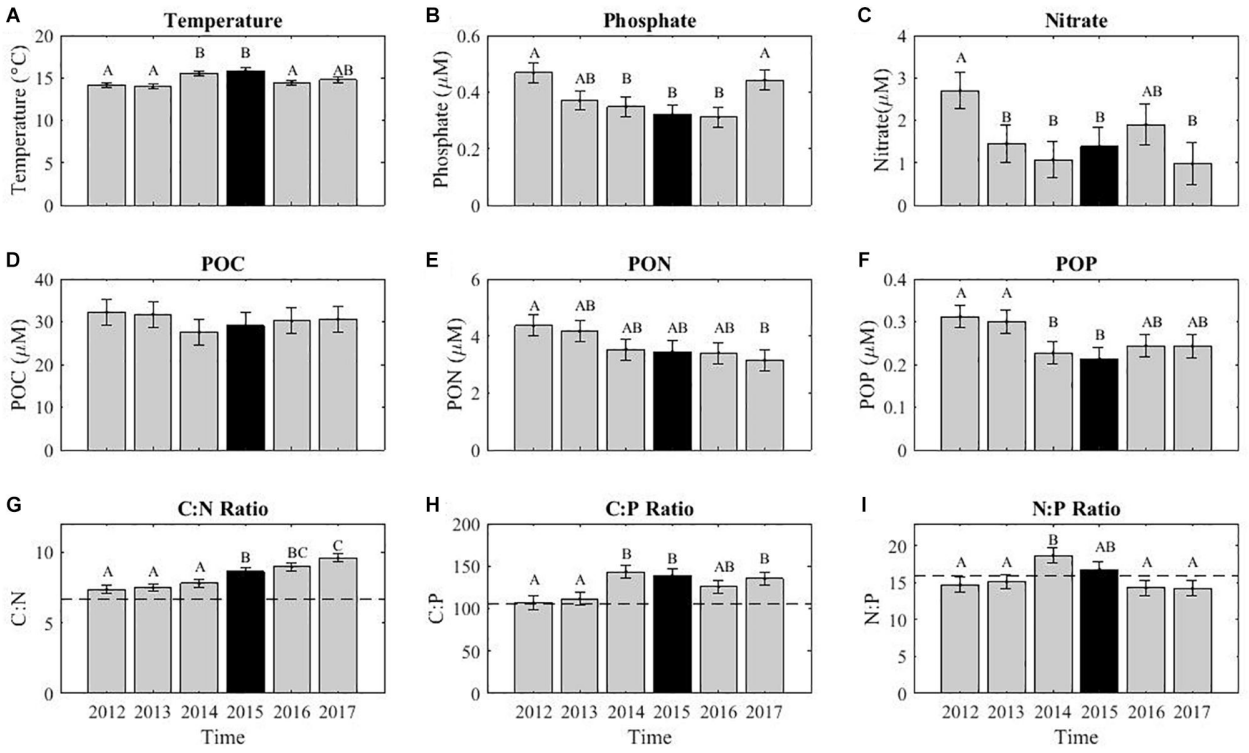

Figure 2.11 The average annual variability in environmental conditions (A–C), POM concentrations (D–F), and stoichiometric ratios (G–I). The annual variations in August quantified using a linear decomposition of annual and monthly variation. Error bars represent the standard deviation. The letters above each bar represent a post hoc Tukey multiple comparison test ($p < 0.05$), where similar letters show no statistical difference. The dashed lines across the stoichiometric ratios indicates the static Redfield ratio (C:N = 6.6, C:P = 106, and N:P = 16), strictly used for comparison purposes.

CHAPTER 3

Marine phytoplankton stoichiometry mediates nonlinear interactions between nutrient supply, temperature, and atmospheric CO_2

Abstract

Marine phytoplankton stoichiometry link nutrient supply to marine carbon export. Deviations of phytoplankton stoichiometry from Redfield proportions (106C:1P) could therefore have a significant impact on carbon cycling, and understanding which environmental factors drive conditions, stoichiometry, and carbon cycling, we compared four different models of phytoplankton C:P: a fixed Redfield model, a model with C:P given as a function of surface phosphorus concentration (P), a model with C:P given as a function of temperature, and a new multi-environmental model that predicts C:P as a function of light, temperature, and P. These stoichiometric models were embedded into a five-box ocean circulation model, which resolves the three major ocean biomes (high-latitude, subtropical gyres, and tropical upwelling regions). Contrary to the expectation of a monotonic relationship between surface nutrient drawdown and carbon export, we found that lateral nutrient transport from lower C:P tropical waters to high C:P subtropical waters could cause carbon export to decrease with increased tropical nutrient utilization. It has been hypothesized that a positive feedback between temperature and $pCO_{2,atm}$ will play an important role in anthropogenic climate change, with changes in the biological pump playing at most a secondary role. Here we show that environmentally driven shifts in stoichiometry make the biological pump more influential, and may reverse the expected positive relationship between temperature and $pCO_{2,atm}$. In the temperature-only model, changes in tropical temperature have more impact on the $\Delta pCO_{2,atm}$ (41 ppm) compared to

subtropical temperature changes (4.5 ppm). Our multi-environmental model predicted a decline in $pCO_{2,atm}$ of 46 ppm when temperature spanned a change of 10°C. Thus, we find that variation in marine phytoplankton stoichiometry and its environmental controlling factors can lead to nonlinear controls on $pCO_{2,atm}$, suggesting the need for further studies of ocean C:P and the impact on ocean carbon cycling.

Keywords: Redfield ratio, traits, carbon cycling

Introduction

The discovery of large-scale deviations of phytoplankton stoichiometry from the Redfield ratio in the past decade (Martiny et al. 2013b,a; Weber & Deutsch 2010) has significant consequences for our understanding of the biological carbon pump and global carbon cycling (Galbraith & Martiny 2015; Moreno & Martiny 2018). Traditionally, the biological pump is thought to be controlled by a combination of the vertical nutrient flux and nutrient utilization efficiency (Sarmiento & Toggweiler 1984). Evidence that elemental stoichiometry is variable thus adds a new dimension to the biological pump, and may lead to higher than currently expected carbon export in subtropical regions (Emerson 2014; Tanioka & Matsumoto 2017; Teng et al. 2014). Global carbon export has been estimated to range between 5 and 12 Pg C yr^{-1} (Boyd & Trull 2007; Henson et al. 2011), but these projections have yet to incorporate the environmental controls on $C:P_{export}$. Variation in $C:P_{export}$ from Redfield proportions can be linked to environmental conditions. There are two leading environmental parameters thought to control $C:P_{export}$: nutrients, predominantly phosphate concentrations, and temperature. Galbraith and Martiny used a simple three-box model to show that variable stoichiometry driven by phosphate availability could enhance the efficiency of the biological pump in the low-latitude ocean

(Galbraith & Martiny 2015). In contrast, Yvon-Durocher et al. (2015) used a meta-analysis of global temperature and stoichiometric ratios to propose that C:P increased 2.6-fold from 0 to 30°C. Thus, it is unclear if differences in nutrient supply or temperature, or some combination of them, control the global variation in C:P of plankton and exported material.

There are two important ingredients missing from published studies that could alter the interactions among phytoplankton stoichiometry, carbon export, and atmospheric pCO_2 ($pCO_{2,atm}$). The first is the presence of two distinct low-latitude biomes, namely the equatorial upwelling regions and the macronutrient-depleted subtropical gyres. In direct observations and inverse model analyses, these two biome types appear to have unique elemental compositions (DeVries & Deutsch 2014; Martiny et al. 2013a; Teng et al. 2014). Thus, in order to properly represent global variations in surface plankton C:P and carbon export, it is essential to separately model macronutrient-limited subtropical gyres and equatorial upwelling zones.

The second missing ingredient is that environmental factors beyond nutrient availability may impact the elemental composition of surface plankton $C:P_{export}$. Temperature, irradiance, and nutrient concentrations are all important environmental factors, which influence the physiology and stoichiometry of phytoplankton. However, surveys of phytoplankton C:P are insufficient to distinguish the separate effects of each factor on C:P due to strong environmental covariance. Cellular trait-based models use detailed studies of phytoplankton physiology to determine how phytoplankton cells should allocate their resources as a function of environmental conditions, allowing us to model the interactive influence of temperature, nutrient concentrations, and irradiance on C:P ratios (Clark et al. 2011; Daines et al. 2014; Shuter 1979; Talmy et al. 2014; Toseland et al. 2013).

Numerous physiological mechanisms have been proposed to explain variation in phytoplankton stoichiometry, including growth rate (Sterner & Elser 2002), photoacclimation (Falkowski & LaRoche 1991; Geider et al. 1996; Leonardos & Geider 2004, 2005), nutrient-limitation responses (Garcia et al. 2016; Goldman et al. 1979; Rhee 1978), and temperature (Rhee & Gotham 1981; Toseland et al. 2013; Yvon-Durocher et al. 2015). Through incorporation of such physiological responses, a trait-based model has revealed that differences in ribosomal content and cell size between warm-water, oligotrophic environments and cold-water, eutrophic environments are important mechanisms driving stoichiometric variation in the ocean (Daines et al. 2014). Thus, linking biome-scale variations in environmental conditions with a detailed trait-based model of phytoplankton resource allocation and elemental composition may enable us to more fully explore interactions among multiple ocean environmental factors, the biological pump, and $pCO_{2,atm}$.

Here, we create a five-box ocean circulation model, incorporating the three major ocean biomes, to study the feedback effects of variable stoichiometry on carbon export and $pCO_{2,atm}$. We will explicitly address the following research questions: (1) How does environmental variability influence marine phytoplankton cellular allocation strategies and in turn the elemental stoichiometric ratio? (2) What are the effects of changing environmental conditions on stoichiometric ratios, carbon export, and $pCO_{2,atm}$? (3) What is the influence of the environmental conditions among the three major surface biomes on carbon export and $pCO_{2,atm}$?

Methods

Box model design

To quantify the feedbacks between phytoplankton stoichiometry, carbon export, and $pCO_{2,atm}$, we formulated a five-box ocean circulation model of the phosphorus and carbon cycles in the ocean coupled to an atmospheric box. The foundation of our model is based on the models introduced in Ito and Follows (2003) and DeVries and Primeau (2009). Phosphorus is used to represent the role of nutrient availability in controlling stoichiometry and C export. We chose this over N because, on long timescales, P is commonly considered the ultimate limited nutrient, whereas N is only limiting productivity and export on short timescales (Tyrrell 1999). On long timescales, nitrogen fixation/denitrification will presumably adjust the N inventory. Our modeling is focused on long-term steady-state outcomes and we would like to avoid issues associated with modeling the N cycle (like getting N-fixation and denitrification rates correct). Thus, we chose to use P as a representative for nutrient availability at long-term steady-state biogeochemical equilibrium. The model includes three surface boxes, each corresponding to one of the major biomes: the tropical equatorial upwelling regions (labeled T), the subtropical gyres (labeled S), and the high-latitude regions (labeled H) (Figure 3.1). We define the oligotrophic subtropical gyre regions where the mean annual phosphate concentration is less than 0.3 μM (Teng et al. 2014), with the remainder of the surface ocean assigned either to box T or box H based on latitude. We use these assignments to calculate the baseline physical properties of each region, including mean annual averaged irradiance and temperature. The subsurface ocean is divided into two regions: the thermocline waters that underlies the subtropical gyres and the equatorial upwelling regions (labeled M), and deep waters (labeled D) (DeVries & Primeau 2009).

To simulate the global transport of water between boxes, our model includes a thermohaline circulation (T_c) that upwells water from the deep ocean into the tropics, laterally transports water into the subtropics and high latitudes, and downwells water from the high-latitude region to the deep ocean. Surface winds produce a shallow overturning circulation (T_w) that transports water from the thermocline to the tropics and then laterally into the subtropics. These circulations create teleconnections of nutrient supply in the surface ocean boxes. A bidirectional mixing term that ventilates the deep box directly through the high-latitude surface box (*fhd* represents deep water formation in the North Atlantic region and around Antarctica (Sarmiento & Toggweiler 1984). The parameters T_c, T_w and *fhd* are considered adjustable parameters, which we calibrate using phosphate data from WOA13 (Garcia et al. 2014a). In order to simulate the movement of particles, we included export fluxes (*Pt*, *Ps*, and *Ph*) of organic phosphorus out of each surface box. The conservation equations of phosphorus are as follows:

$$\frac{dP_T}{dt} = \frac{(P_M - P_T) \cdot Tc + (P_M - P_T) \cdot Tw - (a + b) \cdot Pt}{VT} \quad (1)$$

$$\frac{dP_S}{dt} = \frac{(P_T - P_S) \cdot Tc + (P_T - P_S) \cdot Tw - (a + b) \cdot Ps}{VS} \quad (2)$$

$$\frac{dP_H}{dt} = \frac{(P_S - P_H) \cdot Tc + (P_D - P_H) \cdot fhd - Ph}{VH} \quad (3)$$

$$\frac{dP_M}{dt} = \frac{(P_D - P_M) \cdot Tc + (P_S - P_M) \cdot Tw + a \cdot Pt + a \cdot Ps}{VM} \quad (4)$$

$$\frac{dP_D}{dt} = \frac{(P_H - P_D) \cdot Tc + (P_H - P_D) \cdot fhd + Ph + b \cdot Pt + b \cdot Ps}{VD} \quad (5)$$

where P represents the concentration of phosphorus at a specific box, a represents 0.25 remineralization, b represents 0.75 remineralization, and V represents the volume of the specified box.

Our box model simulates P, alkalinity, and various forms of C; total carbon in the surface boxes is partitioned into carbonate, bicarbonate, and pCO_2. The global mean P is prescribed according to the observed mean value (Garcia et al. 2014a). The export of carbon is linked to phosphorus export using the $C:P_{export}$ ratio. To quantify the breakdown of carbon into these components, we model the solubility pump, using temperature and salinity to determine the partitioning of inorganic carbon among total carbon within a box. The global mean alkalinity is prescribed according to the observed mean ocean values but is also subject to transport (Sarmiento & Toggweiler 1984). Our box model simulates alkalinity and total inorganic carbon, which are conserved tracers from which the speciation of inorganic carbon in seawater can be calculated. Biome-specific salinity and temperature are used to prescribe the solubility constants of CO_2 in seawater and the bromine concentration, which is taken to be proportional to salinity. CO_2 cycles through the atmosphere via the air-sea gas exchange fluxes (*fah*, *fas*, *fat*). We use a uniform piston velocity of 5.5 x 10^{-5} m s^{-1} to drive air-sea gas exchange (DeVries & Primeau 2009; Follows et al. 2002). Quantifying the atmospheric concentration of carbon satisfies:

$$\frac{dC_A}{dt} = [(C_T - C_A) \cdot SolT(temp, sal) \cdot fat + (C_S - C_A) \cdot SolS(temp, sal) \cdot fas +$$

$$(C_H - C_A) \cdot SolH(temp, sal) \cdot fah]/\mathrm{VA} \quad (6)$$

where C represents the concentration of total carbon in a specific box and Sol is the solubility constant in a specified box, calculated from temperature (temp) and salinity (sal).

We calibrated our model parameters (T_c, T_w, *fhd*) so that the macronutrients were at similar average values compared to World Ocean Atlas 2013 dataset for each location. We tested the sensitivity of modeled $p\mathrm{CO}_{2,\mathrm{atm}}$ to the fluxes T_c, T_w, and *fhd* and found that with T_c = 20 Sv and T_w = 5Sv (values that allowed the model to match P and alkalinity), $p\mathrm{CO}_{2,\mathrm{atm}}$ was sensitive to the value of *fhd* (Sarmiento & Toggweiler 1984). Guided by values previously used in the literature, we set *fhd* to 45.6 Sv (Table 3.1) but we also present results for thue nutrient-only stoichiometry model at two extreme values of *fhd* (18 and 108 Sv) (Figure 3.2). The functional dependence of $p\mathrm{CO}_{2,\mathrm{atm}}$ with changing subtropical and tropical P for each extreme value of *fhd* was quite similar, though the value of $p\mathrm{CO}_{2,\mathrm{atm}}$ for the high-*fhd* simulation (Figure 3.2). We found that our value of 45.6 Sv provides a modern $p\mathrm{CO}_{2,\mathrm{atm}}$ value. Although the focus of this study is to determine the impact of low-latitude biogeochemistry on $p\mathrm{CO}_{2,\mathrm{atm}}$, we point out that at Redfield stoichiometry, $p\mathrm{CO}_{2,\mathrm{atm}}$ increases by 100 ppm when *fhd* increased from its default value 45.6 to 108 Sv. For certain values of the parameters, the model produced excessive nutrient trapping in the thermocline. In order to dampen the nutrient trapping, we tuned the remineralization depth. As such, 25% of the total export is respired in the thermocline, with the remaining 75% exported into the deep ocean, leading to a better match between the modeled and observed P in the thermocline box.

Stoichiometric models

To quantify and understand the feedbacks between carbon export and $pCO_{2,atm}$, we embedded four stoichiometric models into our five-box ocean circulation model. Each model differs according to its complexity and how much environmental information they utilize. These are a static Redfield model that assumes that $C{:}P_{export}$ is constant across environmental conditions, a nutrient-only model that uses surface P to predict $C{:}P_{export}$ (from Galbraith and Martiny, 2015) a temperature-only model that uses T to predict $C{:}P_{export}$ (modified from Yvon-Durocher et al., 2015) and a multi-environmental model that uses light, T, and P to predict $C{:}P_{export}$.

Static Redfield model

Our control model uses a static Redfield stoichiometry. The Redfield ratio is based on an average value of organic carbon to phosphorus of 106:1.

Nutrient-only model

The nutrient-only stoichiometric model expressed phytoplankton C:P as a function of the ambient phosphate concentration:

$$C{:}P = \frac{1}{\kappa[P] + [\mathrm{P}]_0} \quad (7)$$

where the parameters κ = 6.9 x $10^{-3}\mu M^{-1}$ and $[\mathrm{P}]_0$ = 6.0 x10^{-3} were obtained by regressing the reciprocal of C:P onto P (Galbraith & Martiny 2015).

Temperature-only model

The temperature-only stoichiometric model expresses phytoplankton C:P as a function of temperature:

$$ln(C{:}P) = \Pi(T - 15°C) + b, \quad (8)$$

where the parameters Π = 0.037°C^{-1} and b = 5.5938 (Yvon-durocher et al. 2015). The temperature-only model was created to determine the temperature responses of log-transformed C:P ratios centered at 15°C.

Multi-environmental model

We created a multi-environmental model, which predicts how cell size, biomass allocations to biosynthesis and photosynthesis, and C:P ratios vary with temperature, light levels, temperature, and phosphorus concentrations. The multi-environmental factor model was derived from a non-dynamic physiological trait-based model. We used a theoretical cellular-allocation trait model based on phytoplankton physiological properties that divides the "cell" into several functional pools which represent cellular investments in biosynthesis, photosynthesis, and structure, and a storage pool, which represents variations in the level of P-rich molecules such as polyphosphates (full model equations can be found on GitHub: https://github.com/georgehagstrom/-bg-2017-367/blob/master/CP.m, last access: 12 April 2018). The functional pools are composed of biological macromolecules such as ribosomes, proteins, carbohydrates, and lipids. The model predicts the size of each pool as a function of light, *T*, and P. The size of each functional pool is modeled by using subcellular resource compartments, which connect the fitness of a hypothetical phytoplankton cell in a given environment to its cellular radius and the relative allocation of cellular material to photosynthetic proteins, ribosomes, and biosynthetic proteins. We assume that real phytoplankton populations have physiological behaviors that cluster around the strategy that produces the fastest growth rate in each environment (Norberg et al. 2001), and use the stoichiometry of this optimal strategy to model the elemental composition of cellular material (Figure 3.1).

Phytoplankton can accumulate large reserves of nutrients that are not immediately incorporated into the functional components of the cell (Diaz et al. 2016; Mino et al. 1998; Mouginot et al. 2015; Van Mooy & Devol 2008). This storage capability varies among phytoplankton species, and depends on the particular nutrient under consideration: the cost for storing physiologically relevant quantities of nutrients is low for nutrients with low quotas such as phosphorus, in comparison to nitrogen and carbon. Thus, the phosphorus storage is assumed highly plastic in comparison to carbon storage (Moore et al. 2013). Further, we assume that each cell dedicates a fixed fraction of its biomass to carbon reserves, and focus our modeling efforts on the variability of the stored phosphorus pool. To predict the size of the storage pool, we assume a linear relationship between stored and phosphorus and ambient environmental phosphorus levels and used statistical modeling of an oceanic C:P dataset (Martiny et al. 2014) to calculate the constant of proportionality . The result is a relatively simple model that both qualitatively and quantitatively predicts the variation of C:P in phytoplankton.

Phytoplankton physiology is modeled through allocations of cell dry mass to three distinct pools: structure ($S(r)$), biosynthesis (E), and photosynthesis (L) (Figure 2.3). Allocations satisfy

$$1 = S(r) + E + L, \tag{9}$$

where the variables S, E, and L represent the specific allocations of cellular biomass.

The specific allocation of biomass to the cell membrane is inversely proportional to the cell radius (Clark et al. 2011), which accounts for the changing relative volume of the cell membrane with radius. The structure pool includes the cell membrane plus wall and

other components (γ), which are not related to photosynthesis or biosynthesis and is given by:

$$S(r) = \frac{\alpha}{r} + \gamma. \tag{10}$$

In an environment specified by T, [P], and light level (I), the growth rate of a cell using a given strategy is the minimum of the following growth rates:

$$\mu = min(\mu_E, \mu_L, \mu_P). \tag{11}$$

Here μ_E is determined by the specific rate of protein synthesis, μ_L is determined by the specific rate of carbon fixation, and μ_P is determined by the specific rate of phosphorus uptake, or

$$\mu_E = k_E(T)E, \mu_L = \frac{f_P(L,I) - \Phi_M(T)}{1+\Phi_S}, \mu_P = \frac{1}{Q_P(r,E)} \frac{V_m(r)[P]}{K_P(r)+[P]}. \tag{12}$$

We assume that part of the energy captured by a cell via photosynthesis is used for maintenance (Φ_M), whereas the rest is used to drive the synthesis of new macromolecules (Φ_M), whereas the rest is used to drive the synthesis of new macromolecules (Φ_S), so that a cell growing at rate μ_L is in energy balance. The efficiency of biosynthesis k_E and the carbon cost of maintenance Φ_M are functions of T, whose dependence is modeled using Q_{10} = 2.0 (Broeze et al. 1978; Shuter 1979; Van Bogelen & Neidhardt 1990). Uptake is regulated by a Monod function with kinetic parameters depending on the radius through the allometric scaling relationships derived from measurements of phytoplankton populations (Edwards et al. 2012):

$$V_m(r) = a_P r^{b_P}, K_P(r) = a_K r^{b_K}. \quad (13)$$

This use of allometric scaling relationships departs from the conventions adopted by Shuter (1979) or Daines et al. (2014), who assume that uptake rates are diffusion-limited.

The phosphorus quota for functional elements of the cell (thus not including any storage) is determined by the allocation to biosynthesis E and the percentage p_{DNA} of cellular dry mass allocated to DNA:

$$Q_{p,biosynthesis}(E, r) = \frac{4}{3}\pi r^3 \rho_{\mathrm{cell}} p_{\mathrm{dry}} \frac{(\alpha_E E P_{\mathrm{rib}} + p_{\mathrm{DNA}} P_{\mathrm{DNA}})}{31}. \quad (14)$$

Here, we assume that there is no contribution to the functional-apparatus P quota from phospholipids, which instead are merged with storage molecules. This differs from Daines et al. (2014), who assumes that phospholipids, occupy 10% of the cell by mass. Phytoplankton can substitute sulfoquinovosdiaglycerol (SQDG) for phospholipids in their cell membranes under low P conditions (Van Mooy et al. 2009). Similarly, P storage molecules are also regulated by P availability. Thus, we treat phospholipids and P storage as one pool.

The function f_{P} is the cellular response to light levels and is chosen to capture the effects of both electron transport and carbon fixation on photosynthesis; it is also closely related to a previous model (Talmy et al. 2013). This prior model included four compartments: electron transport, carbon fixation, photoprotection, and biosynthesis. It was found that photoprotection allocation was not a large or greatly changing component of their allocations. We therefore do not include this within our model due to its high

complexity with little qualitative results. Our biosynthesis was also separately parametrized.

The decomposition of photosynthesis into light harvesting and carbon fixation components is critical and makes our model predictions agree much better with experiments studying the variations of C:P or N:P ratios with irradiance. Models that do not have their decomposition predict too large a decrease in cellular allocations to photosynthesis at high light levels. In a two-compartment model, increases in allocations to carbon fixation cause the overall allocation to light harvesting to have a more mild decrease. The two-compartment treatment also seems more physiologically realistic than a one-compartment treatment, which only models photosynthetic pigments. Thus, we used the functional forms and parameters that were derived (experimentally) previously for carbon fixation and light harvesting (Talmy et al. 2013).

Our model interprets light harvesting allocation, L, as being composed of proteins dedicated to carbon fixation (F_1), such as RuBisCO, and proteins dedicated to light harvesting (F_2), such as photosynthetic pigments. The rate of photosynthetic carbon fixation is a function of allocations to each of these, which satisfy $F_1 + F_2 = L$. The relative allocations together determine the overall photosynthetic rate:

$$P_{\max} = \min\left(k_1 F_{1,} k_2 F_2\right), f_p = P_{\max}\left(1 - exp\left(\frac{-\alpha_{\mathrm{ph}} \phi_M F_2 I}{P_{\max}}\right)\right). \qquad (15)$$

For a given I and L, there is a pair of values ($F_{1,\mathrm{opt}}$, $F_{2,\mathrm{opt}}$) that maximize the photosynthetic rate f_{P}. We estimate the photosynthetic rate $f_{\mathrm{P}}(L, I)$ under the assumption that cells assume the optimal allocations to carbon fixation and electron transport. Our model departs from the developed by Shuter (1979) and Daines et al. (2014), which

assume that energy acquisition is a linear function of light levels leading to functional responses linearly proportional to the cellular investment in light harvesting proteins.

We model photosynthesis as having Q_{10} = 1, which is consistent with physiological studies going back to Shuter (1979) that suggest that photosynthetic efficiency does not depend on temperature over physiologically relevant ranges. The discrepancy between photosynthetic and biosynthetic temperature dependence has traditionally been explained by referring to the differences in the chemistry and physics of the two processes. The electron transport chain relies on quantum mechanical processes, which are unaffected by variations in temperature in a physiologically relevant range (Devault 1980). Required maintenance respiration rates are also modeled as having a Q_{10} = 2.0 (Devault 1980). We model the phytoplankton community residing in a given environment by assuming it consists solely of the phytoplankton type using the highest growth rate strategy in that environment. This strategy is found by solving for the values of r and E and that make

$$\mu = \mu_L = \mu_P = \mu_E. \quad (16)$$

We will now show that under two assumptions that will be true in nearly any realistic situation, a strategy maximizing μ always exists, is unique, and satisfies $\mu = \mu_L = \mu_P = \mu_E$ (Figure 3.4). The function μ_L is a function of the chosen strategy (r, E), and it is an increasing function of r and decreasing function of E. The first assumption is that light levels are sufficiently high that there exists some r_{min} such that $\mu_L (r_{min}, 0) > 0$, which means that light is sufficient for some phytoplankton to be able to overcome maintenance costs. The function μ_P is a monotonically decreasing function of both r and E. As there is a non-zero amount of P contained in the structure pool, and because uptake rates decline to zero with r, there will be some r_{max} at which $\mu_P(r_{max},0) > 0$. The second assumption is that r_{min} <

r_{max}, which will be true for most realistic value of light levels. We note that fixed r, μ_E is a monotonically decreasing function of E. Since none of μ_E, μ_L, or μ_P have critical points, the function μ can only have a maximum at places where two or more of μ_E, μ_L, and μ_P are equal, or at the boundaries of the strategy space. On the boundaries of strategy space, $E = 0$ or $L = 0$ so that $\mu \leq 0$. We can exclude the boundary and focus on places where two or more μ_E, μ_L, and μ_P are equal. We define two curves: one on which $\mu_L = \mu_E$ and the other on which $\mu_E = \mu_P$. The curve for which $\mu_E = \mu_L$ begins at the point $r = r_{min}$ and can be described by a monotonically increasing function $E = g(r)$ on the interval $[r_{min}, \infty]$. This curve exists because $\mu_E = 0$ when $E = 0$, $\mu_L > 0$ when $E = 0$, so that there is always a solution to $\mu_L = \mu_E$ for fixed $r > r_{min}$. To see that the curve is an increasing function of r, consider the function $V(E,r) = \mu_L - \mu_E$ and apply the chain rule to the equation $V(g(r), r) = 0$ to find that along the curve $E = g(r)$:

$$\frac{dE}{dr} = g'^{(r)} = \frac{-\frac{\partial V}{\partial r}}{\frac{\partial V}{\partial E}}. \qquad (17)$$

We consider the terms in Eq. (17) carefully. The function V is an increasing function of r because μ_E is independent of r because μ_L is an increasing function of r (for a fixed investment in photosynthesis and greater photosynthetic growth rate). Thus, the numerator of Eq. (17) is negative. The function V is a decreasing function of E because μ_L is a decreasing function of E (greater investments in biosynthesis at fixed radius lead to smaller investments in photosynthesis) and μ_E is an increasing function of E. Thus the denominator of Eq. (17) is negative, and the quotient on the right-hand side is positive, so $g'(r)$ is positive and describes an increasing curve.

By similar logic, we can define a curve $h(r)$ that solves the equation $\mu_P(h,r) = \mu_E(h,r)$. This curve exists on the finite interval $[r_I, r_{max}]$, where r_I solves the equation $\mu_P(1 - S(r_I), r_I) = \mu_E(1 - S(r_I), r_I)$. Thus, $h(r)$represents a decrasing curve from the point $(1 - S(r_I), r_I)$ to $(0, r_{max})$. We can see that $h(r)$ is always decreasing by using the chain rule on $\mu_P(h, r) - \mu_E(h, r) = 0$, just as in the previous argument.

The growth maximizing strategy must occur somewhere on the curves described by $(g(r), r)$ and $(h(r), r)$. The functions $\mu_1(r) = \mu(g(r), r)$ and $\mu_2(r) = \mu(h(r), r)$ are continuously differentiable functions of r except where $g(r) = h(r)$ (which must exist by the intermediate value theorem). Therefore, the only place where μ can have a maximum is at the place where $g(r)$ and $h(r)$ intersect. This is the strategy that leads to equality of all the growth rates. We refer to this strategy, as a function of environmental conditions, as $\big(r_m(P, I, T), E_m(P, I, T), L_m(P, I, T)\big)$. Using this strategy, we can predict the stoichiometry of the functional components of the phytoplankton population in a given environment.

We assume that real phytoplankton populations cluster near the optimal strategy in the local environment (Norberg et al. 2001):

$$(E_m, r_m) = \text{argmax}_{(E,r)}\mu. \qquad (18)$$

For all values of environmental parameters used in this study, the unique maximum of the growth rate occurs for the set of parameter values that lead to co-limitation by nutrients, photosynthesis, and biosynthesis, analogously to the predictions of Klausmeier and co-workers (2004). The optimal strategy determines the model prediction of the C:P of functional components in a given environment by taking the quotient of the carbon and phosphorus quotas. The carbon quota is calculated as:

$$Q_C = \frac{\left(\frac{m_{lip}{}^{\alpha}}{r} p_{lip} C_{lip} + p_{carb} C_{carb} + \alpha_E E C_{\mathrm{rib}} + \left((1-\alpha_E)E + L + \frac{m_{prot}{}^{\alpha}}{r}\right) C_{prot} + p_{\mathrm{DNA}} C_{\mathrm{DNA}}\right)}{\frac{4}{3}\pi r^3 \rho_{\mathrm{cell}} p_{\mathrm{dry}}}. \quad (19)$$

Here we see the contributions of carbon contained in both functional and storage pools, the latter of which are assumed to occupy a fixed fraction of the cell independent of the environment (but linked to cell size).

Measurements of cellular P partitioning indicate that the ribosomal RNA can sometimes contribute only 33% of the total P quota (Garcia et al. 2016). The additional phosphorus includes membrane phospholipids and storage compounds, each of which can be up- or down-regulated in response to phosphorus availability in the environment. To model this phenomenon, we assume the existence of an additional stored P pool, whose size is a linear function of environmental P, or:

$$(P{:}C)_{storage} = \epsilon[P], \quad (20)$$

where ϵ is determined by the best fit to the Martiny et al. (2014) data. Our model then predicts C:P as:

$$C{:}P = \frac{1}{(P{:}C)_{(E_m, r_m)} + \epsilon[P]}. \quad (21)$$

The model parameter ϵ is calculated by minimizing the residuals of the P:C ratio predicted by Eq. (19) in comparison to the global dataset on particulate organic matter stoichiometry compiled by Martiny et al. (2014). To maintain consistency with the linear regression model of Galbraith and Martiny (2015), we restrict the dataset to observations from the upper 30 m of the water column containing particulate organic phosphorus and carbon concentrations of greater than 5 nM. Observations from the same station and the same day, but at different depths in the water column are averaged together. The P:C ratio

of the functional apparatus is calculated using irradiance, T, and P data from the World Ocean Atlas (Garcia et al. 2014b; Locarnini et al. 2013 oceancolor.gsfc.nasa.gov/data/10.5067/AQUA/MODIS/L3B/PAR/2014/, last access: 12 April 2018.), which are used to estimate environmental conditions at the location and date of particulate organic matter measurements. Light levels are computed by averaging irradiance over the top 50 m of the water column, assuming an e-folding depth of 20 m. Linear regression determines $\epsilon = 2500\ \mathrm{M}^{-1}$ which fits the data with an $R^2 = 0.28$. All parameters for the model are listed in Table 3.2.

Experimental Design

To address how changing environmental conditions affected stoichiometric ratios, carbon export, and $p\mathrm{CO}_{2,\mathrm{atm}}$ we performed two tests: a change in nutrients and a change in sea surface temperature. These tests allowed us to observe how the relationships between environmental conditions, carbon export and $p\mathrm{CO}_{2,\mathrm{atm}}$ depend on the mechanisms responsible for stoichiometric variation in the ocean. In order to account for the effects of particulate inorganic carbon (PIC) export, we multiply model predicted $\mathrm{C{:}P}_{\mathrm{export}}$ by 1.2, consistent with previous studies (Broecker 1982; Sarmiento & Toggweiler 1984).

The first set of numerical experiments examined the sensitivity of $p\mathrm{CO}_{2,\mathrm{atm}}$ to nutrient availability in the tropical and subtropical boxes for each of the three stoichiometric models. We varied tropical P from 0.15 to 1.5 μM and subtropical P from $1\mathrm{x}10^{-3}$ to 0.5 μM by adjusting the implied biological export and determined the equilibrium $p\mathrm{CO}_{2,\mathrm{atm}}$ values.

The second set of experimental tests was done to quantify how temperature modifies carbon export and $p\mathrm{CO}_{2,\mathrm{atm}}$ for each stoichiometric model. Temperature influences

carbon cycling in two ways within our model: through the solubility of inorganic carbon in seawater and through changes in phytoplankton stoichiometry within the temperature-only and multi-environmental models. Due to the well-known effects of temperature on CO_2 solubility, it is generally predicted that there is to be a positive feedback between $pCO_{2,atm}$ and temperature mediated by declining CO_2 solubility at high temperatures. To study the relative strengths of the temperature solubility feedback and the temperature regulation of C:P feedback, we performed a numerical experiment in which we varied the sea surface temperature by 5°C in either direction of modern sea surface temperature. This represents a plausible range of variation under both ice-age and anthropogenic climate change scenarios. We varied tropical temperature from 21 to 31°C and subtropical temperature from 19 to 29°C, determining equilibrium $pCO_{2,atm}$ values for combinations of temperature conditions.

Results

To quantify the linkages between phytoplankton and physiology, elemental stoichiometry, and ocean carbon cycling, we divide our results into two parts. The first is a direct study of the stoichiometric models, comparing their predictions about the relationship between stoichiometry and environmental conditions, and in the case of the trait-based model, illustrating how cellular physiology is predicted to vary across these conditions. In the second part, we show how variable stoichiometry influences carbon export and $pCO_{2,atm}$, under changing phosphorus concentrations and temperature. Within these results, we distinguish the influence or lack thereof off the three distinct biomes; in particular the equatorial upwelling regions and the macronutrient depleted subtropical gyres.

Multi-environmental and physiological controls on plankton stoichiometry

Out multi-environmental model captured several major mechanisms hypothesized to be environmental drivers of C:P ratios, including a temperature dependence of many cellular processes, a link between growth rate and ribosome abundance, and storage drawdown during nutrient limitation. The predicted relationship between environmental conditions and C:P can be understood through the environmental regulation of three factors: (i) the balance between photosynthetic proteins and ribosomes, (ii) the cell radius and associated allocation to structural material, and (iii) the degree of phosphorus storage. Our model predicted that for an optimal strategy, specific protein synthesis rates will match specific rates of carbon fixation. Thus the ratio of photosynthetic machinery to biosynthetic machinery is primarily controlled by irradiance and temperature. Increases in light levels lead to higher photosynthetic efficiency, higher ribosome content, smaller cells (due to a lower requirement for photosynthetic machinery), and lower C:P ratios (Figure 3.5). The response of C:P to light levels predicted by our model was muted in comparison to other subcellular compartment models because we separately modeled electron transport and carbon fixation (Talmy et al. 2013), and our predictions were consistent with the weak relationship between irradiance and C:P (Thrane et al. 2016) (Figure 3.5A).

Increases in temperature increase the efficiency of biosynthesis, but not photosynthesis. Therefore elevated temperature lead to a reduced ribosome content relative to photosynthetic proteins and higher C:P ratios (Figure 3.6A). This leads to a non-monotonic, concave relationship between temperature and cell size, which is due to a subtle interaction between biosynthesis efficiency (which varies greatly with temperature), maintenance costs, and size-dependent uptake rates.

Nutrient concentrations do not affect the ratio of biosynthetic to photosynthetic machinery but positively relate to both P storage and cell radius. Cell radius directly influences the specific rate of nutrient uptake and indirectly influences biosynthesis and photosynthesis as the cell membrane and wall affects the space available for other investments. This effect is pronounced in oligotrophic conditions (P< 100nM). Here, cell radius declines below 1 μm, resulting in decreasing allocations to both photosynthesis and biosynthesis and elevated C:P ratios. Higher values of the cell radius are observed in nutrient-rich conditions.

P concentrations also influenced C:P through the direct control of P storage. We plotted the relative contribution of the storage compartment and the functional compartment to the P quota, as a function of environmental conditions. The impact of the residual pool on the overall size of the P pool is heavily dependent on environmental conditions, varying from a minimum of close to 0% to a maximum of just under 50%. In the vast majority of the parameter range considered here, the contribution of the residual pool is much more modest (10-20%). High values occur when phosphorus is available and the temperature is high. In these conditions, ribosomal contributions are decreased but the residual contribution is high. In cold water, high P ecosystems, the residual contribution is approximately 25% and in oligotrophic ecosystems it is close to 0. Thus, C:P was predicted to be a decreasing function of P with two distinct regimes: a moderate-sensitivity regime for P above 100nM, and a high-sensitivity regime for P below 100 nM.

We next used the outcome of the trait model as a multi-environmental model to predict C:P ratios in the modern ocean based on annual mean light, *T*, and P. Our predictions reproduced the global pattern (Martiny et al. 2013a) with C:Pratios above the

Redfield ratio in subtropical gyres and C:P ratios below the Redfield ratio in equatorial and coastal upwelling regions and subpolar gyres (Figure 3.7A). Additionally, our model also reproduced basin-scale stoichiometric gradients among similar biomes in each ocean, predicting the highest C:P ratios in the western Mediterranean Sea and the western North Atlantic Subtropical Gyre, and somewhat elevated C:P ratios in the South Atlantic Subtropical Gyre as well as the North and South Pacific subtropical gyres.

To study the potential impact of sea surface temperature on phytoplankton resource allocation and stoichiometry, we used our multi-environmental model to predict C:P in ocean conditions both 5°C colder (cooling environments) and warmer (warming environments) than the modern ocean. According to our model, a 5°C increase (or decrease) in sea surface temperature would cause a 15% rise (or fall) in C:P ratios (Figure 3.7). This sensitivity suggested that the relative effect of T on biochemical processes could have large implications for biogeochemical cycles, making it important to determine the relative importance of physiological mechanisms regulating C:P ratios.

We compared the multi-environmental model to the predictions made by two other models: the nutrient-only model used by the Galbraith and Martiny model (2015), and our temperature-only model modified from Yvon-Durocher et al. (2015). These two models also successfully predicted the qualitative pattern of stoichiometric variation in the ocean, but they were unable to replicate the full range of variation observed in the data (Figure 3.8). In particular, there were mismatches in the North Atlantic Subtropical Gyre and the Southern Ocean, where the C:P ratio is at the extreme (Figure 3.8A, B). The nutrient-only model has a tendency to predict lower C:P ratios than the multi-environmental model in warm tropical and subtropical waters, and predict higher C:P ratios in cold waters (Figure

3.8A). This difference is driven by the *T* sensitivity of biosynthesis in the multi-environmental model, leading to increasing C:P in all warm-water regions and decreasing C:P in cold-water regions (Figure 3.8C). The multi-environmental model predicted a wider range of C:P in the ocean. The temperature-only model overall had higher C:P ratios globally compared with the multi-environmental model (Figure 3.8B) but suggested lower C:P in the gyres and higher C:P in high latitudes, especially in the Southern Ocean (Figure 3.8D).

Impact of nutrient availability on carbon export and atmospheric pCO_2

We next quantified the impact of nutrient availability in the tropics and subtropics on stoichiometry, carbon export, and $pCO_{2,atm}$ (Figure 3.9A-L). Using a constant Redfield model (or the temperature-only model), we replicated the previously observed approximately linear relationship between surface P and $pCO_{2,atm}$ (equivalent to how pre-formed P will influence $pCO_{2,atm}$) (Ito & Follows 2003; Sigman & Boyle 2000). We found that P drawdown in the subtropical box had a greater impact on carbon export, since export from the high-latitude box was not enhanced by the P supply from the subtropical box (Figure 3.9A, D, G). In the Redfield model, $pCO_{2,atm}$ appeared to be much more sensitive to subtropical P than tropical P, which was partially due to enhanced carbon export in the subtropical box and partially due to the larger surface area of the subtropical box (implying a greater potential for CO_2 exchange) (Figure 3.9J).

In contrast to the predictions made using Redfield stoichiometry, when we used the nutrient-only model for phytoplankton stoichiometry, we observed a nonlinear relationship between surface P and $pCO_{2,atm}$ (Figure 3.9B, E, H, K). At fixed tropical P, there was a strong relationship between subtropical P drawdown, export, and $pCO_{2,atm}$ in

accordance with the findings of Galbraith and Martiny (2015) (Figure 3.9B, E, H). The total decline in $pCO_{2,atm}$ as subtropical P declined from 0.4 to 1 x 10^{-3} μM could be more than 60 ppm, which was more than twice the decline that occurred in the fixed stoichiometry experiment (Figure 3.9K). We found a nonlinear monotonic relationship between tropical P and $pCO_{2,atm}$: when tropical P was high, declines in tropical P led to lower carbon export and increased $pCO_{2,atm}$. However, this trend reversed when tropical P was further drawn down (Figure 3.9K). The counter-intuitive decline in $pCO_{2,atm}$ with higher export from the tropics was driven by a teleconnection in nutrient delivery between the subtropical and tropical boxes. Increases in export in the tropical box due to P drawdown decreased the supply of P to the subtropics, which led to a decrease in the more efficient (higher C:P) subtropical export. Thus, the nutrient-only model predicted a greater decrease in subtropical export than the increase in tropical export.

The multi-environmental model also predicted a nonlinear relationship between P drawdown, carbon export, and $pCO_{2,atm}$. However, the pattern was somewhat distinct from that of the nutrient-only model results (Figure 3.9C, F, I, L). First, subtropical P drawdown had a nonlinear relationship with $pCO_{2,atm}$: when subtropical P was high, declines in tropical P led to slight declines in $pCO_{2,atm}$, and when subtropical P is low, small declines in tropical P lead to large declines in $pCO_{2,atm}$. This intensification of the relationship between subtropical P and $pCO_{2,atm}$ was due to the nonlinear relationship between P and C:P predicted by the trait-based model (Figure 3.9I). The multi-environmental model predicted extremely high tropical export, but only when P was lower than 0.05 μM (Figure 3.9C, F, I). Second, the effect of tropical P levels on $pCO_{2,atm}$ was strongly modulated by subtropical P, reversing from a negative to a positive relationship as subtropical P decline (Figure 3.9I, L).

The difference between the nutrient-only model and the multi-environmental model arose because the multi-environmental model incorporated a temperature impact on resource allocation and elemental ratios. Although we were not varying temperatures in these experiments, we did represent regional temperature differences between the different boxes. The result in that a large stoichiometric contrast between the tropical and subtropical regions only arose when there was a large difference in nutrient levels between the two regions (Figure 3.9L). However, both the nutrient-only model and the multi-environmental model predicted that carbon export and $pCO_{2,atm}$ were sensitive to the interaction between regional nutrient availability and $C:P_{export}$.

Interactive effect of temperature on stoichiometry, carbon export, and atmospheric pCO_2

We next quantified the impact of sea surface temperature (SST) in the tropics and subtropics on $C:P_{export}$, carbon export, and $pCO_{2,atm}$ (Figure 3.10A-D). The Redfield model predicts that increases in temperature lead to a decline in the solubility of CO_2 in seawater and consequently an increase in $pCO_{2,atm}$ from 288 to 300 ppm ($\Delta\ pCO_{2,atm} = 12$) (Figure 3.10A). This feedback was present with the same strength in the nutrient-only model (with no *T* dependence on C:P), in which $pCO_{2,atm}$ ranged from 268 to 280 ppm ($\Delta\ pCO_{2,atm} = 12$) (Figure 3.10B).

In contrast to the Redfield and nutrient-only models, the temperature-only model predicted a negative linear relationship between $pCO_{2,atm}$ and tropical sea surface *T* and a positive linear relationship between $pCO_{2,atm}$ and subtropical sea surface *T* (Figure 3.10C). The decline in $pCO_{2,atm}$ with tropical SST was driven by an enhancement of export due to increased C:P at higher temperatures (Figure 3.11). At 5°C below modern ocean

temperature, the model predicted C:P in the tropics was 131 and subtropical was 121, resulting in a $pCO_{2,atm}$ of 305 ppm. At 5°C above modern ocean temperature, the model predicts a C:P ratio in the tropics of 189 and C:P ratio of 175 in the subtropics, resulting in a $pCO_{2,atm}$ of 263 ppm. Tropical SST had more impact with $\Delta\ pCO_{2,atm}$ = 41 ppm compared to subtropical SST, with a $\Delta\ pCO_{2,atm}$ ranging from 4 to 5 ppm (Figure 3.11).

Similar to the temperature-only model, the multi-environmental model predicted a negative linear relationship between $pCO_{2,atm}$ and tropical SST and a positive linear relationship between $pCO_{2,atm}$ and subtropical SST (Figure 3.10D). The decline in $pCO_{2,atm}$ with tropical SST was driven by an enhancement of export due to increased C:P at higher temperatures (Figure 3.11). In the subtropical region, the expected increase in export was mitigated by a decline in solubility. At 5°C below modern ocean temperature, the trait-based model predicted that C:P in the tropics was 147 and that C:P in the subtropics was 155, resulting in an increase in $pCO_{2,atm}$ to 279 ppm (Figure 3.11). Variation in tropical SST over a 10°C span led to a significant decline in $pCO_{2,atm}$, with a $\Delta\ pCO_{2,atm}$ of approximately 46, and tropical C:P ranging from 147 to 210 (Figure 3.11). Because the subtropical box has a large surface area, the decrease in surface CO_2 solubility at high temperatures is sufficient to overcome the increase in export due to higher C:P leading to a positive relationship between $pCO_{2,atm}$ and subtropical temperatures.

Discussion

Here, we found that variable stoichiometry of exported organic material moderates the interaction between low-latitude nutrient fluxes and ocean carbon cycling. A full connecting circulation allows for complete movement of nutrients between ocean regions resulting in strong linkages between nutrient supply ratios and cellular stoichiometric

ratios (Deutsch & Weber 2012). It has been shown that the inclusion of an oceanic circulation connecting high- and low-latitude regions results in a feedback effect between high-latitude nutrient export and relative nutrient supply in low-latitudes (Sarmiento et al. 2004; Weber & Deutsch 2010). Together, the inclusion of lateral transport between ocean regions and of deviations from Redfield stoichiometry within our model led us to predict the existence of strong teleconnections between the tropics and the macronutrient-limited subtropics. The degree of nutrient drawdown in the tropics had a strongly non-monotonic relationship with $pCO_{2,atm}$ because this drawdown influenced both nutrient supply to the subtropics and tropical C:P. The idea of biogeochemical teleconnections has been proposed before, but we found that variations in stoichiometry greatly enhance the importance and strength of such linkages (Sarmiento & Toggweiler 1984). Thus biome-scale variations in phytoplankton elemental stoichiometry may change the sensitivity of the carbon pump to other phenomena that regulate patterns of nutrient drawdown. We also see that the degree of nutrient drawdown had a strong impact on predicted (and observed) C:P leading to highly nonlinear controls on $pCO_{2,atm}$, whereby increased export in the topics counter-intuitively leads to increasing $pCO_{2,atm}$. Large-scale gradients in stoichiometry can alter the regional efficiency of the biological pump: P supplied to high C:P regions leads to a larger export of carbon than P supplied to low C:P regions. This lends an important role to details of ocean circulation and other processes that alter nutrient supply and phytoplankton physiological responses in different surface ocean regions. Therefore, biome-scale variations in phytoplankton elemental stoichiometry can lead to a fundamental change in the partitioning of carbon between the atmosphere and the ocean.

We have created a box model to simulate the impact of the low-latitude stoichiometric ratios, its environmental controlling factors, and the relationships to $pCO_{2,atm}$. Low-latitude phosphorus concentrations can be set in one of two fashions; through iron limitation and through nutrient supply. Here we will briefly discuss how iron limitation would play a significant role on phosphorus concentrations and associated C:P. The biogeochemical functioning of tropical regions are commonly influenced by iron availability in such a way that macronutrients cannot be fully drawn down by phytoplankton (Coale et al. 1996; Moore 2004; Raven et al. 1999). The degree of nutrient drawdown has a strong impact on predicted (and observed) C:P. This environmental control on C:P could lead to highly nonlinear controls on $pCO_{2,atm}$, whereby increased iron availability lead to increased P drawdown and export in the tropics. However, as we have shown this may lead to increasing rather than commonly assumed decreasing $pCO_{2,atm}$. This link between iron and export would differ in the subtropics, where iron is thought to stimulate nitrogen levels through nitrogen fixation. This would result in elevated phosphate drawdown, higher C:P, and higher export. Thus, iron availability may play a complex role depending on whether there is an increased delivery in upwelling zones (leading to a potential declining global C export) or in the subtropical gyres (leading to a potential increase in global C export).

Past studies using box models have found $pCO_{2,atm}$ to be insensitive to low-latitude nutrients (Follows et al. 2002; Ito & Follows 2003; Sarmiento & Toggweiler 1984; Toggweiler 1999). This phenomenon was explored by DeVries and Peimeau (2009), who showed that the strength of the thermohaline circulation is the strongest control on $pCO_{2,atm}$, and that changes in low-latitude export have a minor impact. Unlike our study,

such earlier work relied on a uniform Redfield stoichiometry. However, we find that when stoichiometric variation is included, carbon export and $pCO_{2,atm}$ become dependent on details of low-latitude processes.

It is important to recognize that a five-box model is an incomplete description of ocean circulation and that it is here used to illustrate important mechanisms, not to make precise quantitative predictions. In order for our model to adequately reflect important features of the carbon and phosphorus nutrient distributions, we had to carefully select the values of the thermohaline and wind-driven upper ocean circulations that lead to reasonable nutrient fluxes and standing stocks. The value of thermocline circulation, T_c, has been calibrated in different box models to range from 12 to 30 Sv (DeVries & Primeau 2009; Galbraith & Martiny 2015; Sarmiento & Toggweiler 1984; Toggweiler 1999). Variations in the thermohaline circulation influence the abundance of nutrients in different boxes. Depending on the strength of this circulation, our model accumulated nutrients in the thermocline box and we tuned this parameter to most accurately mimic nutrient variation across ocean regions. Other caveats relates to our choice of the wind driven overturning circulation and the two-way flux values. Similar to the circulation values, a wide range of two-way flux values have been used in the literature. We therefore performed sensitivity experiments to find the best value for our full model setup, but the qualitative trends observed are insensitive to the choice of such fluxes.

Nutrient availability and temperature have been alternatively proposed as drivers of variation in stoichiometric ratios in the global ocean, and the strong statistical correlation between temperature and nutrients throughout the ocean has prevented identification of the relative importance of each factor (Martiny et al. 2013b; Moreno &

Martiny 2018). We see that although temperature regulation of $C:P_{export}$ can influence $pCO_{2,atm}$, this regulation is strongly dependent on the detailed physiological control mechanisms and also generally diverge from expectations based on the solubility pump. The decrease in surface CO_2 solubility at elevated temperature is sufficient to overcome the increase in export due to higher C:P leading to a positive relationship between $pCO_{2,atm}$ and subtropical temperatures. It is important to point out that the relative importance of the two competing effect depends critically on the physical circulation of the ocean. Predicted increases in stratification are often invoked as mechanisms that would decrease the vertical supply of nutrients, which one might think would further compensate for the effect of higher C:P. However, the strength of the biological pump in the subtropics is also influences by lateral transport of nutrients (Letscher et al. 2015) as such we argue that it is unclear if you should expect increasing, unchanged, or decreasing C export in low-latitude regions with ocean warming and stratification. Similarly, it is unclear how increases in stratification might affect the strength of the solubility pump. The sensitivity of $pCO_{2,atm}$ to changes in subtropical surface temperatures depends critically on the volume of the ocean ventilated form the subtropics, i.e., on the volume of the thermocline box in our model. How this volume might change in response to a warming world is a complicated dynamical problem that is beyond the scope of the present work.

Our results do not identify whether temperature or nutrient concentrations is the most important driver of phytoplankton C:P, but they do suggest that the physiological effect of temperature could be important for ocean carbon cycling. Both the temperature-only and multi-environmental models predict that temperature increases enhance tropical export, causing substantial decreases in $pCO_{2,atm}$ with temperature. This relationship is the

reverse of that predicted by the nutrient-only and Redfield models and represents a sizable potential negative feedback on carbon cycling. The multi-environmental model also predicted that C:P responds in a nonlinear fashion to P, with significantly increased sensitivity in highly oligotrophic conditions. Thus, a deeper understanding of the physiological mechanisms regulating phytoplankton C:P ratios is key to understanding the carbon cycle.

Our derivations of the multi-environmental model relies on several important assumptions. The growth rate in the multi-environmental model is determined by a set of environmental conditions and quantified by the specific rate of protein synthesis, carbon fixation, and phosphorus uptake. The effect of growth rate on stoichiometry will likely be dependent on whether light, a specific nutrient, or temperature control growth (Moreno & Martiny 2018). The magnitude of Q_{10} leads to uncertainty in our multi-environmental model because the range of possible values is highly dependent on the cell or organism being tested. In a study examining Q_{10} of photochemical processes ranged from 1.0 to 2.08, and for carboxylase activity of RuBisCO to be 2.66 (Raven & Geider 1988). In addition to the high uncertainty between Q_{10} values, there is high ambiguity associated with cellular inorganic P stores (e.g., polyphosphates and phospholipids) (Kornberg et al. 1999). P storage, such as polyphosphates, can serve as both energy and nutrient storage that may be regulated by unique environmental factors. Thus, we recognize multiple caveats within the trait-based model but expect that it improves our ability to link environmental and phytoplankton stoichiometry variation.

Conclusions

We find that processed that affect nutrient supply in oligotrophic gyres, such as the strength of the thermohaline circulation, are particularly important in setting $pCO_{2,atm}$ but via a complex link with $C:P_{export}$. By explicitly modeling the shallow overturning circulation, we showed that increased export in the tropics, which might be influenced by increased atmospheric iron dust deposition, may lead to increases, rather than decreases, in $pCO_{2,atm}$. Increased P drawdown in the tropics shifts export away from the subtropical gyres and changes the mean export C:P in the low-latitude ocean. Additionally, we find that it is difficult to separate nutrient supply and temperature controls on marine phytoplankton stoichiometry, carbon export, and $pCO_{2,atm}$ and we need better physiological experiments and field data to fully understand the relative impact of the two factors. Nevertheless, it is likely that both play a key role in regulating phytoplankton stoichiometry, $C:P_{export}$, and ultimately ocean carbon cycling.

References

Boyd PW, Trull TW. 2007. Understanding the export of biogenic particles in oceanic waters: Is there consensus? *Prog. Oceanogr.* 72(4):276–312

Broecker WS. 1982. Ocean chemistry during glacial time. *Geochim. Cosmochim. Acta*. 47(8):1539–40

Broeze RJ, Solomon CJ, Pope DH. 1978. Effects of low temperature on in vivo and in vitro protein synthesis in *Escherichia coli* and *Pseudomonas fluorescens. J. Bacteriol.* 134(3):861–74

Clark JR, Daines SJ, Lenton TM, Watson AJ, Williams HTP. 2011. Individual-based modelling of adaptation in marine microbial populations using genetically defined physiological parameters. *Ecol. Modell.* 222(23–24):3823–37

Coale KH, Fitzwater SE, Gordon RM, Johnson KS, Barber RT. 1996. Control of community growth and export production by upwelled iron in the equatorial Pacific Ocean. *Nature*. 379(6566):621–24

Daines SJ, Clark JR, Lenton TM. 2014. Multiple environmental controls on phytoplankton growth strategies determine adaptive responses of the N : P ratio. *Ecol. Lett.* 17:414–25

Deutsch C, Weber T. 2012. Nutrient ratios as a tracer and driver of ocean biogeochemistry. *Ann. Rev. Mar. Sci.* 4:113–41

Devault D. 1980. Quantum mechanical tunnelling in biological systems. *Q. Rev. Biophys.* 13(4):387–564

DeVries T, Deutsch C. 2014. Large-scale variations in the stoichiometry of marine organic matter respiration. *Nat. Geosci.* 7(12):890–94

DeVries T, Primeau F. 2009. Atmospheric pCO2 sensitivity to the solubility pump: Role of the low-latitude ocean. *Global Biogeochem. Cycles*. 23(4):1–13

Diaz JM, Bjorkman KM, Haley ST, Ingall ED, Karl DM, et al. 2016. Polyphosphate dynamics at Station ALOHA, North Pacific subtropical gyre. *Limnol. Oceanogr.* 61(1):227–39

Edwards KF, Thomas MK, Klausmeier CA, Litchman E. 2012. Allometric scaling and taxonomic variation in nutrient utilization traits and maximum growth rate of phytoplankton. . 57(2):554–66

Emerson S. 2014. Annual net community production and the biological carbon flux in the ocean. *Global Biogeochem. Cycles*. 28(1):14–28

Falkowski PG, LaRoche J. 1991. Acclimation to spectral irradiance in algae. *J. Phycol.* 27:8–14

Follows MJ, Ito T, Marotzke J. 2002. The wind-driven, subtropical gyres and the solubility pump of CO2. *Global Biogeochem. Cycles*. 16(4):9pp

Galbraith ED, Martiny AC. 2015. A simple nutrient-dependence mechanism for predicting the stoichiometry of marine ecosystems. *Proc. Natl. Acad. Sci. U. S. A.* 112(27):8199–8204

Garcia HE, Locarnini RA, Boyer TP, Antonov JI, Baranova OK, et al. 2014a. World Ocean Atlas 2013: Dissolved Inorganic Nutrients (phosphate, nitrate, silicate). In *NOAA Atlas NESDIS 75*

Garcia HE, Locarnini RA, Boyer TP, Antonov JI, Baranova OK, et al. 2014b. World Ocean Atlas 2013: Dissolved Oxygen, Apparent Oxygen Utilization, and Oxygen Saturation. In *NOAA Atlas NESDIS 75*

Garcia NS, Bonachela JA, Martiny AC. 2016. Interactions between growth-dependent changes in cell size, nutrient supply and cellular elemental stoichiometry of marine *Synechococcus*. *ISME J*. 10(11):2715–24

Geider RJ, Macintyre HL, Kana TM. 1996. A dynamic model of photoadaptation in phytoplankton. *Limnol. Oceanogr.* 41(1):1–15

Goldman JC, McCarthy JJ, Peavy DG, Peavey DG. 1979. Growth rate influence on the chemical composition of phytoplankton in oceanic waters. *Nature*. 279(5710):210–15

Henson SA, Sanders R, Madsen E, Morris PJ, Le Moigne F, Quartly GD. 2011. A reduced estimate of the strength of the ocean's biological carbon pump. *Geophys. Res. Lett.* 38(4):10–14

Ito T, Follows MJ. 2003. Upper ocean control on the solubility pump of CO2. *J. Mar. Res.* 61(4):465–89

Klausmeier CA, Litchman E, Levin SA. 2004. Phytoplankton growth and stoichiometry under multiple nutrient limitation. *Limnol. Oceanogr.* 49(4):1463–70

Kornberg A, Rao NN, Ault-Riche D. 1999. Inorganic polyphosphate: A molecule of many functions. *Annu. Rev. Biochem.* 68:89–125

Leonardos N, Geider RJ. 2004. Responses of elemental and biochemical composition of *Chaetoceros muelleri* to growth under varying light and nitrate: phosphate supply ratios and their influence on critical N : P. *Limnol. Oceanogr.* 49(6):2105–14

Leonardos N, Geider RJ. 2005. Elemental and biochemical composition of *Rhinomonas reticulata* (Cryptophyta) in relation to light and nitrate-to-phosphate supply ratios. *J. Phycol.* 41(3):567–76

Letscher RT, Moore JK, Teng Y-C, Primeau F. 2015. Variable C : N : P stoichiometry of dissolved organic matter cycling in the Community Earth System Model. *Biogeosciences*. 12(1):209–21

Locarnini RA, Mishonov A V., Antonov JI, Boyer TP, Garcia HE, et al. 2013. World Ocean Atlas 2013. Vol. 1: Temperature.

Martiny AC, Pham CTA, Primeau FW, Vrugt JA, Moore JK, et al. 2013a. Strong latitudinal patterns in the elemental ratios of marine plankton and organic matter. *Nat. Geosci.* 6(5):1–5

Martiny AC, Vrugt JA, Lomas MW. 2014. Concentrations and ratios of particulate organic carbon, nitrogen, and phosphorus in the global ocean. *Sci. Data*. 1:

Martiny AC, Vrugt JA, Primeau FW, Lomas MW. 2013b. Regional variation in the particulate organic carbon to nitrogen ratio in the surface ocean. *Global Biogeochem. Cycles*. 27(3):723–31

Mino T, Van Loosdrecht MCM, Heijnen JJ. 1998. Microbiology and biochemistry of the enhanced biological phosphate removal process

Moore CM, Mills MM, Arrigo KR, Berman-Frank I, Bopp L, et al. 2013. Processes and patterns of oceanic nutrient limitation. *Nat. Geosci*. 6(9):701–10

Moore JK. 2004. Upper ocean ecosystem dynamics and iron cycling in a global three-dimensional model. *Global Biogeochem. Cycles*. 18(4):1–21

Moreno AR, Martiny AC. 2018. Ecological stoichiometry of ocean plankton. *Ann. Rev. Mar. Sci.* 10(1):43–69

Mouginot C, Zimmerman AE, Bonachela JA, Fredricks H, Allison SD, et al. 2015. Resource allocation by the marine cyanobacterium *Synechococcus* WH8102 in response to different nutrient supply ratios. *Limnol. Oceanogr.* 60(5):1634–41

Norberg J, Swaney DP, Dushoff J, Lin J, Casagrandi R, Levin SA. 2001. Phenotypic diversity and ecosystem functioning in changing environments: a theoretical framework. *Proc. Natl. Acad. Sci.* 98(20):11376–81

Raven JA, Evans MCW, Korb RE. 1999. The role of trace metals in photosynthetic electron transport in O-2-evolving organisms. *Photosynth. Res.* 60(2–3):111–49

Raven JA, Geider RJ. 1988. Temperature and algal growth. *New Phytol.* 110(4):441–61

Rhee G-Y, Gotham IJ. 1981. The effect of environmental factors on phytoplankton growth: Temperature and the interactions of temperature with nutrient limitation

Rhee GY. 1978. Effects of N-P atomic ratios and nitrate limitation on algal growth, cell composition, and nitrate uptake. *Limnol. Oceanogr.* 23(1):10–25

Sarmiento JL, Slater R, Barber R, Bopp L, Doney SC, et al. 2004. Response of ocean ecosystems to climate warming. *Global Biogeochem. Cycles*. 18(3):

Sarmiento JL, Toggweiler JR. 1984. A new model for the role of the oceans in determining atmospheric PCO2. *Nature*. 308(5960):621–24

Shuter B. 1979. A model of physiological adaptation in unicellular algae. *J. Theor. Biol.* 78(4):519–52

Sigman DM, Boyle EA. 2000. Glacial/interglacial variations in atmospheric carbon dioxide. *Nature*. 407(October):859–69

Sterner RW, Elser JJ. 2002. *Ecological Stoichiometry: The Biology of Elements from Molecules to the Biosphere*. Princeton, NJ: Princeton University Press

Talmy D, Blackford J, Hardman-Mountford NJ, Dumbrell AJ, Geider RJ. 2013. An optimality model of photoadaptation in contrasting aquatic light regimes. *Limnol. Oceanogr.* 58(5):1802–18

Talmy D, Blackford J, Hardman-Mountford NJ, Polimene L, Follows MJ, Geider RJ. 2014. Flexible C : N ratio enhances metabolism of large phytoplankton when resource supply is intermittent. *Biogeosciences*. 11(17):4881–95

Tanioka T, Matsumoto K. 2017. Buffering of Ocean Export Production by Flexible Elemental Stoichiometry of Particulate Organic Matter. *Global Biogeochem. Cycles*. 31(10):1528–42

Teng Y-C, Primeau FW, Moore JK, Lomas MW, Martiny AC. 2014. Global-scale variations of the ratios of carbon to phosphorus in exported marine organic matter. *Nat. Geosci.* 7(12):895–98

Thrane JE, Hessen DO, Andersen T, Hillebrand H. 2016. The impact of irradiance on optimal and cellular nitrogen to phosphorus ratios in phytoplankton. *Ecol. Lett.* 19(8):880–88

Toggweiler JR. 1999. Variation of atmospheric CO2 by ventilation of the ocean's deepest

water. *Pale*. 14(5):571–88

Toseland A, Daines SJ, Clark JR, Kirkham A, Strauss J, et al. 2013. The impact of temperature on marine phytoplankton resource allocation and metabolism. *Nat. Clim. Chang.* 3(11):979–84

Tyrrell T. 1999. The relative influences of nitrogen and phosphorus on oceanic primary production. *Nature*. 400:525–31

Van Bogelen RA, Neidhardt FC. 1990. Ribosomes as sensors of heat and cold shock in *Escherichia coli*. *Proc. Natl. Acad. Sci.* 87(15):5589–93

Van Mooy BAS, Devol AK. 2008. Assessing nutrient limitation of *Prochlorococcus* in the North Pacific Subtropical gyre by using an RNA capture method. *Limnol. Oceanogr.* 53(1):78–88

Van Mooy BAS, Fredricks HF, Pedler BE, Dyhrman ST, Karl DM, et al. 2009. Phytoplankton in the ocean use non-phosphorus lipids in response to phosphorus scarcity. *Nature*. 458(7234):69–72

Weber TS, Deutsch C. 2010. Ocean nutrient ratios governed by plankton biogeography. *Nature*. 467(7315):550–54

Yvon-durocher G, Dossena M, Trimmer M, Woodward G, Allen AP. 2015. Temperature and the biogeography of algal stoichiometry. . 562–70

Yvon-Durocher G, Dossena M, Trimmer M, Woodward G, Allen AP. 2015. Temperature and the biogeography of algal stoichiometry. *Glob. Ecol. Biogeogr.* 24(5):562–70

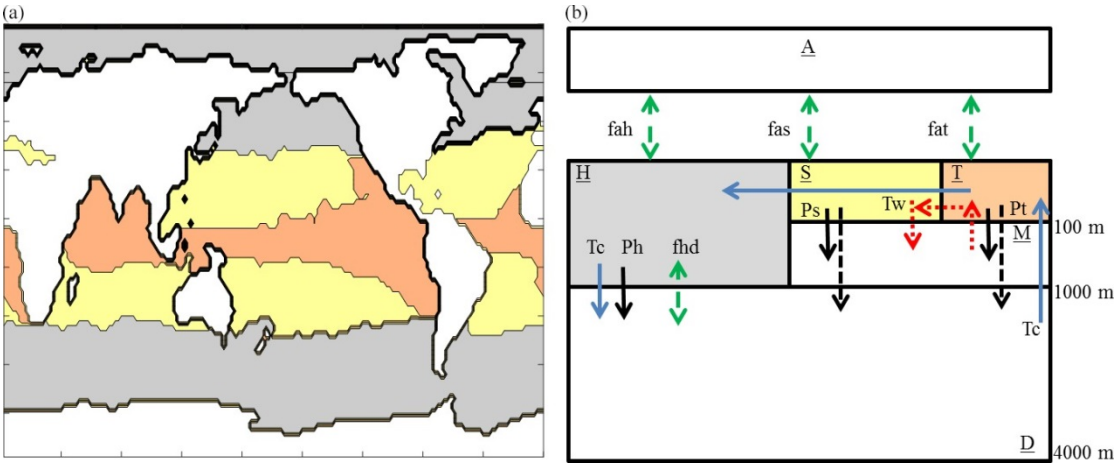

Figure 3.12 Box model design. (a) Sea surface breakdown by region. All peach-colored regions represent the tropical surface ocean box, the cream-colored regions represent the subtropical surface ocean box, and grey regions represent the high-latitude surface ocean box. (b) The model includes tropical (T), subtropical (S), and high-latitude (H) surface ocean boxes, a mixed thermocline (M) box, and a deep water (D) box. The thermohaline circulation T_C is set to 20 Sv, while the wind driven shallow overturning circulation is set to 5 Sv. The high-latitude mixing flux *fhd* is set to 45.6 Sv. The thickness of box H is 1000 m, and box M is 900 m. Box T has a temperature of 26°C, box S has a temperature of 24°C, and box H has a temperature of 7°C. Box S covers 39 % and box T covers 25% of the ocean surface area.

Table 3.2 High-latitude deep water exchange range.

RANGE OF FHD [SV]	SOURCESOURCE
38.1	(Sarmiento and Toggweiler, 1984)
3-300	(Toggweiler, 1999)
60	(DeVries and Primeau, 2009)
30-130	(Galbraith and Martiny, 2015)
18-108 (default value 45.6)	This Study

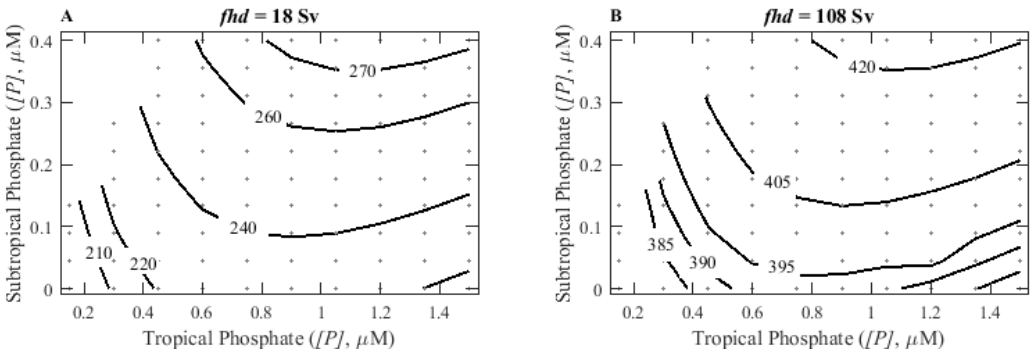

Figure 3.13 $pCO_{2,atm}$ (ppm) sensitivity to extreme *fhd* values under changing surface phosphate concentrations. (a) Range of $pCO_{2,atm}$ (ppm) using an *fhd* value of 18 Sv. (b) Range of $pCO_{2,atm}$ (ppm) using an *fhd* value of 108 Sv.

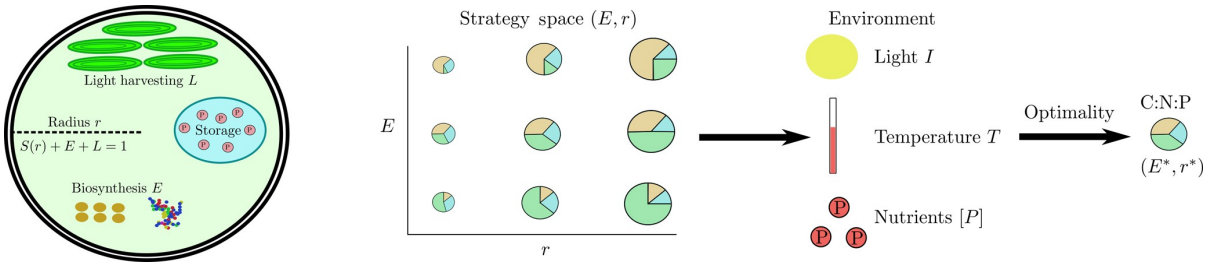

Figure 3.14 Diagram of physiological model. Phytoplankton strategies are represented in a two-dimensional strategy space (*E, r*). Each strategy is assigned a fitness in each environment using physiological principles, and the strategy with the highest fitness is selected to represent the local population. The stoichiometry of cellular components is used to calculate the stoichiometry of the functional pools in the cell.

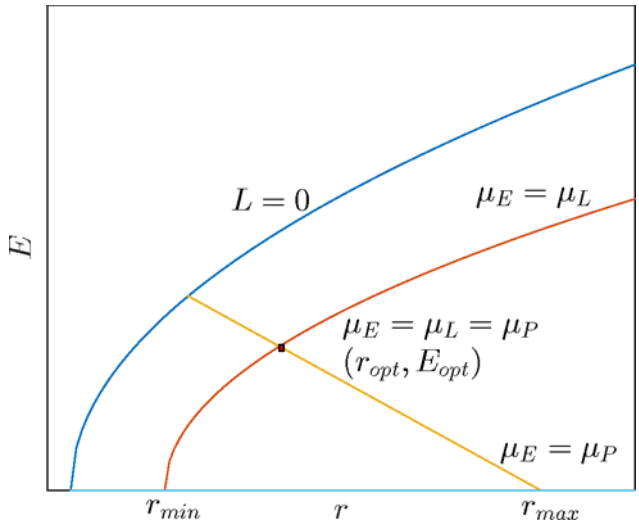

Figure 3.15 Diagram of strategy space. The *(r, E)* plane is divided into a region in the first quadrant where $L > 0$ corresponds to the set of allowable strategies. The optimal strategy occurs at the point r_{opt}, E_{opt} , denoted by the red rectangle, where $\mu = \mu_L = \mu_P = \mu_E$.

Table 3.3 Physiological Model Constants

PARAMETER	DESCRIPTION	VALUE	UNITS	SOURCE
α	Proportionality coefficient for radius	0.12	-	(Toseland et al., 2013)
γ	Percent dry mass devoted to structure other than membrane	0.2	-	(Toseland et al., 2013)
k_{E0}	Synthesis rate of biosynthesis apparatus at T_0=25	0.168	hr^{-1}	(Shuter, 1979)
$Q_{10,E}$	Q_{10} of biosynthetic apparatus	2.0		(Shuter, 1979)
Φ_{M0}	Specific carbon cost of maintenance at T_0=25	10^{-3}	hr^{-1}	(Shuter, 1979)
$Q_{10,M}$	Q_{10} of maintenance	2.0	-	(Shuter, 1979)
$Q_{10,P}$	Q_{10} of photosynthesis	1.0		(Shuter, 1979)
ΦS	Carbon cost of synthesis	0.67	-	(Shuter, 1979)
aP	Allometric scaling constant for VMP	1.04×10^{-16}	$(mol\ P)(hr)^{-1}$	(Edwards et al., 2012)
bP	Allometric scaling exponent for VMP	3.0	-	(Edwards et al., 2012)
aK	Allometric scaling constant for KP	6.4×10^{-8}	$(mol\ P)(L)^{-1}$	(Edwards et al., 2012)
bK	Allometric scaling exponent for KP	1.23	-	(Edwards et al., 2012)
ρcell	Cell Density	10^6	g/m^3	(Shuter, 1979)
pdry	Fraction of dry mass in cell	0.47	-	(Toseland et al., 2013)
αE	Fraction of dry mass in biosynthetic apparatus	0.55	-	(Toseland et al., 2013)

	devoted to ribosomes			
Prib	Fraction of ribosomal mass in phosphorus	0.047	-	(Sterner and Elser, 2002)
pDNA	Fraction of cell dry mass in DNA	0.01	-	(Toseland et al., 2013)
PDNA	Fraction of DNA mass in phosphorus	0.095	-	(Sterner and Elser, 2002)
k1	Specific Efficiency of Carbon Fixation Apparatus	0.373	hr^{-1}	(Talmy et al., 2013)
k2	Specific Efficiency of Electron Transport Apparatus	0.857	hr^{-1}	(Talmy et al., 2013)
αPh	Light Absorption	1.97	m^2/gC	(Morel and Bricaud, 1981)
ϕM	Maximum Quantum Efficiency	10^{-6}	gC/μmol photons	(Falkowski and Raven, 1997)
m_{lip}	Fraction of cell membrane composed of lipids	0.3	-	(Toseland et al., 2013)
m_{prot}	Fraction of cell membrane composed of protein	0.7	-	(Toseland et al., 2013)
p_{lip}	Fraction of cell dry mass in storage lipids	0.1	-	(Sterner and Elser, 2002)
p_{carb}	Fraction of cell dry mass in storage carbohydrates	0.04	-	(Sterner and Elser, 2002)
C_{DNA}	Fraction of DNA mass in Carbon	0.36	-	(Sterner and Elser, 2002)
C_{rib}	Fraction of ribosomal mass in Carbon	0.42	-	(Sterner and Elser, 2002)
C_{prot}	Fraction of protein mass in Carbon	0.53	-	(Sterner and Elser, 2002)

C_{lip}	Fraction of lipid mass in Carbon	0.76	-	(Sterner and Elser, 2002)
C_{carb}	Fraction of carbohydrate mass in Carbon	0. 4	-	(Sterner and Elser, 2002)

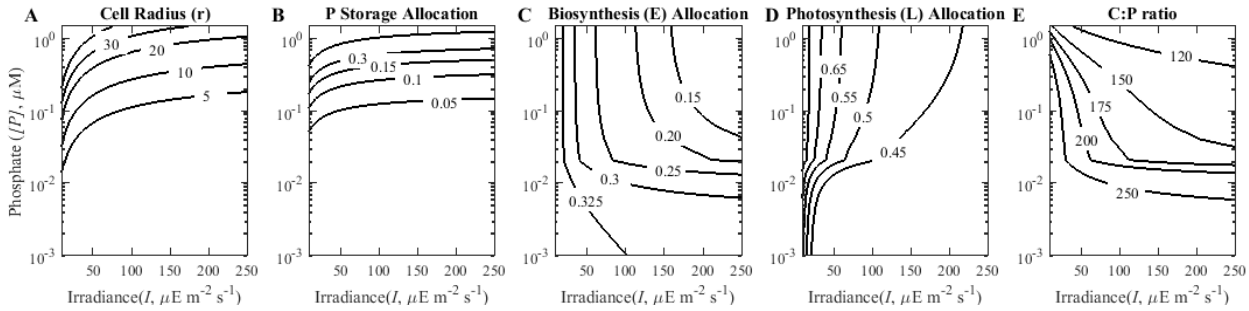

Figure 3.16 Influence of phosphate concentration and irradiance on cellular stoichiometry and cellular traits, at a constant T = 25°C. A) Cell radius (r). B) P storage allocation. C) Biosynthesis allocation. D) Photosynthesis (L) allocation. E) The C:P ratio. As irradiance increases, there is a tendency towards greater allocation to biosynthesis and lesser allocation to photosynthesis, which leads to lower C:P ratios. When phosphorus is very low, there is a large decrease in both biosynthesis and photosynthesis allocations due to the large relative allocation to the cell membrane. C:P ratios are inversely proportional to phosphorus concentration, driven by an increase in luxury storage and ribosomal content as P increases.

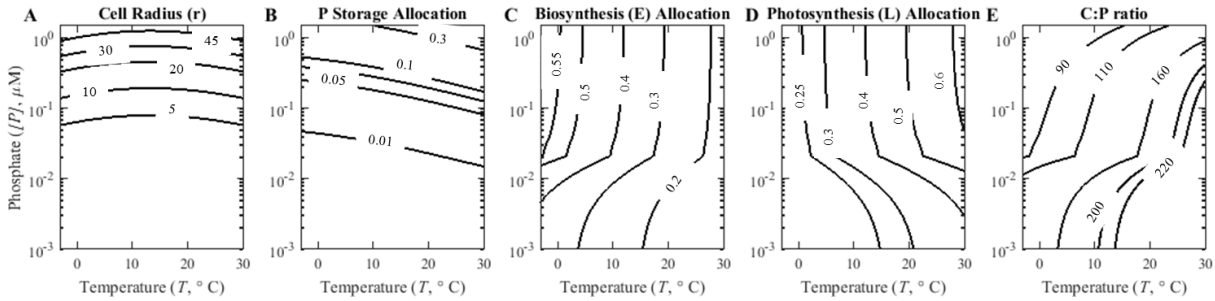

Figure 3.17 Influence of phosphate concentration and temperature on cellular stoichiometry and cellular traits, at a constant irradiance I = 50μEm^{-2}s^{-1}. A) Cell radius (r). B) P storage allocation. C) Biosynthesis allocation. D) Photosynthesis (L) allocation. E) The C:P ratio. Consistent with the translation compensation hypothesis, increases in T led to a reduction in the allocation to biosynthesis and an increase in C:P.

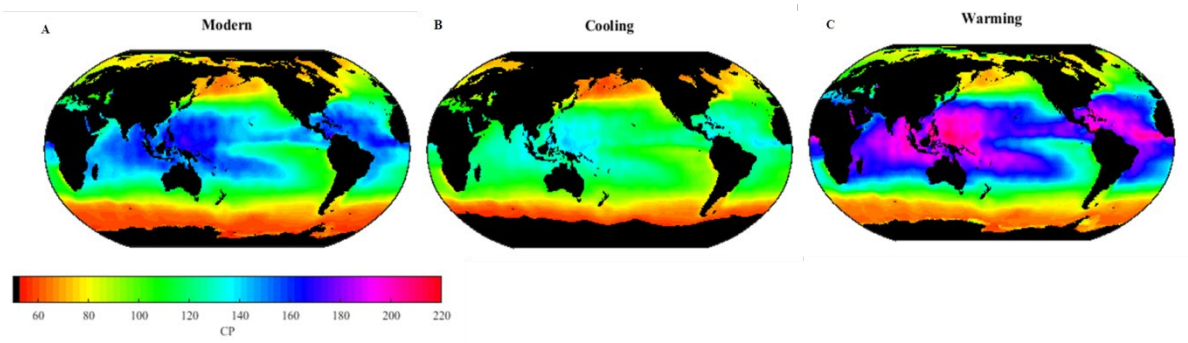

Figure 3.18 Predicted C:P ratios in the global ocean in differing climatic regimes. (a) C:P ratio under modern ocean conditions. Large differences in C:P are predicted between distinct types of ocean biome, with low C:P in equatorial upwelling regions and subpolar gyres, and high C:P in subtropical gyres. Regional differences between biomes of similar type are observed as well, with the low-phosphorus Atlantic having a higher C:P than the Pacific. (b) C:P ratio under cooling temperature conditions (5°C from the modern ocean). (c) C:P ratio under warming temperature conditions (5°C from the modern ocean). Each 5°C change leads to a shift of 15 % in the mean C:P ratio of organic matter.

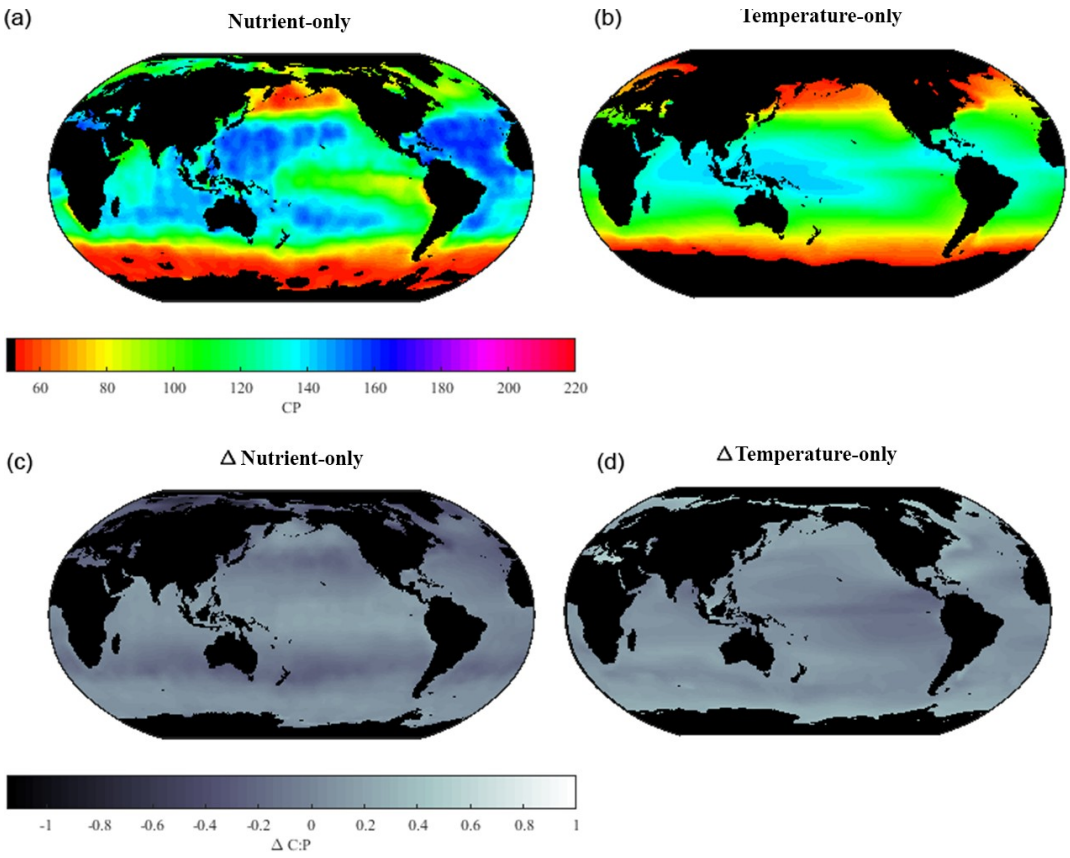

Figure 3.19 Comparison of C P between the multi-environmental model and the nutrient-only model and temperature-only model. The upper panels show predicted C:P for the global ocean under the nutrient-only (a) and temperature-only (b) models, and the lower panels show the normalized difference, i. e. $\frac{C:P_{subcell}-C:P_{other}}{C:P_{subcell}}$, between the C : P in the subcellular model (c, d).

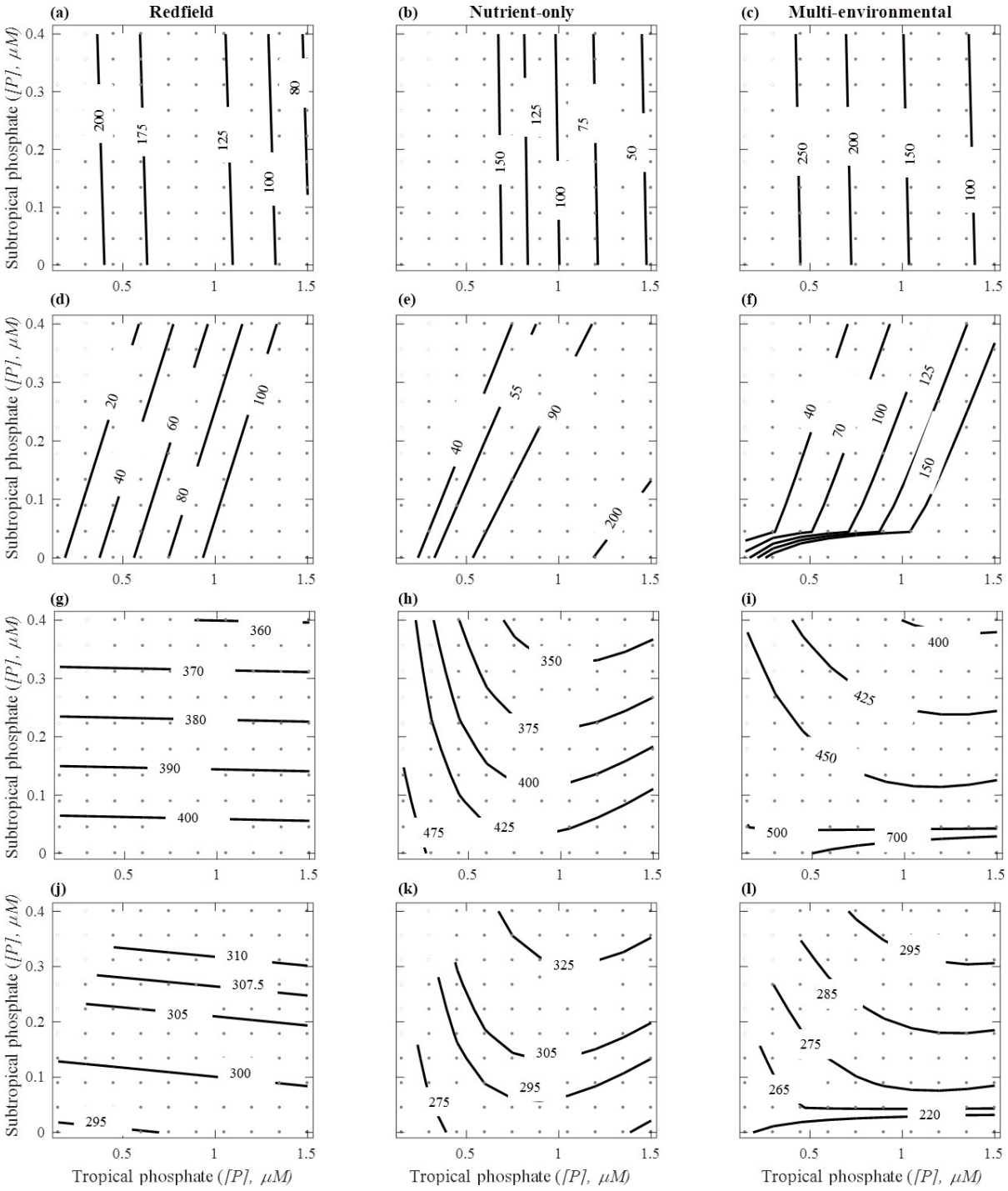

Figure 3.20 Carbon export (T mol C yr^{-1}) and $pCO_{2,atm}$ (ppm) in changing surface phosphate concentrations. Columns correspond to type of stoichiometry: Redfield (a, d, g, j), nutrient-only (b, e, h, k), and multi-environmental model (c, f, i, l). Rows correspond to either tropical carbon export (a–c), subtropical carbon export (d–f), total carbon export (g–i), or atmospheric pCO_2 (j–l). The grey points represent where $pCO_{2,atm}$ was calculated, between spaces are interpolated.

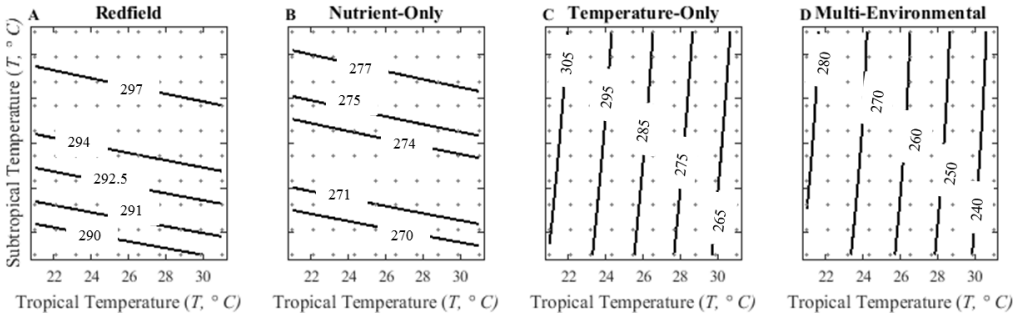

Figure 3.21 $pCO_{2,atm}$ (ppm) as a function of changing surface temperature concentrations. Based on (a) Redfield (fixed) stoichiometry model, (b) nutrient-only stoichiometry model, (c) temperature-only stoichiometry model, and (d) multi-environmental stoichiometry model.

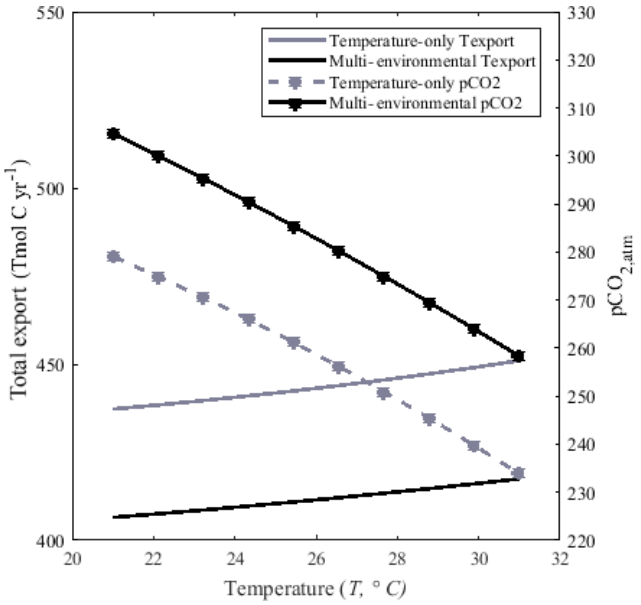

Figure 3.22 The effect of changing sea surface temperature (°C) on $pCO_{2,atm}$ and total carbon export (T mol C yr^{-1}) in the temperature-only and multi-environmental model. Phosphate concentrations are 0.3 µM in the tropical and 0.05 µM in the subtropical box. Multi-environmental model total carbon export is the solid grey line, and $pCO_{2,atm}$ is the dashed grey line. Temperature-only model total carbon export is the solid black line, and $pCO_{2,atm}$ is the dashed black line.

CHAPTER 4

Latitudinal gradient in the carbon-to-oxygen respiration quotient and the implications for ocean oxygen availability

Abstract

We show that the concentration of dissolved oxygen in the ocean is strongly sensitive to the respiratory oxygen demand of exported organic matter. Relatively small changes in the amount of oxygen consumed per unit of organic carbon respiration (i.e., the respiration quotient, $r_{-O2:C}$) produce large changes in oxygen minimum zones with strong feedbacks on primary productivity through the nitrogen inventory. Because $r_{-O2:C}$ has rarely been measured in the ocean, this result conveys a large uncertainty for future deoxygenation. We present direct measurements of $r_{-O2:C}$ along a Pacific Ocean meridional transect that traverses all major biomes. Our measured $r_{-O2:C}$ ranged from 0.73 to 1.54 with a positive temperature relationship and a mean of 1.15. An independent inverse model constrained with global nutrients, oxygen, and carbon concentrations support this positive relationship between $r_{-O2:C}$ and temperature. These results imply that future deoxygenation in response to warming will be more intense than previously anticipated.

Keywords: Respiration quotient, oxygen levels

Introduction

Global warming is presently driving an observed marine deoxygenation, which is predicted to amplify in the future (Schmidtko et al. 2017). The resulting changes in oxygen levels will impact the size of oxygen minimum zones (OMZs) (Gruber 2011; Oschlies et al. 2008) and could lead to increased loss of fixed nitrogen. Furthermore, the combination of ocean warming and declining oxygen levels may reduce the habitat range for many marine animals and possibly lead to mass extinction as seen at the end of the Permian period (Penn et al. 2018).

One of the main uncertainties in predicting current and future oxygen levels is the regulation of the biological respiration demand (Oschlies et al. 2018). The respiration quotient describes the amount of oxygen needed during the consumption of one mole of organic carbon and is thus controlled by the carbon oxidation state (signified by z):

$$C_x(H_2O)_w(NH_3)_yH_zH_3PO_4 + \left(x + \frac{1}{4}z\right)O_2 \rightarrow xCO_2 + yNH_3 + H_3PO_4 + \left(w + \frac{1}{2}z\right)H_2O \quad (1)$$

$$r_{-O2:C} = \frac{\left(x+\frac{1}{4}z\right)}{x}, \quad (2)$$

with an additional oxygen demand due to nitrification:

$$y\,NH_3 + 2y\,O_2 \rightarrow yHNO_3 + yH_2O, \quad (3)$$

yielding the total respiration quotient ($r_{\Sigma-O2:C}$) describing the full oxidation of particulate organic matter:

$$r_{\Sigma-O2:C} = \frac{\left(x+\frac{1}{4}z+2y\right)}{x}. \quad (4)$$

Despite the great importance of linking carbon export to ocean oxygen loss, the respiration quotient has rarely been measured directly in the field (Karl & Grabowski 2017). Alfred Redfield implicitly assumed that all planktonic organic carbon consisted of carbohydrates (setting z to zero) and thus $r_{-O2:C}$ = 1.0 and $r_{\Sigma-O2:C}$ = 1.3 (Redfield et al. 1963). However, carbohydrates represent a somewhat oxidized form of organic carbon and other macromolecules (especially lipids) are further reduced. Based on a theoretical estimation of phytoplankton biomass composition, Anderson (1995) and Laws (2000) independently estimated the respiration quotient to be ~1.1 and proposed limited biological variation. Ocean biogeochemical models and theories assume a constant respiration quotient but disagree on the exact value (Paulmier et al. 2009).

There is some biological and geochemical evidence for a varying respiration quotient. The macromolecular composition of plankton differs across lineages (Finkel et al. 2016b) and physiological states (Fraga et al. 1998) leading to predicted shifts in the respiration quotient (Fig. S4.1). A limited set of full elemental analyses of particulate organic matter provide support for variation in the carbon oxidation state (Chen et al. 1996; Hedges et al. 2002). End-member mixing models of oxygen and DIC concentrations along isopycnal surfaces suggest large variance in $r_{-O2:C}$ between ocean basins (Li 2002), but this method can have large biases (Schneider et al. 2005). Inverse model studies constrained by observations, find large-scale gradients in the $r_{-O2:P}$ and $r_{C:P}$ for the regeneration of organic matter (DeVries & Deutsch 2014; Teng et al. 2014). Simply dividing these two ratios suggests that $r_{\Sigma-O2:C}$ could range between 0.7 to 2.1. Such independent studies challenge the notion of a static link between the oxygen and carbon cycles, but the drivers, magnitude, and regional differences of the respiration quotient are unknown.

Based on a set of prognostic ocean biogeochemical model simulations, direct chemical measurements from diverse biomes, and a global inverse model analysis, we address the following research questions: (i) what are the global biogeochemical implications of changing $r_{-O2:C}$, (ii) what is the regional average and variation in $r_{-O2:C}$, and (iii) does the regional variation in $r_{-O2:C}$ systematically relate to specific environmental conditions?

MATERIALS AND METHODS

Sample Collection

Seawater samples were collected during the GO-SHIP P18 cruise aboard R/V *Ronald H. Brown* from November 11, 2016 to February 3, 2017 between 32.72° N, 117.16°W off

San Diego, CA to 77.85°S, 166.67°E near Antarctica (Fig. S4.2). Samples for particulate organic carbon (POC) and chemical oxygen demand (PCOD) were taken from 198 stations from the underway system. The underway intake was located at a depth of 5.3 m from the sea surface. All carboys were rinsed twice with filtered seawater before sampling. Triplicate samples for POC and sextuplicate samples for PCOD were taken every four hours with a one hour shift forward each day. Water was pre-filtered with a 30 µm nylon mesh (Small Parts #7050-1220-000-12) to remove rare large particles from the sample. Additional samples (triplicate for POC and sextuplicate for PCOD) were taken by removing the 30 µm nylon mesh, allowing all particles to collect in order to determine the total particulate organic matter from station 159 to 198. All samples were collected on pre-combusted 500°C GF/F filters (Whatman, GE Healthcare, Little Chalfont, Buckinghamshire, UK) for the analysis of POC and PCOD. Sample volume was determined on a per station basis, ranging from 3 to 8 l. All filters were then folded in half, sealed inside pre-combusted aluminum foil, and stored at -20°C until analysis.

Particulate Organic Carbon (POC)

Filters were dried at 55°C (24 h) and then stored in a desiccator with concentrated hydrochloric acid fumes for 24 h to remove inorganic carbonates. The filters were dried for 48 h at 55°C before being folded and pelletized into pre-combusted tin capsules (CE Elantech, Lakewood, New Jersey). Tin capsules were then analyzed on a Flash EA 1112 NC Soil Analyzer (Thermo Scientific, Waltham, Massachusetts) using an atropine ($C_{17}H_{23}NO_3$) standard.

Particulate Chemical Oxygen Demand (PCOD) Assay

Quantifying the Chemical Oxygen Demand is commonly used for wastewater and freshwater samples. The assay is based on the determination of residual potassium dichromate following organic matter oxidation with silver sulfate as catalyst under strongly acidic and high temperature (150°C) conditions (Baumann 1974; Moore et al. 1949; Vyrides & Stuckey 2009). As dichromate does not oxidize ammonium, the assay only quantifies the oxygen demand from organic carbon. A major obstacle for using the method with seawater POM samples is the interference of chloride ions. As such, chloride is oxidized by dichromate and cause precipitation of silver chloride. Several efforts have been made to apply this method to seawater samples and the main solution is the addition of mercuric sulfate (Dobbs & Williams 1963). Thus, the method has the potential for quantifying the oxygen demand in POM.

Here, we modified the assay to quantify the chemical oxygen demand from marine POM collected on GF/F filters. Specifically, GF/F filters with collected POM samples were dried overnight at 55°C. We then added the filter and 2 ml milli-Q water to HACH COD HR+ reagent vials (Product # 2415915 containing mercuric sulfate) and digested the samples at 150˚C for 2 h. We learned that the major obstacle for this assay was uneven precipitation of silver chloride following digestion. Thus, we modified the assay to include a subsequent precipitation step by adding 92.1 µL of 9.5 M NaCl (minimum amount of chloride to induce consistent precipitation) to each vial. Vials were immediately inverted twice and centrifuged for 30 min at 2500 rpm to remove any precipitate. Finally, we quantified the remaining dichromate by absorbance at 600 nm using HACH certified COD standards (Fig. S4.3).

To validate the modified technique, we (i) tested for any interference using standard additions, (ii) established a linear relationship between input amounts and absorbance, and (iii) optimized the technique to achieve a variance similar to other POM analyses. First, we were quantitatively able to recover experimentally added organic carbon to seawater samples suggesting limited sample interference (Fig. S4.3). Second, we found that increasing sample volume (and associated amount of PCOD captured on filters) corresponded linearly to an increase in measured PCOD (Fig. S4.3C). Third, the coefficient of variance for PCOD and $r_{-O2:C}$ corresponded to the coefficient of variance for POC and $r_{C:P}$, respectively (Fig. S4.3F). We did not fully explore the detection limit for our assay as the method was much more sensitive than one used for POC. Thus, our sampling strategy focused on recovering enough POC. These method development and optimization steps suggested that our assay provided an unbiased and sensitive method to quantify PCOD.

$r_{-O2:C}$ was computed from the mean concentrations of PCOD and POC. The standard deviation for $r_{-O2:C}$ was calculated as a pooled sample:

$$\sigma_{r_{-O2:C}} = \frac{PCOD_{aver}}{POC_{aver}} \times \sqrt{\left(\left(\frac{\sigma_{PCOD}}{POC_{aver}}\right)^2 + \left(\frac{\sigma_{POC}}{POC_{aver}}\right)^2\right)}. \quad (5)$$

The coefficient of variance was calculated as a pooled sample:

$$cv_{r-O2:C} = \frac{\sigma_{r-O2:C}}{r_{-O2:C,aver}}. \quad (6)$$

Statistical linear models were fitted using one or two predictor variables (Temperature (°C; T), Nutricline Depth (m; Z_{NO3} = 1 µM NO_3), Phosphate (P), and N:P_{surf}).

Our standard POM assay quantifies particles less than 30 µm to avoid the stochastic presence of rare large particles. However, large phytoplankton are an important contributor to POM in the Southern Ocean. To address any uncertainties with this size

selection, we also collected POM with no size fractionation between 54° S and 69° S (Fig. S4.4A). We found that total [POC] or [PCOD] were only significantly different from the <30 μm fraction at a few stations. Furthermore, $r_{-O2:C}$ was not statistically different between the total and below <30 μm fractions. This suggested that capping the POM sample at a particle size of 30 μm did not affect the outcome of our analysis (Fig. S4.4C).

Prognostic CESM Simulations

A modified version of Community Earth System Model (CESM) was used for our 300-year simulations, which included a prescribed $r_{-O2:C}$ ranging between 0.8 and 1.3 in 0.1 increments across model experiments. Model output was averaged over the last 20 simulation years for analysis to remove short term variability. The model includes three phytoplankton functional groups (small, large, and diazotrophic phytoplankton) and multiple potentially growth-limiting nutrients (N, P, Fe, Si). The model has been used in CESM climate simulations (Moore et al. 2013, 2018). The ecosystem-biogeochemistry model code is a preliminary version of the CESM V2.1 code set, run within the coarse-resolution CESM V1.2.1. ocean circulation model (Wang et al. 2019). Water column denitrification is initiated in the model when oxygen levels fall below 7 μM, with complete denitrification and no oxic remineralization below 5 μM (Moore et al. 2013). Additional documentation and model source code for CESM2.0 are available online (www2.cesm.ucar.edu). To quantify the changes in oxygen levels, denitrification rates, and net primary production, we subtracted the model output using a fixed $r_{-O2:C}$ of 0.8 (Figure 3.1A, D, and G) and 1.3 (Figure 3.1B, E, and H) from the simulation with fixed $r_{-O2:C}$ of 1.0 (Redfield quotient).

Analysis of CMIP5 Model Output

We obtained output from the Coupled Model Intercomparison Project Phase 5 (CMIP5) models from the Earth System Grid Federation (Taylor et al. 2012). We calculated the changes in ocean oxygen content and rates of denitrification between the simulated 1990s and 2090s for available biogeochemical models following the historical and Representative Concentration Pathway 8.5 (RCP8.5). This is the high-end, business as usual, emissions scenario with strong global warming over the 21st century.

Bayesian Inverse Model Estimate of $r_{-\mathrm{O2:C}}$

The formulation of the biogeochemical inverse model builds on our previous inverse modeling work for the phosphorus and nitrogen cycles (Wang et al. 2019) by adding governing equations for the cycling of carbon and dissolved oxygen. The model also carries explicit tracers for the chemical-oxygen-demand (COD) so that it can keep track of organic carbon with different oxidative states. The governing equations for the biogeochemical model are given subsequently. Here, we give a brief overview of the source and sink terms and introduce the parameters that need to be estimated from the data.

The optimal solution for the marine nitrogen cycle computed serves as the starting point for the new model (Wang et al. 2019). From that solution, the rate of organic nitrogen production is used to prescribe the rate of organic carbon production via a constant C:N=106:16 ratio:

$$P_{\mathrm{Corg}} = r_{\mathrm{C:N}} P_{\mathrm{Norg}}.$$

The rate of COD production is then diagnosed from the organic carbon production rate via a respiration quotient that varies spatially through its dependence on the sea-surface temperature (SST), i.e. $r_{-\mathrm{O2:C}} = m(SST - 15°\mathrm{C}) + b$:

$$P_{\mathrm{COD}} = r_{-\mathrm{O2:C}} r_{\mathrm{C:N}} P_{\mathrm{Norg}}.$$

The photosynthetic oxygen production is then diagnosed by combining the COD production rate with the rates of new and recycled organic N:

$$P_{\mathrm{O_2}} = P_{\mathrm{COD}} + 2RP_{\mathrm{Norg}} - \frac{3}{4}(1-R)P_{\mathrm{Norg}},$$

where 1-R denotes the fraction of organic matter production tied to new sources of fixed N (either due to microbial N fixation or due to inputs from atmospheric deposition and rivers). A fraction σ of P_{Corg} and P_{COD} is allocated to the dissolved phase, i.e. to DOC and DCOD while the remaining is allocated to a sinking particulate phase. An estimate of the climatologically-averaged circulation constrained by temperature, salinity, mean sea surface height, natural radiocarbon, CFC-11 and the air-sea exchange of heat and freshwater is used to compute the transport and mixing of tracers in the dissolved phase (DeVries & Primeau 2011; Primeau et al. 2013). Tracers in the particulate phase (POC and PCOD) are transported downward using a depth-dependent sinking speed with a constant dissolution rate so as to produce a powerlaw flux attentuation profile with exponent b_{C}. Particulate inorganic carbon is transported downward using a constant sinking speed and dissolution rate so as to produce an exponentially decaying flux attenuation profile. All the POC and PCOD cycle through their corresponding dissolved phases before being respired according to a respiration rate coefficient, $\kappa_{d\mathrm{C}}$. The oxygen consumption rate is diagnosed from the respiration of carbon and the remineralization of organic nitrogen after correcting for the substitution of nitrate as the electron acceptor in the presence of water-column and sedimentary denitrification:

$$L_{\mathrm{O_2}} = \kappa_{d\mathrm{C}}\mathrm{DCOD} + 2\kappa_{d\mathrm{N}}\mathrm{DON} - \frac{5}{4}(D_{\mathrm{wc}} + D_{\mathrm{sed}}),$$

where $\kappa_{d\mathrm{N}}$DON is remineralization rate of organic N, and $D_{\mathrm{wc}} + D_{\mathrm{sed}}$ is the fixed-N loss rate due to denitrification and anammox reactions.

As formulated, the new inverse model includes five biogeochemical parameters that were not part of the previous N-cycle model: m, b, σ, $\kappa_{d\mathrm{C}}$, and b_{C}. Only the parameters m and b that determine $r_{-\mathrm{O2:C}}$ are of direct interest, but the additional parameters are uncertain and must also be estimated from the data. We use a Bayesian inversion procedure to account for their contribution to the uncertainty of $r_{-\mathrm{O2:C}}$ (Wang et al. 2019). In this approach, the model-predicted concentrations of dissolved oxygen, DO_2, dissolved organic carbon, DOC, and dissolved inorganic carbon, DIC, are used to define the mean of a multivariate normal probability distribution for the observations of O_2, DOC, and DIC in the GLODAPv2 database (Key et al. 2015; Olsen et al. 2016). The resulting probability distribution, conditioned on the structural choice of our biogeochemical model, specifies the likelihood function for the Bayesian inversion procedure. Flat prior probability densities are assumed for m and b, whereas flat priors are assumed for the logarithms of σ, $\kappa_{d\mathrm{C}}$, and b_{C}. A trust-region optimization procedure is used to find the parameter values that maximize the posterior probability distributions. Parameter uncertainties are determined by approximating the posterior distribution near its maximum using a multivariate normal distribution.

Results

A change in the respiration quotient can have widespread impacts on ocean oxygen, nitrogen, and carbon processes. We conducted sensitivity simulations with a prognostic ecosystem and biogeochemistry model (Primeau et al. 2013; Wang et al. 2019) in which we varied $r_{-O2:C}$ between 0.8 and 1.3. An increase from Redfield proportions ($r_{-O2:C}$ = 1) to a

high value ($r_{-O2:C}$ = 1.3) caused a 7% decrease in global dissolved oxygen levels and a 187% expansion of OMZs volumes ([O_2] <25μM; Fig. 1). This expansion as well as decreased oxygen concentrations at the water-sediment interface caused a 218% increase in total denitrification. Indirectly, through the loss of N, net primary production and carbon export at 100 m decreased by 4.9% and 5.1%, respectively. Thus, the respiration quotient is a first-order control on ocean biogeochemical cycles.

The changes to ocean biogeochemical cycles from a varying respiration quotient are comparable in magnitude to business-as-usual climate change impacts by year 2100 (Fig. S4.5, Table S4.1). Climate simulations performed under scenario RCP8.5 showed a decline in the total dissolved oxygen content of the ocean between 3.1% and 4.7% by year 2100 (Figure S4.5, Table S4.1). Climate warming impacts on ocean oxygen were similar in magnitude to a change in $r_{-O2:C}$ of ~0.2. Therefore, changes in the respiration quotients rival generally accepted thermodynamic and physical impacts on ocean oxygen levels and could serve as an important feedback to climate change.

To quantify the respiration quotient, we combined field measurements of particulate organic carbon (POC) and the required oxygen demand for respiration along the Eastern Pacific Ocean. We measured oxygen consumption by modifying and calibrating a method commonly used for measuring the particulate chemical oxygen demand (PCOD) in wastewater (Vyrides & Stuckey 2009). We then estimated the respiration quotient ($r_{-O2:C}$) across 198 stations along line P18 (Fig. S4.6). The cruise covered the Eastern boundary of the North Pacific Ocean subtropical gyre, the eastern Pacific Ocean equatorial upwelling region, the South Pacific Ocean subtropical gyre, and finally crossed several fronts in the Southern Ocean. Based on past biome delineations (Reygondeau et al. 2013)

and our environmental observations, we classified the transect into nine distinct regions (Table S4.2). Sea-surface temperature steadily decreased from 29.5°C to approximately 0°C (Figure 3.2A). A deep nutricline was detected in regions 1:CAMR - 3:TPEQ, and 5:SPSG marking the location of subtropical gyre conditions (**Figure 3.1**B). Nitrate was mostly drawn down to detection limit in several regions, whereas residual phosphate was present throughout the Eastern Pacific Ocean (Fig. S4.7). As a result, the dissolved nitrate to phosphate ($N:P_{surf}$) ratio was low in the subtropical North Pacific, approached Redfield proportions in high nutrient regions south of the equator, decreased again in the southern subtropical gyre, and finally continually increased entering the Southern Ocean (Figure 3.1). This low $N:P_{surf}$ suggested N limitation in oligotrophic regions. As such, our samples covered all major biome types.

We observed distinct but highly correlated POM concentration levels across regions. [POC] and [PCOD] were tightly correlated ($r^2_{Pearson} = 0.93$, $p < 0.0001$) (Figure 3.2D, E) and showed parallel regional shifts. Thus, our optimized PCOD assay accurately quantified marine organic matter. Specifically, [POC] and [PCOD] were low in the gyre regions (1:CAMR, 2:PNEC, and 5:SPSG), slightly higher in equatorial Pacific Ocean waters (4:PEQD), and very high in the Southern Ocean regions (6:SST – 9:APLR) (Figure 2D, E). Changes in POM concentrations followed the nine regions that arose from the combination of environmental conditions.

We detected significant a clear latitudinal gradient in the respiration quotient. $r_{-O2:C}$ averaged 1.15 but ranged between 0.73 and 1.54 (Table S4.3, Fig. 2F). The highest regional average $r_{-O2:C}$ of $1.26^{1.48}_{1.10}$ (range set by the minimum and maximum value) was found on the warm edge of the North Pacific Subtropical Gyre (1:CAMR, Fig. S4.7), and the lowest

average $r_{-O2:C}$ ratio at $0.99^{1.18}_{0.79}$ was detected near the ice edge in the Southern Ocean (9:APLR). Regions 1:CAMR through 7:SANT were significantly different from the Redfield quotient, whereas regions 1:CAMR through 4:PEQD and 9:APLR deviated from Anderson's higher quotient (Fig. S4.8). Alas, the observed respiration quotients were different from the theoretical values across multiple ocean regions.

The respiration quotient was significantly related to ocean environmental conditions. We tested all linear combinations of environmental factors and $r_{-O2:C}$ (Table S4.4). A significant positive relationship between temperature and $r_{-O2:C}$ suggested an increase in $r_{-O2:C}$ of ~ 0.2 between polar and tropical regions (Figure 3.3A). We saw indications of an additional regulation of $r_{-O2:C}$ by nutrient availability and/or nitrogen. A deeper nutricline led to a slightly depressed quotient in comparison to waters with the same temperature but higher nutrients. A positive relationship between temperature and the respiration quotient was also observed for a small set of previously analyzed samples from the Western North Pacific Ocean (Fig. S4.7). Temperature emerged as the best predictor, but additional factors may exert a secondary control on the respiration quotient.

We tested if the observed temperature dependence of $r_{-O2:C}$ could be detected via the imprint on the large-scale three-dimensional distribution of oxygen and carbon in the ocean. To achieve this, we constructed an inverse biogeochemical model constrained by the GLODAP.2016v2 and WOA2013 databases of hydrographic measurements of nutrients, carbon, and oxygen concentrations (Key et al. 2015; Olsen et al. 2016). We relied on previous inverse-modeling efforts for the carbon, nitrogen, and phosphorus cycles (Primeau et al. 2013; Teng et al. 2014; Wang et al. 2019) but with an added oxygen cycling model. The resulting biogeochemical model tracks the dissolved oxygen concentration as

well as the oxidation and reduction of nitrogen and carbon. Through a Bayesian inversion procedure, we estimated $r_{-O2:C}$ = $1.121^{1.123}_{1.119}$ at 15°C and a temperature dependence ($0.0197^{0.0201}_{0.0193}$°C^{-1}) (± 1 std; Figure 3.3B). The temperature dependence for the respiration quotient estimated from the inverse model is stronger than what we measured in the suspended particles. However, both the inverse model and the direct measurements agree on the midpoint value at 15˚C and a positive relationship with temperature (Figure 3.3). Accordingly, we have multiple lines of evidence for a regional varying respiration quotient.

Discussion

There is increasing evidence for regionally distinct elemental ratios of marine organic matter (Moreno & Martiny 2018). Extending this work, we find strong support for a latitudinal gradient in the respiration quotient ranging between 0.73 and 1.54. This range is somewhat outside the bounds of biochemical predictions (Anderson 1995; Laws et al. 2000) but still within a plausible range. Previously detected shifts in the C:H:O ratio of POM in the Western Pacific Ocean corresponds to a respiration quotient ranging between 0.6 and 1.6 (Chen et al. 1996) and several studies have detected 40% variation in the C:H ratio (Karl & Grabowski 2017). Platt and Irwin observed a 30% variation in the caloric content of fresh organic matter (Platt & Irwin 1972). As the carbon oxidation state and caloric content of organic matter are closely tied (Karl & Grabowski 2017), one should expect a parallel range in the respiration quotient. Finally, the observed values are firmly within the bounds proposed using endmember mixing models (Li 2002). Previous studies have tended to downplay or dismiss evidence for changes in the respiration quotient because of an inability to distinguish signal from noise. However, the large number of new

measurements and their spatial coherence strongly support a systematically varying respiration quotient.

The observed latitudinal gradient for the respiration quotient must be linked to changes in the underlying molecular composition of surface POM and plankton. The exact nature of this relationship remains to be quantified, but we hypothesize it is driven by an increased proportion of lipids relative to proteins and carbohydrates. The proportion of biochemical components across major phytoplankton groups follow an allometric relationship (Finkel et al. 2016a) leading to an elevated lipid-to-carbohydrate/protein ratio in small plankton. Smaller cells have a higher surface-to-volume ratio and an associated high contribution of the lipid-rich membrane to total carbon. The high abundance of small picoplankton in warm tropical and subtropical regions could result in a higher lipid fraction and higher respiration quotient of exported organic matter. Another biological mechanism is the accumulation of lipids following nitrogen starvation response in many phytoplankton (Shifrin & Chisholm 1981). We observed the highest respiration quotient in warm regions with low $N{:}P_{surf}$. Thus, shifts in plankton biogeography and/ or physiology could regulate the observed changes in the respiration quotient.

There are several noteworthy caveats to our conclusions. First, the direct observations are limited to surface samples from a single Eastern Pacific Ocean transect. It is plausible that measurements from other regions or seasons will identify additional controls on the respiration quotient. Second, it is unclear if the POM oxidative state will change during sinking and aging. The O:C ratio is higher in surface vs. deep dissolved organic matter (DOM) suggesting preferential remineralization of oxidized forms of organic carbon (Letscher et al. 2013). In this study, H:C decrease concurrently and it is the balance

of O:C and H:C that ultimately controls the respiration quotient. Furthermore, there is limited variation in the O:C and H:C ratios for DOC between deep Atlantic (young) and Pacific Ocean (old) DOM (Bercovici et al. 2018). Thus, it is difficult at present to predict if the respiration quotient will change with depth and future vertical profiles are needed. Third, we did not measure the respiration quotient of DOM even though this fraction is an important component of the ocean carbon cycle (Roshan & Devries 2017). Hence, it is unclear if POM and DOM will display the same level and biome patterns in $r_{-O2:C}$. Fourth, the chemical assay has oxidative limitations and some compounds are not fully oxidized (Baker et al. 1999). Thus, there may be negative biases in the respiration quotient for some samples although extensive work on sewage material has not uncovered any systematic biases in COD measurements (McCrady 2008). Fifth, we observed covariance between $r_{-O2:C}$ and environmental parameters other than sea surface temperature. The uncertainty estimates we have provided from our inverse model analysis are conditioned on the model structure. Exploring more complex relationships between $r_{-O2:C}$ and a broader suite of environmental variables in the lab, *in situ*, and by the inverse model should improve our understanding of the respiration quotient. Nevertheless, our independent methods strongly support our conclusion that the respiration quotient varies between regions.

The observed variation in the respiration quotient is expected to have large biological and biogeochemical impacts. The production of more reduced organic carbon in tropical and subtropical regions implies a higher caloric content and perhaps a superior food source (Karl & Grabowski 2017). On the other hand, an upshift in the respiration quotient can initiate a biogeochemical cascade leading to lower ocean oxygen levels, higher rates of denitrification, N loss and declining productivity. These biogeochemical changes

could have devastating impacts on marine life (Penn et al. 2018). Thus, a biological feedback whereby warmer temperature leads to the production of more reduced organic carbon can have a large future control on marine ecosystem functioning and biogeochemistry.

References

Anderson LA. 1995. On the hydrogen and oxygen content of marine phytoplankton. *Deep Sea Res. Part I Oceanogr. Res. Pap.* 42(9):1675–80

Aumont O, Bopp L. 2006. Globalizing results from ocean in situ iron fertilization studies. *Global Biogeochem. Cycles*. 20(2):

Baker JR, Milke MW, Mihelcic JR. 1999. Relationship between chemical and theoretical oxygen demand for specific classes of organic chemicals. *Water Res.* 33(2):327–34

Baumann FJ. 1974. Dichromate reflux chemical oxygen demand. Proposed method for chloride correction in highly saline wastes. *Anal. Chem.* 46(9):1336–38

Bercovici SK, Koch BP, Lechtenfeld OJ, McCallister SL, Schmitt-Kopplin P, Hansell DA. 2018. Aging and Molecular Changes of Dissolved Organic Matter Between Two Deep Oceanic End-Members. *Global Biogeochem. Cycles*. 32:1449–56

Chen CTA, Lin CM, Huang BT, Chang LF. 1996. Stoichiometry of carbon, hydrogen, nitrogen, sulfur and oxygen in the particulate matter of the western North Pacific marginal seas. *Mar. Chem.* 54(1–2):179–90

DeVries T, Deutsch C. 2014. Large-scale variations in the stoichiometry of marine organic matter respiration. *Nat. Geosci.* 7(12):890–94

DeVries T, Primeau F. 2011. Dynamically and Observationally Constrained Estimates of Water-Mass Distributions and Ages in the Global Ocean. *J. Phys. Oceanogr.*

41(12):2381–2401

Dobbs RA, Williams RT. 1963. Elimination of chloride interference in the chemical oxygen demand test. *Anal. Chem.* 35(8):1064–67

Dunne JP, John JG, Shevliakova S, Stouffer RJ, Krasting JP, et al. 2013. GFDL's ESM2 global coupled climate-carbon earth system models. Part II: Carbon system formulation and baseline simulation characteristics. *J. Clim.* 26(7):2247–67

Finkel Z V., Follows MJ, Irwin AJ. 2016a. Size-scaling of macromolecules and chemical energy content in the eukaryotic microalgae. *J. Plankton Res.* 38(5):1151–62

Finkel Z V, Follows MJ, Liefer JD, Brown CM, Benner I, Irwin AJ. 2016b. Phylogenetic diversity in the macromolecular composition of microalgae. *PLoS One*. 11(5):e0155977

Fraga F, Rios AF, Perez FF, Figueiras FG. 1998. Theoretical limits of oxygen:carbon and oxygen:nitrogen ratios during photosynthesis and the mineralization of the organic matter inthe sea. *Sci. Mar.* 62(1–2):161–68

Gruber N. 2011. Warming up, turning sour, losing breath: ocean biogeochemistry under global change. *Philos. Trans. R. Soc. a-Mathematical Phys. Eng. Sci.* 369(1943):1980–96

Hedges JI, Baldock JA, Gélinas Y, Lee C, Peterson ML, Wakeham SG. 2002. The biochemical and elemental compositions of marine plankton: A NMR perspective. *Mar. Chem.* 78(1):47–63

Ilyina T, Six KD, Segschneider J, Maier-Reimer E, Li H, Núñez-Riboni I. 2013. Global ocean biogeochemistry model HAMOCC: Model architecture and performance as component of the MPI-Earth system model in different CMIP5 experimental realizations. *J. Adv. Model. Earth Syst.* 5(2):287–315

Karl DM, Grabowski E. 2017. The importance of H in particulate organic matter

stoichiometry, export and energy flow. *Front. Microbiol.* 8(MAY):1–7

Key RM, Olsen A, van Heuven S, Lauvset SK, Velo A, et al. 2015. Global Ocean Data Analysis Project, Version 2 (GLODAPv2)

Laws EA, Falkowski PG, Smith WO, Ducklow H, McCarthy JJ. 2000. Temperature effects on export production in the open ocean. *Global Biogeochem. Cycles*. 14(4):1231–46

Letscher RT, Hansell DA, Carlson CA, Lumpkin R, Knapp AN. 2013. Dissolved organic nitrogen in the global surface ocean: Distribution and fate. *Global Biogeochem. Cycles*

Li Y-H. 2002. Latitudinal change of remineralization ratios in the oceans and its implication for nutrient cycles. *Global Biogeochem. Cycles*. 16(4):77-1-77–16

McCrady MH. 2008. Standard Methods for the Examination of Water and Waste-water. *Am. J. Public Heal. Nations Heal.*

Moore JK, Doney SC, Kleypas JA, Glover DM, Fung IY. 2002. An intermediate complexity marine ecosystem model for the global domain. *Deep Sea Res. Part II Top. Stud. Oceanogr.* 49(1–3):403–62

Moore JK, Fu W, Primeau F, Britten GL, Lindsay K, et al. 2018. Sustained climate warming drives declining marine biological productivity. *Science (80-.).* 359:1139–43

Moore JK, Lindsay K, Doney SC, Long MC, Misumi K. 2013. Marine ecosystem dynamics and biogeochemical cycling in the Community Earth System Model [CESM1 (BGC)]: Comparison of the 1990s with the 2090s under the RCP4. 5 and RCP8. 5 scenarios. *J. Clim.* 26(23):9291–9312

Moore WA, Kroner RC, Ruchhoft CC. 1949. Dichromate reflux method for determination of oxygen consumed. *Anal. Chem.* 21(8):953–57

Moreno AR, Martiny AC. 2018. Ecological stoichiometry of ocean plankton. *Ann. Rev. Mar.*

Sci. 10(1):43–69

Olsen A, Key RM, Heuven S Van, Lauvset SK, Velo A, et al. 2016. The Global Ocean Data Analysis Project version 2 (GLODAPv2) – an internally consistent data product for the world ocean. *Earth Syst. Sci. Data*. 8:297–323

Oschlies A, Brandt P, Stramma L, Schmidtko S. 2018. Drivers and mechanisms of ocean deoxygenation. *Nat. Geosci.* 11(July):467–73

Oschlies A, Schulz KG, Riebesell U, Schmittner A. 2008. Simulated 21st century's increase in oceanic suboxia by CO2-enhanced biotic carbon export. *Global Biogeochem. Cycles*. 22(4):

Palmer JR, Totterdell IJ. 2001. Production and export in a global ocean ecosystem model. *Deep. Res. I*. 48:1169–98

Paulmier A, Kriest I, Oschlies A. 2009. Stoichiometries of remineralisation and denitrification in global biogeochemical ocean models. *Biogeosciences*. 6:923–35

Penn JL, Deutsch C, Payne JL, Sperling EA. 2018. Temperature-dependent hypoxia explains biogeography and severity of end-Permian marine mass extinction. *Science (80-.).* 362(1130):

Platt T, Irwin B. 1972. Caloric content of phytoplankton. *Limnol. Oceanogr.* 18(2):306–10

Primeau FW, Holzer M, DeVries T. 2013. Southern Ocean nutrient trapping and the efficiency of the biological pump. *J. Geophys. Res. Ocean.* 118(5):2547–64

Redfield AC, Ketchum BH, Richards FA. 1963. The influence of organisms on the composition of sea-water. *sea ideas Obs. Prog. study seas. Vol. 2.* 26–77

Reygondeau G, Longhurst A, Martinez E, Beaugrand G, Antoine D, Maury O. 2013. Dynamic biogeochemical provinces in the global ocean. *Global Biogeochem. Cycles*. 27(4):1046–

58

Roshan S, Devries T. 2017. Efficient dissolved organic carbon production and export in the oligotrophic ocean. *Nat. Commun.* 8(2036):

Schmidtko S, Stramma L, Visbeck M. 2017. Decline in global oceanic oxygen content during the past five decades. *Nature*. 542(7641):335–39

Schneider B, Karstensen J, Oschlies A, Schlitzer R. 2005. Model-based evaluation of methods to determine C:N and N:P regeneration ratios from dissolved nutrients. *Global Biogeochem. Cycles*. 19(2):1–18

Shifrin NS, Chisholm SW. 1981. Phytoplankton lipids: interspecific differences and effects of nitrate, silicate and light-dark cycles

Taylor KE, Stouffer RJ, Meehl GA. 2012. An overview of CMIP5 and the experiment design. *Bull. Am. Meteorol. Soc.* 93(4):485–98

Teng Y-C, Primeau FW, Moore JK, Lomas MW, Martiny AC. 2014. Global-scale variations of the ratios of carbon to phosphorus in exported marine organic matter. *Nat. Geosci.* 7(12):895–98

Tjiputra JF, Roelandt C, Bentsen M, Lawrence DM, Lorentzen T, et al. 2013. Evaluation of the carbon cycle components in the Norwegian Earth System Model (NorESM). *Geosci. Model Dev.* 6(2):301–25

Vyrides I, Stuckey DC. 2009. A modified method for the determination of chemical oxygen demand (COD) for samples with high salinity and low organics. *Bioresour. Technol.* 100(2):979–82

Wang W, Moore JK, Martiny AC, Primeau FW. 2019. Convergent estimates of marine nitrogen fixation. *Nature*. 566:205–11

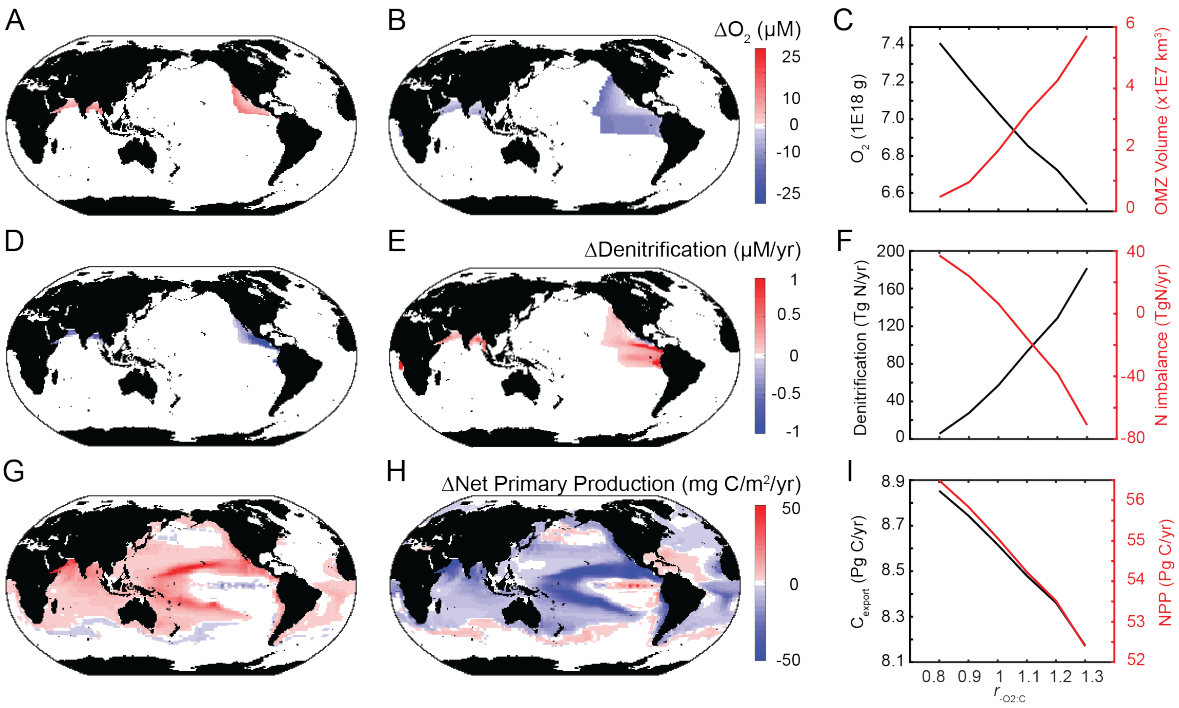

Figure 4.23 Impact of a changing respiration quotient on ocean biogeochemical processes. A. Change in OMZ (O_2 ≤25 μM) extent and intensification when $r_{-O2:C}$ shifts from 1 to 0.8, B. Change in OMZ extent and intensification when $r_{-O2:C}$ shifts from 1 to 1.3. C. Total oxygen levels and OMZ volume as a function of the respiration quotient. D. Change in denitrification zones and intensity when $r_{-O2:C}$ shifts from 1 to 0.8. E. Change in denitrification zones and intensity when $r_{-O2:C}$ shifts from 1 to 1.3. F. Annual denitrification rates and global ocean N balance as a function of the respiration quotient. G. Change in ocean net primary production when $r_{-O2:C}$ shifts from 1 to 0.8. H. Change in ocean net primary production when $r_{-O2:C}$ shifts from 1 to 1.3. I. Annual net primary production and carbon export (at 100 m) as a function of the respiration quotient.

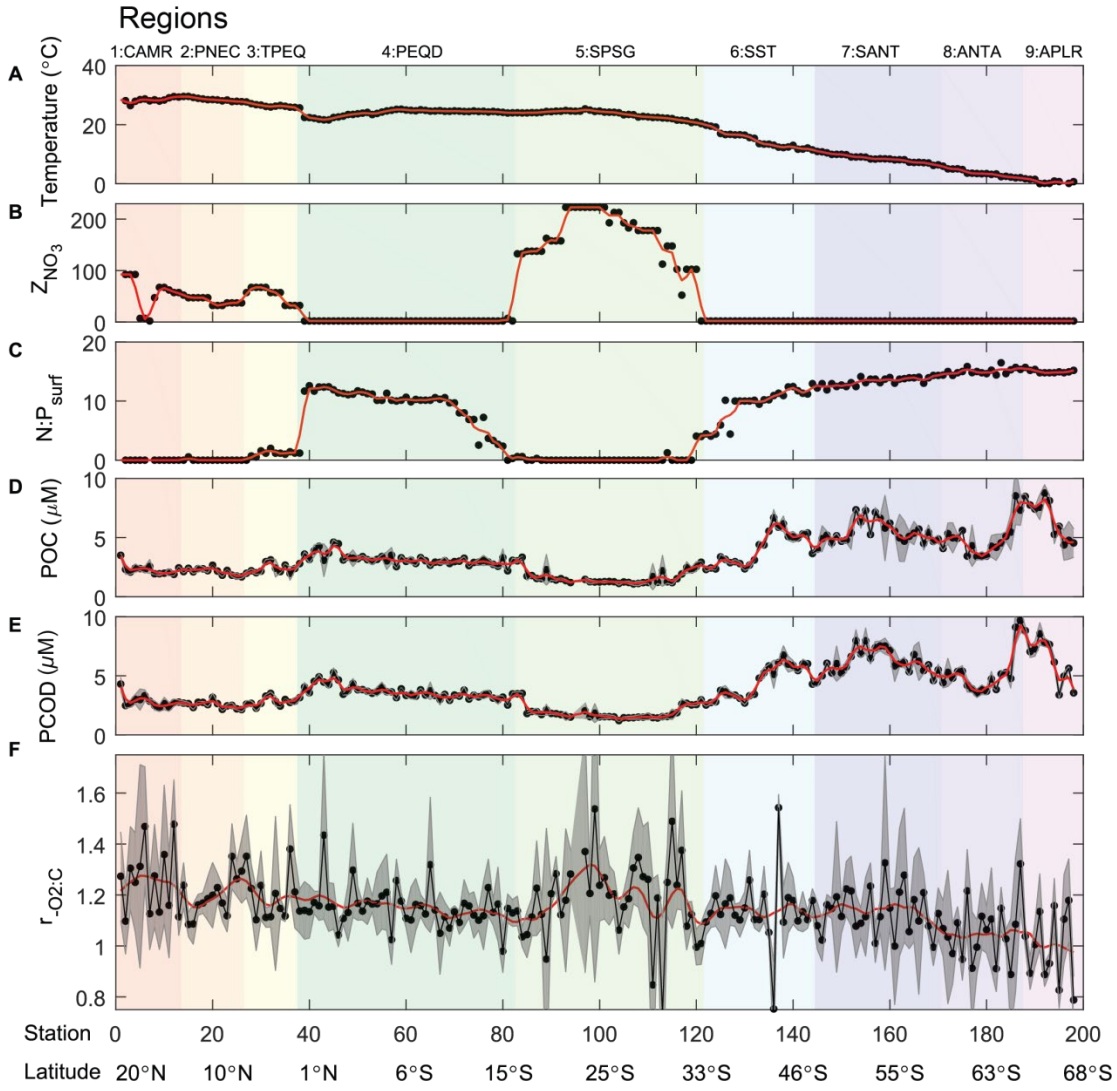

Figure 4.24 Environmental conditions, POM concentrations and the respiration quotient across the eastern Pacific Ocean. A. Sea-surface temperature, B. Nutricline depth (depth at which nitrate is 1 μM), C. Dissolved nitrate to phosphate ($N:P_{surf}$) ratios at the surface, D. Particulate organic carbon (POC), E. Particulate chemical oxygen demand (PCOD), and F. Respiration Quotient. Averaged data are marked as black dots. In panels A-E, the red line represents a 4-station moving average. In panels D-F, the grey shaded regions represent the standard deviation of the replicates. In panel F, the red line represents an 8-station moving average.

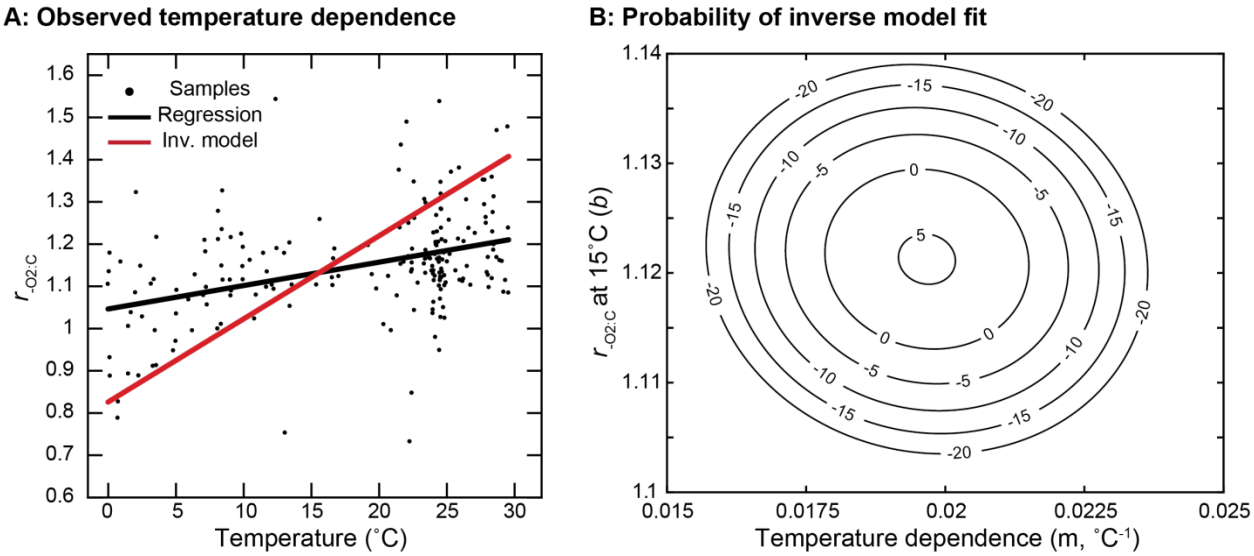

Figure 4.25 Relationship between temperature and the respiration quotient. A. Observed temperature dependence for surface POM $\boldsymbol{r_{-O2:C}}$ = 1.0465 + (0.0055383/°C) *SST*, (R^2 = 0.154) and equivalent relationship inferred from the inversion of hydrographic data. B. The logarithmic marginal posterior probability density for the temperature dependence (m) and intercept (b) in the relationship $\boldsymbol{r_{-O2:C} = m(SST - 15°C) + b}$ estimated from the inversion of the hydrographic data.

Table S4.1 Model change in oxygen levels.

ESM Model	Ocean module	Depth layers	O_2 (Pg)	Resolution	Reference
CESM1-BGC	BEC	60	-289	1.125˚/0.27˚-0.53˚	(Moore et al. 2002)
GFDL-ESM2G	TOPAZ2	63	-281	0.3–1˚	(Dunne et al. 2013)
GFDL-ESM2M	TOPAZ2	50	-312	0.3–1˚	(Dunne et al. 2013)
HadGEM2-ES	Diat-HadOCC	40	-303	0.3–1˚	(Palmer & Totterdell 2001)
IPSL-CM5A-LR	PISCES	31	-322	0.5–2˚	(Aumont & Bopp 2006)
IPSL-CM5A-MR	PISCES	31	-254	0.5–2˚	(Aumont & Bopp 2006)
MPI-ESM-LR	HAMOCC5.2	40	-249	1.5˚	(Ilyina et al. 2013)
MPI-ESM-MR	HAMOCC5.2	40	-229	0.4˚	(Ilyina et al. 2013)
NorESM1-ME	HAMOCC5.1	53	-206	1.125˚	(Tjiputra et al. 2013)
CESM1-BGC $\mathbf{\Delta r_{-O2:C}}$= -0.2	BEC	60	382	1.125˚/0.27˚-0.53˚	This study
CESM1-BGC $\mathbf{\Delta r_{-O2:C}}$= -0.1	BEC	60	186	1.125˚/0.27˚-0.53˚	This study
CESM1-BGC $\mathbf{\Delta r_{-O2:C}}$= 0	BEC	60	0	1.125˚/0.27˚-0.53˚	This study
CESM1-BGC $\mathbf{\Delta r_{-O2:C}}$= 0.1	BEC	60	-177	1.125˚/0.27˚-0.53˚	This study
CESM1-BGC $\mathbf{\Delta r_{-O2:C}}$= 0.2	BEC	60	-308	1.125˚/0.27˚-0.53˚	This study
CESM1-BGC $\mathbf{\Delta r_{-O2:C}}$= 0.3	BEC	60	-493	1.125˚/0.27˚-0.53˚	This study

Table S4.2 Regional environmental characteristics. Observed environmental conditions in each defined biome [mean (minimum – maximum)].

Region	Stations	Temperature	Nutricline	$N:P_{surf}$
1: CAMR	1 - 13	28.4 (26.5 -29.5)	54.3 (1.9 - 92.4)	Below detection
2: PNEC	14 - 26	28.5 (27.8 - 29.6)	40.9 (32.1 - 52.2)	0.04 (0 - 0.56)
3: TPEQ	27 - 37	26.4 (25.9 - 27.7)	54.0 (32.1 - 67.2)	1.1 (0 - 2)
4: PEQD	38 - 82	24.0 (21.6 - 25.7)	2.7 (1.9 - 32.1)	8.9 (0 - 12.6)
5: SPSG	83 - 121	23.4 (20.3 - 25.3)	164.3 (1.9 - 223.1)	0.3 (0 - 4.1)
6: SSTC	122 - 144	14.8 (11.5 - 19.8)	1.9	9.5 (4.1 - 12.9)
7: SANT	145 - 170	8.6 (6.2 - 10.9)	1.9	13.3 (11.9 - 14.3)
8: ANTA	171 - 187	3.6 (2.0 - 5.9)	1.9	15.0 (14.3 – 16.5)
9: APLR	188 - 198	0.7 (0 - 1.7)	1.9	15.0 (14.8 - 15.7)

Table S4.3 The respiration quotient across regions

Region	Average	Range	Standard Error	n
1: CAMR	1.26	1.10 – 1.48	0.036	13
2: PNEC	1.19	1.08 – 1.35	0.022	13
3: TPEQ	1.20	1.10 – 1.38	0.029	11
4: PEQD	1.15	0.98 - 1.43	0.011	45
5: SPSG	1.18	0.73 – 1.54	0.026	39
6: SSTC	1.14	0.75 – 1.54	0.027	23
7: SANT	1.13	0.99 – 1.33	0.017	26
8: ANTA	1.05	0.89 – 1.32	0.028	17
9: APLR	0.99	0.79 – 1.18	0.042	11

Table S4.4 Statistical $r\text{-}_{O2:C}$ models. SE represents the coefficient of variation.

	Intercept	SE	Temperature	SE	Nutricline	SE	Phosphate	SE	NP_{surf}	SE
$r\text{-}_{O2:C}(T, Z_{NO3}, P, NP_{surf})$	1.11	8.1e-2	3.2e-3	2.4e-3	2.0e-4	1.9e-4	-9.6e-1	7.6e-2	5.2e-3	4.9e-3
$r\text{-}_{O2:C}(T, Z_{NO3}, P)$	1.10	5.9e-2	3.7e-3*	1.8e-4	1.1e-4	1.6e-4	-3.2e-2	3.6e-2		
$r\text{-}_{O2:C}(T, Z_{NO3}, NP_{surf})$	1.04	5.7e-2	5.3e-3*	1.7e-3	2.0e-4	1.9e-4			5.6e-4	3.2e-3
$r\text{-}_{O2:C}(T, P, NP_{surf})$	1.15	7.3e-2	2.5e-3	2.3e-3			-9.4e-2	7.6e-3	2.8e-3	4.3e-3
$r\text{-}_{O2:C}(Z_{NO3}, P, NP_{surf})$	1.21	2.2e-2			1.4e-4	1.9e-4	-1.7e-1*	5.4e-2	6.2e-3	4.8e-3
$r\text{-}_{O2:C}(T, Z_{NO3})$	1.05	1.9e-2	5.e-3*	1.0e-3	1.8e-4	1.4e-4				
$r\text{-}_{O2:C}(T, P)$	1.12	5.3e-2	3.4e-3*	1.7e-3			-4.5e-2	3.2e-2		
$r\text{-}_{O2:C}(T, NP_{surf})$	1.07	4.5e-2	4.6e-3*	1.6e-3					-1.7e-3	2.4e-3
$r\text{-}_{O2:C}(Z_{NO3}, P)$	1.21	2.1e-2			5.1e-5	1.6e-4	-9.4e-2*	2.1e-2		
$r\text{-}_{O2:C}(Z_{NO3}, NP_{surf})$	1.20	2.2e-2			-1.6e-5	1.8e-4			-7.4e-3*	2.0e-3
$r\text{-}_{O2:C}(P, NP_{surf})$	1.23	1.6e-2					-1.5e-1*	5.2e-2	4.2e-3	4.1e-3
$r\text{-}_{O2:C}(T)$	1.05	1.9e-2	5.5e-3*	9.3e-4						
$r\text{-}_{O2:C}(Z_{NO3})$	1.13	1.0e-2			4.7e-4*	1.3e-4				
$r\text{-}_{O2:C}(P)$	1.22	1.5e-2					-9.8e-1*	1.7e-2		
$r\text{-}_{O2:C}(NP_{surf})$	1.20	1.3e-2							-7.3e-3*	1.4e-3

*p<0.05

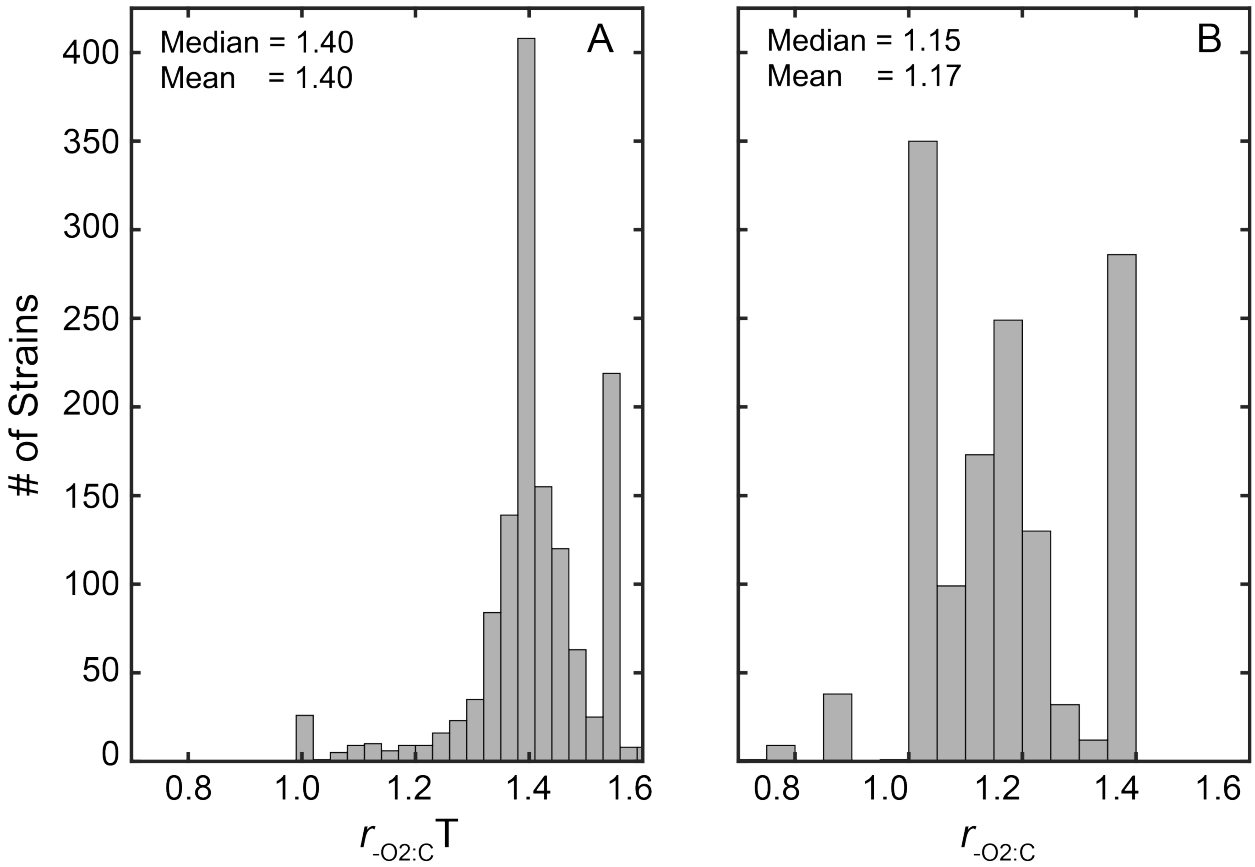

Figure S4.1 Predicted distribution of the respiration quotient across microalgae species. A. The total respiration quotient ($r_{\Sigma-O2:C}$) and B. the respiration quotient ($r_{-O2:C}$). The predictions are based on the biochemical composition of 1562 phytoplankton cultures (Finkel et al. 2016b).

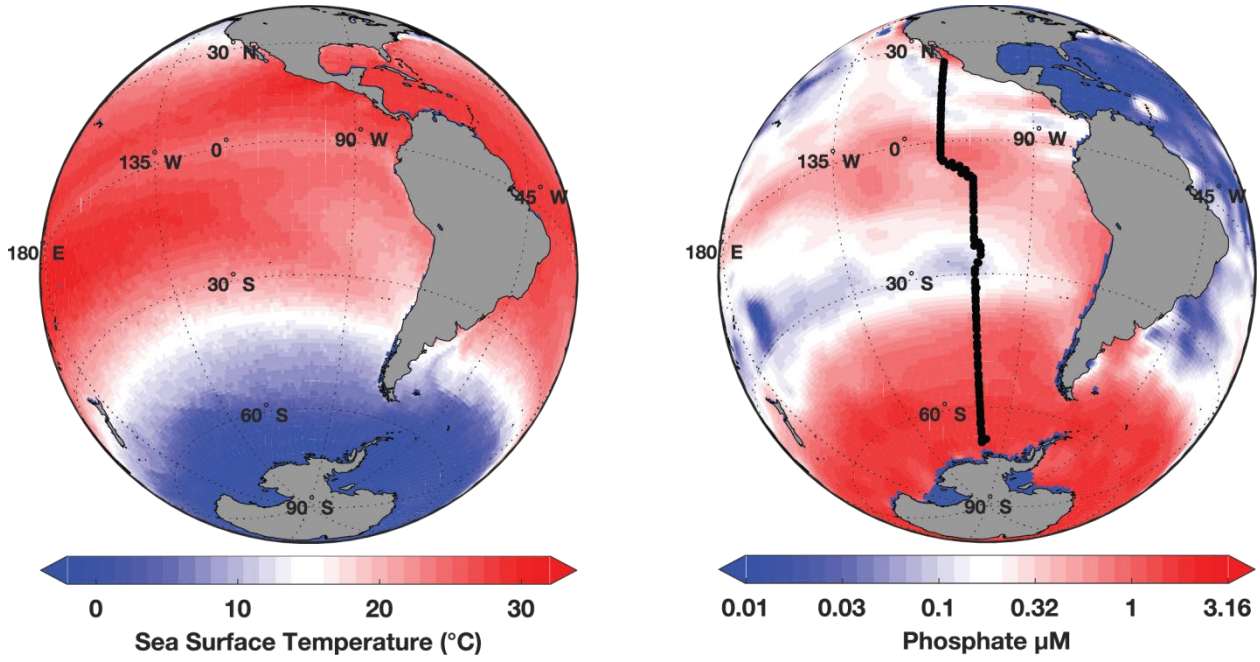

Figure S4.2 P18 GO-SHIP Cruise track locations from San Diego, CA (32.72° N, 117.16°W) to Antarctica (77.85°S, 166.67°E). Background phosphate concentrations are from the GLODAPv2 database (Key et al. 2015; Olsen et al. 2016).

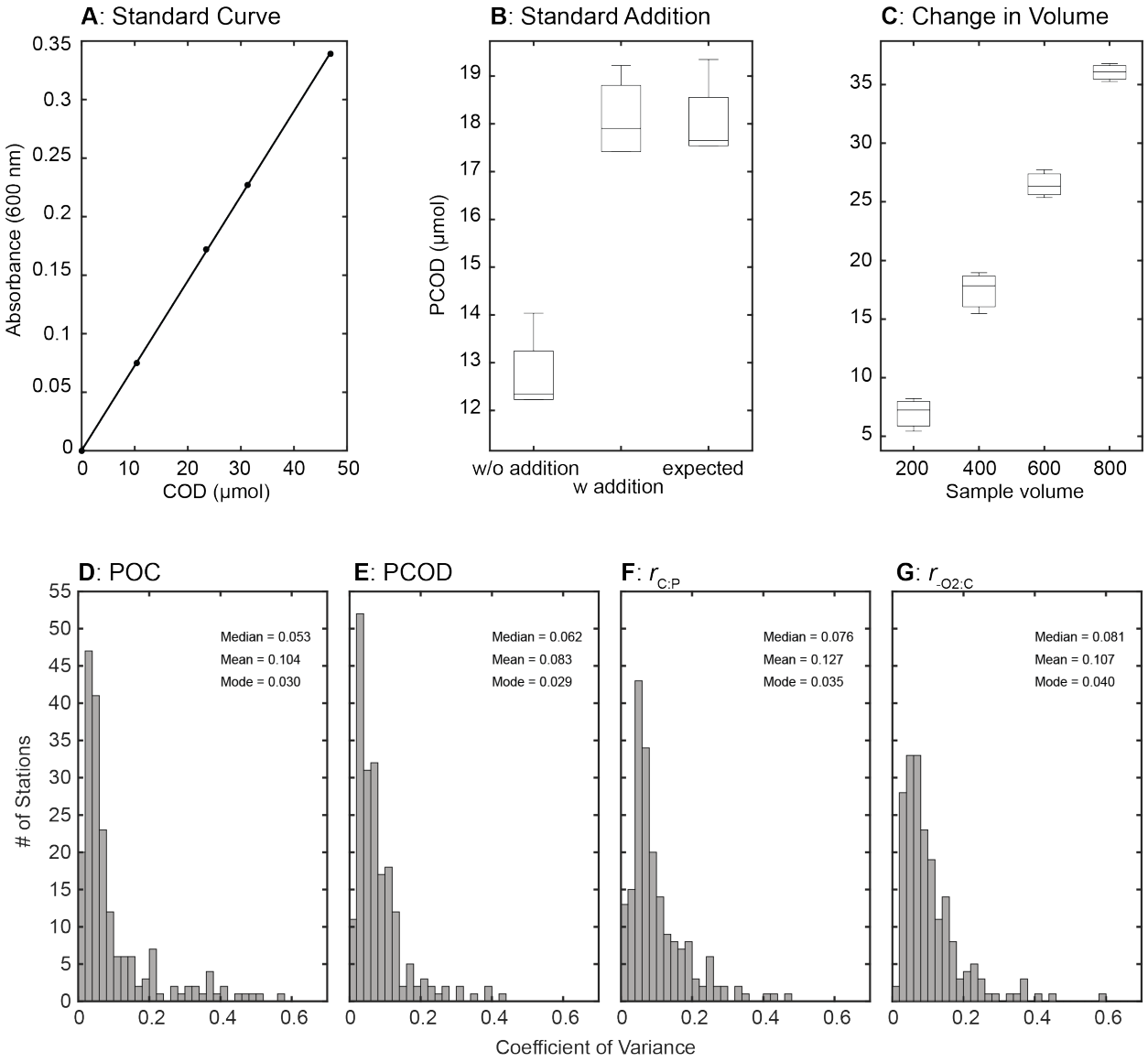

Figure S4.3 Optimization and evaluation of a method for quantifying the oxygen demand of marine POM. A: PCOD standard curve. B: Recovery of the PCOD after experimentally adding organic material to a seawater sample. C: 1:1 relationship between sample volume and measured PCOD. Coefficient of variance in D: [POC], E: [PCOD], F: $r_{C:P}$, and G: The respiration quotient.

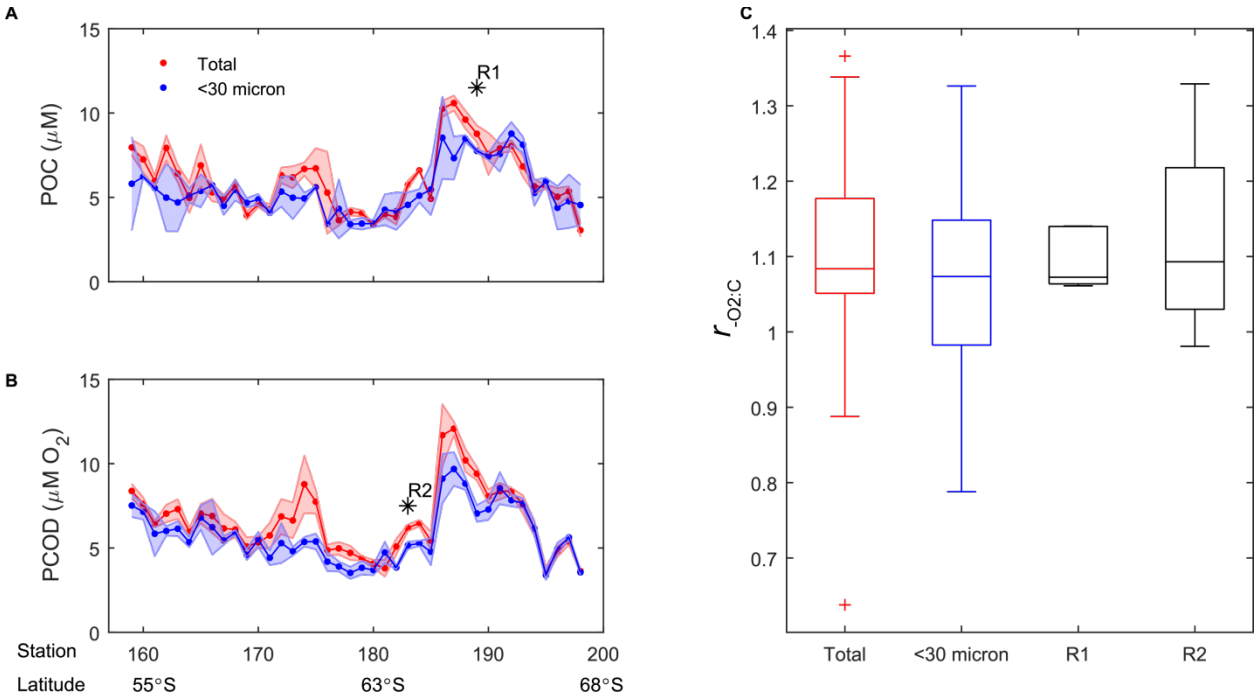

Figure S4.4 Comparison of PCOD concentrations in different size fractions. A. Particulate organic carbon in samples <30 µm and total. B: Particulate chemical oxygen demand in samples <30 µm and total. C: The respiration quotient for <30 µm and total samples as well as for two regions with significant POM concentration differences (R1 and R2).

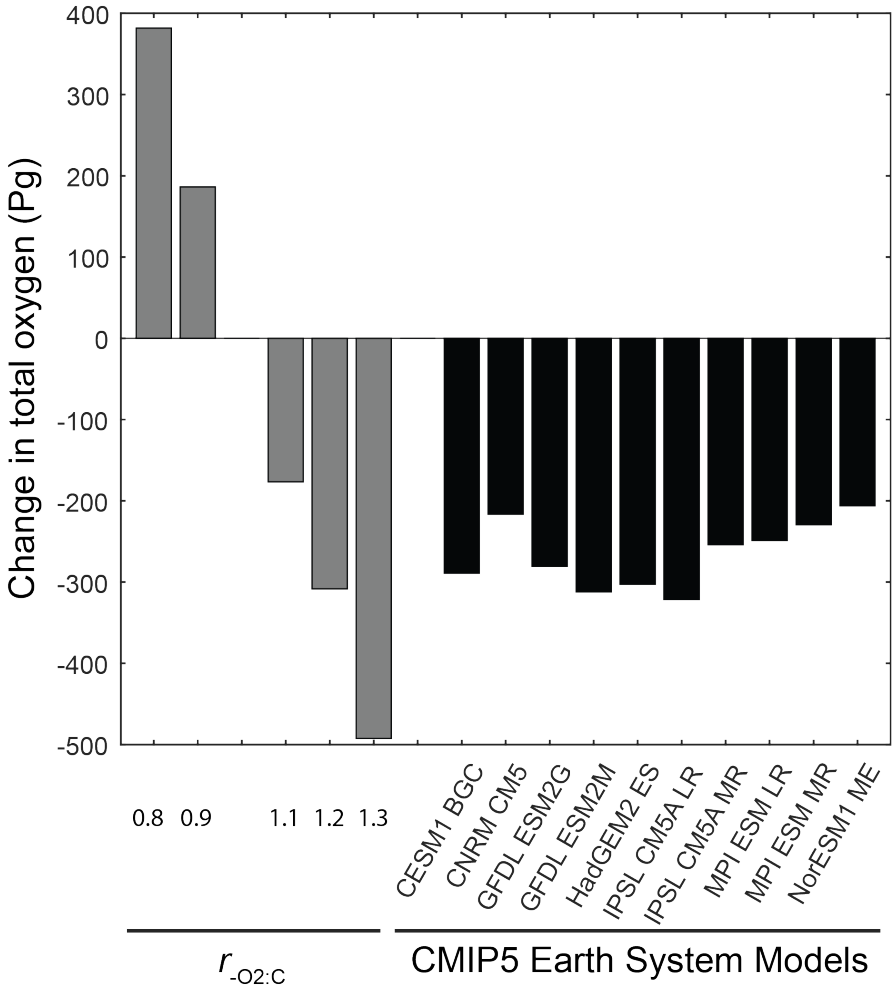

Figure S4.5 Comparison of changes to oxygen levels via changes to the respiration quotient or climate change. A. Changes in global marine oxygen levels by a changing respiration quotient or B. 2100 under the climate change scenario RCP8.5. The climate model outputs are from CMIP5.

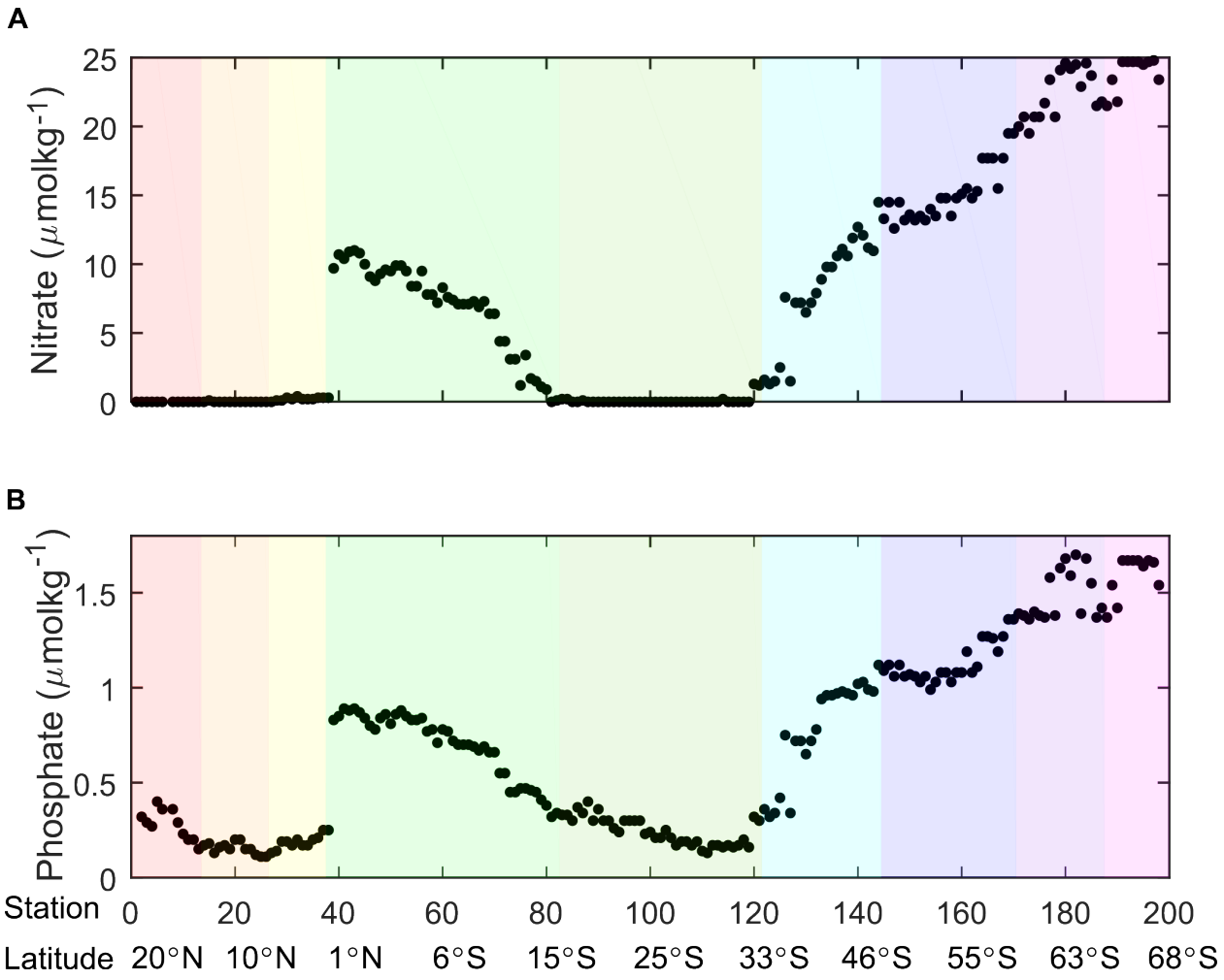

Figure S4.6 Observed nitrate (a) and phosphate (b) concentrations across the P18 cruise track. Colored background represents each ocean biome region.

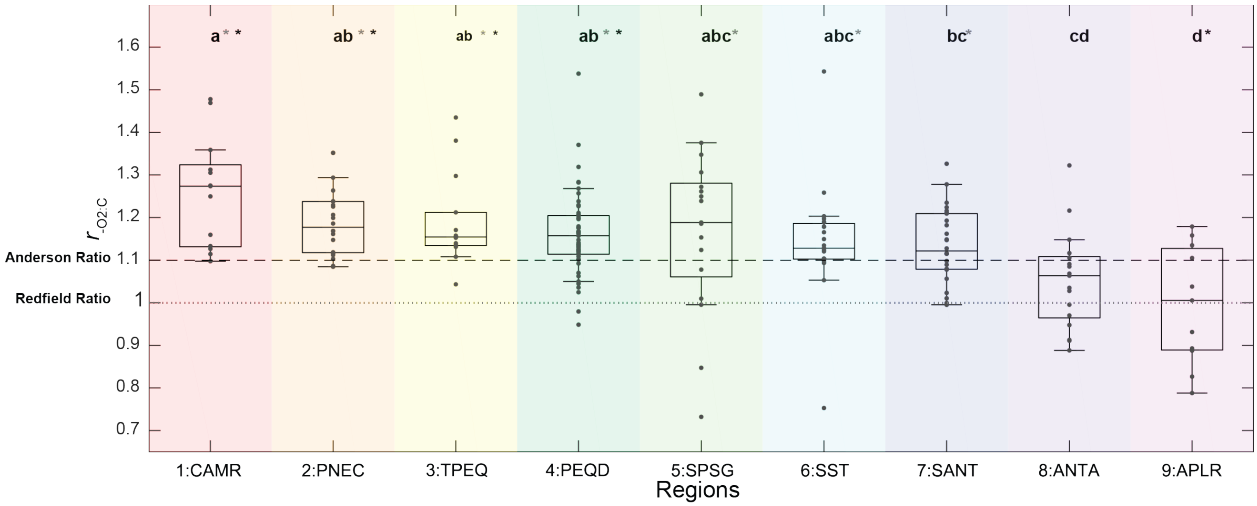

Figure S4.7 Variation in the respiration quotient across eastern Pacific Ocean biomes. 1:CAMR (Central American Coast), 2:PNEC (North Pacific Equatorial Counter Current), 3:TPEQ (Transitional Pacific Equatorial Divergence), 4:PEQD (Pacific Equatorial Divergence), 5:SPSG (South Pacific Gyre), 6:SSTC (South Subtropical Convergence), 7:SANT (Sub-Antarctic Water Ring), 8:ANTA (Antarctic), and 9:APLR (Austral Polar). The variation across biomes (letters above each box) were evaluated by a 1-way ANOVA (p-value <0.05 and Tukey post hoc test). The black and grey dashed line represents Anderson's (1.11) and Redfield's (1.0) respiration quotient. A black or grey asterisks denote a biome average that is statistically different from Anderson's or Redfield's quotient (t-test, p-value <0.05).

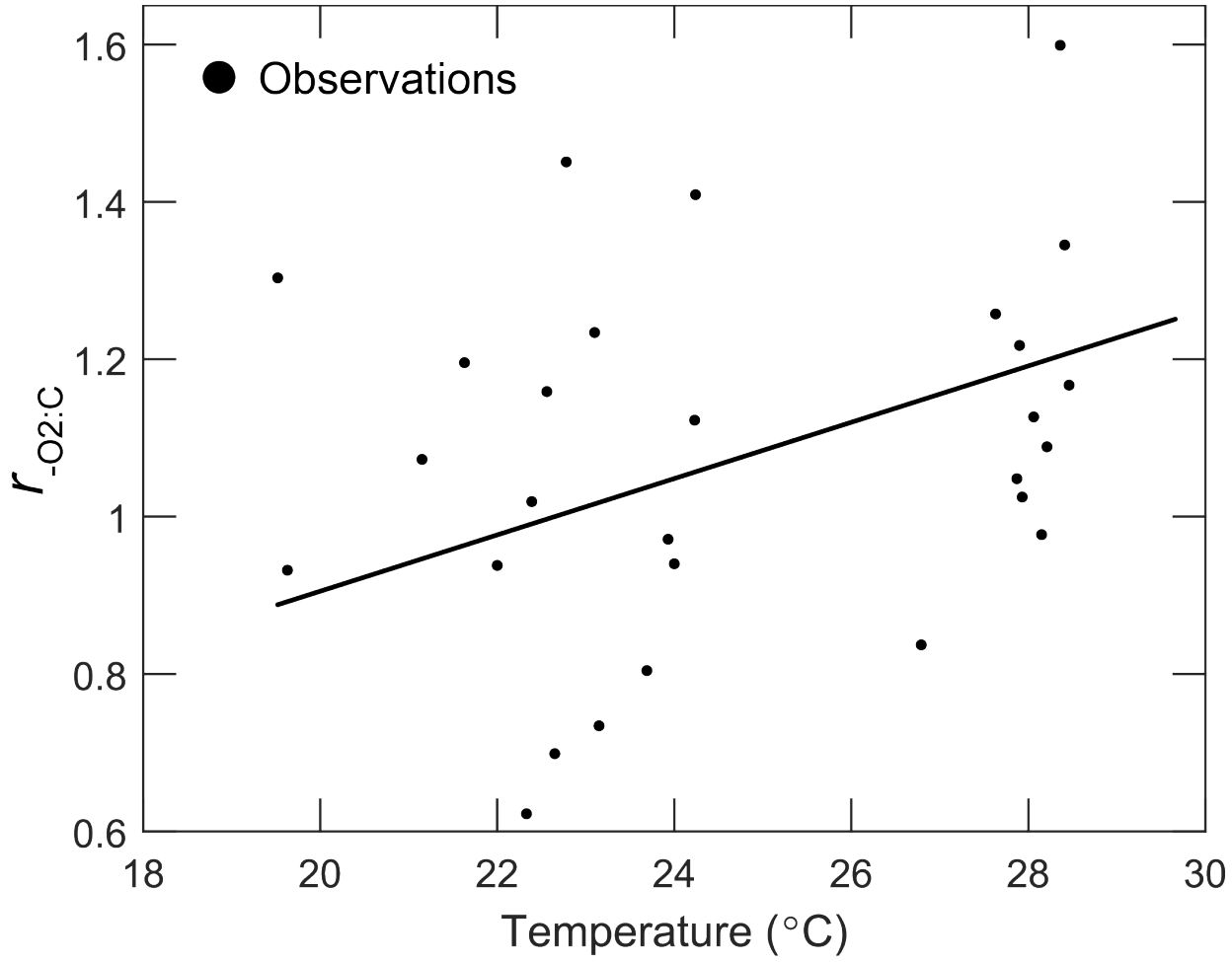

Figure S4.8 Relationship between temperature and the respiration quotient derived from a CHNOPS elemental analysis of marine POM from the Western North Pacific Ocean (Chen et al. 1996). The line represents a linear fitted model of temperature and $r_{-O2:C}$ ($r_{-O2:C}$ = 0.19 + (0.036/°C) *SST*.